
Nordic
Innovation
Mineral to Metal Traceability
A Proof-Of-Concept Study of Rare Earth Elements in the Nordic Region

Mineral to Metal Traceability: A Proof-Of-Concept Study of Rare Earth Elements in the Nordic Region

Authors

Xuan Liu, Jakob Kløve Keiding, Nolwenn Coint, Erik Jonsson, Henrik Stendal, Þorvaldur Þórðarson, Martiya Sadeghi, Nynke Keulen, Benjamin Heredia, Toni Eerola, Magdalena Huyskens, Rune Joachim Clausen, Bjarni Gautason, Jason Yang, Ármann Höskuldsson, Eyþór Rafn Þórhallsson, Hjalti Fransson, Yann Lahaye

Affiliations

Xuan Liu, Toni Eerola, Jason Yang, Yann Lahaye
xuan.liu@gtk.fi; yann.lahaye@gtk.fi; toni.eerola@gtk.fi, jason.yang@gtk.fi
Geological Survey of Finland (GTK)
P.O. Box 96, FI-01251 Espoo, Finland

Jakob Kløve Keiding, Nynke Keulen, Rune Joachim Clausen, Benjamin Heredia
jkk@geus.dk; ntk@geus.dk; rjc@geus.dk; behe@geus.dk
Geological Survey of Denmark and Greenland (GEUS)
Øster Voldgade 10, 1350 Copenhagen, Denmark

Nolwenn Coint, Magdalena Huyskens
Nolwenn.coint@ngu.no; Magdalena.huyskens@ngu.no
Geological Survey of Norway (NGU)
Leiv Eirikssons vei 39, 7040 Trondheim, Norway

Erik Jonsson, Martiya Sadeghi
Erik.jonsson@sgu.se; martiya.sadeghi@sgu.se
Geological Survey of Sweden (SGU)
Box 670, SE-75128 Uppsala, Sweden

Henrik Stendal
Hdal@nanoq.gl
Ministry of Mineral Resources, Government of Greenland
P.O. Box 930, 3900 Nuuk, Greenland

Þorvaldur Þórðarson, Ármann Höskuldsson
torvth@hi.is; armh@hi.is
University of Iceland
Sturlugata 7, 102 Reykjavík, Iceland

Bjarni Gautason, Hjalti Fransson
bjarni.gautason@isor.is; hjaltif@simnet.is
Iceland GeoSurvey
Orkugardur, Rangarvellir 2, 603 Akureyri, Iceland

Eyþór Rafn Þórhallsson
eythor@ru.is
University of Reykjavík
Menntavegur 1, IS-102, Reykjavík, Iceland

Suggested citation

Liu, X., Keiding, J.K., Coint, N., Jonsson, E., Stendal, H., Þórðarson, Þ., Sadeghi, M., Keulen, N., M., Heredia, Eerola, T., Huyskens, M., Clausen, R.J., B. Gautason, B., Yang, J., Höskuldsson Á., Þórhallsson E.R., Fransson H., Lahaye, Y. 2024. Mineral to Metal Traceability: A proof-of-concept study of rare earth elements in the Nordic nations. Nordic Innovation Report.

Design and publication drafting were managed by Kati Kiviniemi.
Layout Elvi Turtiainen Oy.

The photo on p.29, p.50, p.57, p.63 shows underground tunnels of the Løkken VMS deposit, Norway (credit: Leonardo Feltrin); the photo on p.35 shows a pegmatitic grennaite from Norra Kärr, Sweden, featuring pale reddish eudialyte (sensu lato) and thin, yellow laths of a rosenbuschite-like mineral (credit: Erik Jonsson).

Disclaimer: This publication is part of the program Sustainable Minerals by Nordic Innovation. Geological Survey of Finland, Geological Survey of Sweden, Geological Survey of Denmark and Greenland, Ministry of Mineral Resources of the Government of Greenland, Geological Survey of Norway, University of Iceland, and Icelandic Geosurvey are responsible for its content.

Front cover: iStock

Table of contents

Executive Summary 4

1. Introduction 6

1.1 Background 6
1.2 REE value chain 7
1.3 REE resources in the Nordics 9
1.4 Existing traceability approaches 11
1.5 Geo-based traceability methodology 15

2. Main results 18

2.1 NSM REE traceability methodology 18
2.2 Geo-fingerprinting pilot study: REE minerals 21
2.2.1 Homogeneity test 21
2.2.2 Conservativity test 59
2.2.3 Uniqueness test 61
2.3 Geo-forensic pilot study: Nd magnets 62
2.3.1 Analytical workflow 62
2.3.2 Phase characterization 63
2.3.3 Trace elements 67
2.3.4 Nd isotopes 70

3. Discussion 72

3.1 Feasibility analysis 72
3.2 Major challenges 74
3.3 Outlook 75

4. Conclusion 77

Acknowledgement 77
References 78
Table of figures 82

Appendices 85

Appendix 1.
Sample preparation and analytical method 85

Appendix 2.
REE oxalate production with hydrometallurgy 90

Executive Summary

Traceability, when fully functional, is considered imperative for ensuring the transparency, accountability and sustainability of intertwined global supply chains of minerals and metals. The ability to trace and track the flow and transformation of these mineral raw materials requires full documentation and transmission of information relevant to the material flow. Equally important, if not more so, is to have a holistic understanding of the minerals and their metals and all their derivative products with respect to their geological, mineralogical, geochemical and isotopic characteristics. The former, known as document- or paper-based traceability, has been under active investigation by many research initiatives, while the latter, known as geo-based traceability, is the focal point of this research, supported by the Nordic Sustainable Minerals (NSM) project.

Taking rare earth minerals and their contained metals as a main example, this study explored the concept of geo-based traceability by using a tailored methodology that delves into three pivotal cornerstones of the technique. These include precise knowledge of the ore deposits in terms of their mineralogical and geochemical homogeneity, the magnitude of alteration of the geo-signatures due to mineral processing, and the uniqueness of the geo-signatures as compared to other deposits worldwide. A pilot study on four rare earth element (REE) targets in the Nordic region suggests that mineral association, micro-texture, trace element and isotope compositions are variably homogeneous in space and time, depending on the deposit type. Alkaline intrusion-related deposits (Kringlerne in Greenland and Norra Kärr in Sweden) are relatively more likely to have homogeneous and unique geo-signatures compared to carbonatite-related deposits (Fen in Norway and Sokli in Finland). This difference is caused by the distinctive mechanisms and evolution of ore formation and deposit modification. It is noted, however, that geochemically similar elemental pairs, such as Zr/Hf and REE ratios, are the most homogeneous geo-signatures due to their similar geochemical properties, and they are thus relatively insensitive to variations in external conditions (e.g., temperature, pressure). In addition, geo-signatures in carbonatite systems may vary significantly on a deposit scale, but they may be distinctive and unique compared to other deposit worldwide. These sub-deposit-scale signatures might also be important for differentiating a given deposit.

A lab-scale replication of mineral processing from REE ores to individual metals, which we termed a conservativity test, unsurprisingly revealed dramatic loss of geo-signatures at different stages, from mineral beneficiation (producing mineral concentrates) through hydrometallurgical leaching and separation (producing mixed and individual REE compounds) to molten salt electrolysis (producing individual metals). Rock textures and almost entire mineral associations and textures may be completely obliterated due to crushing, grinding and concentration (e.g., by magnetic separation). In some cases, major gangue minerals might survive, such as the nepheline–arfvedsonite–sodalite–aenigmatite residues in the eudialyte concentrates of Kringlerne. Element and isotope compositions are expected to survive, since mineral beneficiation does not involve high temperatures and strong chemical treatment, which can alter and redistribute elements in the minerals. Subsequent hydrometallurgical

treatment, by contrast, considerably alters the elemental composition, as the process involves leaching and sometimes dissolution of the mineral by acid. Nevertheless, the ratios between REEs (e.g., Sm/Nd) remain largely the same due to the very similar chemical properties of rare earth elements. These REE ratios, however, would be completely altered in the succeeding stage of REE separation, which selectively enriches Nd and Nd–Pr over other REEs for making Nd magnets.

The only geo-signatures that survive the entire refining and manufacturing process are perhaps the isotope compositions. Isotope analyses of REE oxalate produced by hydrometallurgical treatment (leaching with green chemistry) from the Kringlerne eudialyte concentrates revealed nearly identical $^{143}Nd/^{144}Nd$ ratios compared to those of original eudialytes. This observation is further verified by our magnet pilot study, the Nd isotope analyses of which revealed the man-made magnets had "natural" Nd isotopic ratios, for instance $^{146}Nd/^{145}Nd$, meaning that the metal refining, alloying and magnet-making process did not change the isotope compositions. Even though mostly conservative, the ratios between stable isotopes are not very useful for tracing, since their ratios remain largely the same across different natural reservoirs. ^{143}Nd, which is the only radiogenic isotope amongst all seven long-lived Nd isotopes, changes in response to the radioactive decay of ^{147}Sm, and thus the ratio $^{143}Nd/^{144}Nd$ varies according to the age and material source of the REE deposits. It is also notable that most trace element compositions in the original minerals are very probably changed in downstream processing, as mentioned above, and new elements might be introduced due to the use of chemicals (e.g., acids used for leaching and precipitation, substituent and dopant elements used in the making of Nd magnets to improve magnet performance). The addition of other elements, however, may well serve as a forensic tool for fingerprinting the origin of magnets and rare earth metals, as evidenced by the clear discrimination of Nd magnets produced in different years and thus presumably originated from different ore deposits. Given this, the availability of the recipe of processing agents and particular substituent and doping elements is important for traceability. A wild speculation is that the substituting and doping process may provide an excellent opportunity for tagging certain end products, such as Nd magnets, and this may therefore offer a complementary means of traceability.

We conclude that the development of geo-based traceability of minerals and metals is a very complicated and challenging task, as is the task of developing a document-based approach, and it will most likely require long-term and most importantly in-depth research to identify homogeneous, conservative and unique geo-signatures, in addition to building a comprehensive database of these traceability signatures. The ideas and results obtained in this project are by no means conclusive, and at best represent a proof of concept that validates the use of mineralogical and geochemical signatures to discriminate and identify the source of minerals and derivative metals, analogous to the use of biological features (e.g., fingerprints, DNA) for identifying a person.

1. Introduction

1.1 Background

Humanity is facing a climate crisis due to its fossil fuel-based industrial and societal developments, which have been proven to be a main source of greenhouse gas (GHG) emissions and a major cause of rapid global warming in the past century (IPCC 2021). Scientific studies have found irrefutable evidence that human-induced climate change is causing widespread adverse and irreversible impacts on both nature and society (IPCC 2022). In order to minimize and mitigate further impacts of such global warming, society and industry, at least in the industrial world, are undertaking a fundamental shift away from fossil energy, which accounted for over 60% of total CO_2 emissions in 2020 (Climate Watch 2023). However, the transition to a mineral-based economy requires the development of both infrastructure and technologies that demand significantly more critical and strategic minerals (CSM) compared to conventional technologies (IEA 2021). In particular, the demand for certain minerals and metals that are key components of these technologies is increasing very rapidly, and will likely do so for the foreseeable future (Alves Dias et al. 2020). According to a recent foresight study, the International Energy Agency (IEA) concluded that in a scenario that aims to meet the Paris Agreement goals, clean energy technologies' share of the total demand rises significantly over the next two decades to over 40% for copper and rare earth elements, 60–70% for nickel and cobalt, and almost 90% for lithium. On top of that, studies on the socio-environmental influence of mining such "energy metals" have demonstrated that over half of all global CSM resources of special metals such as platinum, cobalt, copper, nickel, rare earths and lithium have medium to very high environment-social-governance (ESG) risks (Lèbre et al. 2020). To avoid the conversion of the "carbon crisis" to a "mineral crisis", a sustainable supply of renewable energy minerals and metals should be pursued, even though this is very far from where we are today. Among other important pathways, improving or constructing traceability systems for mineral raw materials, particularly CSMs, has been considered a potential solution (e.g., Sovacool et al. 2020).

Among its multiple uses in metrology, health care and others, the traceability of raw materials refers to the ability to identify and trace information of the ingredient materials used in making a part or end product in a supply chain (UN Global Compact report 2014). In the case of minerals and metals, two main types of information are typically involved, alongside the flow of the materials, which include information of the material itself and that related to the material movement. The former type includes the place of origin and the processing/refining method, to name the most important ones. The latter includes sustainability claims and transactions. The availability and proper transmission of the aforementioned information is crucial for ensuring supply chain transparency and accountability, as well as improving product values (Garcia-Torres et al. 2019). As such, the technique is widely considered a key enabler for pursuing ecological and societal goals set by the UN's Sustainable Development Goals and the EU's Critical Raw Materials Act (2023).

This study aimed to test the potential for the establishment of a comprehensive traceability system for rare earth elements (REEs) and basalt fibres specifically produced in the Nordic countries. The focus was on REEs, which are CSMs essential to the green transition and having a number of identified resources in the Nordic countries, here encompassing Greenland and the Fennoscandian Shield (Finland, Norway and Sweden). These raw materials are characterized by highly complex and non-transparent global supply chains. Implementing traceability could be a crucial facilitator for increased transparency. Basalt fibres are deemed as having significant potential in Iceland and are expected to play an important role in Iceland's future economy and were included here as the second case study on traceability. However, the focus of this report is on the REEs.

1.2 REE value chain

Rare earth elements (REEs) are a group of 17 elements, comprising the 15 lanthanide elements, namely lanthanum (La), cerium (Ce), praseodymium (Pr), neodymium (Nd), promethium (Pm), samarium (Sm), europium (Eu), gadolinium (Gd), terbium (Tb), dysprosium (Dy), holmium (Ho), erbium (Er), thulium (Tm), ytterbium (Yb) and lutetium (Lu), together with scandium (Sc) and yttrium (Y), as defined by the International Union of Pure and Applied Chemistry. Typically, however, scandium is not included among the REEs when classified geologically, as this metal characteristically does not follow the others in the majority of geological processes. These elements are considered as critical and strategic minerals (CSM) in many nations, including the EU, because of their irreplaceable role in high-tech industries, including renewable energy technologies, as well as paramount supply risks (Natural Resources Canada 2021, Department of Industry, Science, Energy and Resources 2022, Grohol 2023). These elements are widely used in catalysts, alloys, polishing compounds, phosphors, and in nuclear-reactor and defence-related applications (Gielen & Lyons 2022). In particular, Pr, Nd, Tb and Dy are essential ingredients in rare earth magnets, which are vital components of high-performance wind turbines and electric vehicle (EV) traction motors.

In a nutshell, the value chain of REEs, like most other metals, consists of a primary chain and a secondary recycling loop. The primary chain, illustrated in Figure 1, starts with upstream exploration and mining, which locates and extracts REE-bearing ores from Earth's crust, followed by midstream mineral processing and metal refining in smelters and refineries. The refined metals are then transferred to production plants, where alloys are made, which are used in the downstream production of semi-final products such as Nd–Fe–B magnets. The semi-final products end up in the manufacturing of final products, such as electric vehicles. At the end of life (EoL) of the final products, they can be reused/repurposed, disposed of in landfill or be recycled. The value chain of secondary REE resources is not included in the current study, but the overall recycling of REEs currently contributes less than 1% of the global demand (Kalvig 2022) and is thus neglectable. For more information on the recycling of REEs and other critical raw materials, the interested reader is referred to the WP2 report of the NSM project by Feltrin et al. (2024).

REE mineral resources mainly consist of monazite and bastnäsite, and subordinately of xenotime, apatite group minerals, allanite, loparite, eudialyte and steenstrupine from carbonatite, alkaline igneous rock, iron oxide and

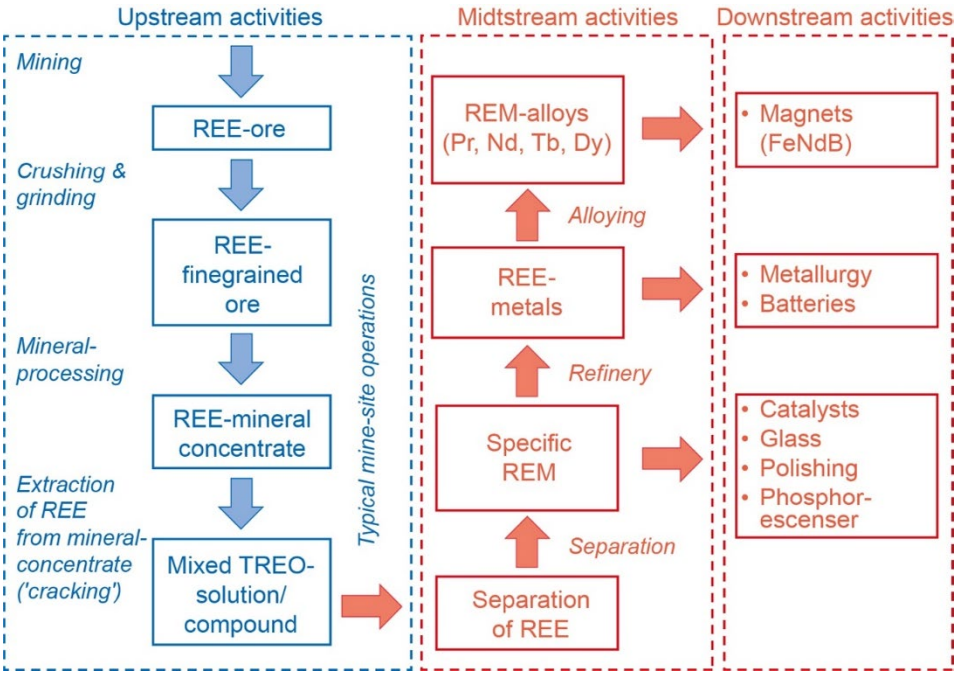


Figure 1. Generic diagram showing the primary value chain of REEs from mine to finished product. The upstream activities (in blue) are generally performed in or near the mining facility. The mid- and downstream activities (in red) involve advanced processing stages, each handled by companies specializing in that particular phase. These steps are primarily dominated by Chinese companies. Figure from Kalvig (2022).

hydrothermal type deposits, ionic clays, placers and marine sediments (Kalvig 2022, Liu et al. 2023). After extraction, REE ores undergo mineral beneficiation and processing by physicochemical methods (e.g., gravity, electrostatic and magnetic separation, froth flotation) to produce mineral concentrates, which are then further processed by hydrometallurgy, electrometallurgy and pyrometallurgy to produce intermediate REE compounds in the form of carbonates, oxides and oxalates. REE compounds are then subject to reduction to make pure individual metals, typically by molten salt electrolysis. The separated REE metals can subsequently be used in end products or further alloyed with other metals, for instance with Fe and B to produce Nd–Fe–B magnets, by a series of physical grinding, heat treatment, sintering and magnetization.

China dominates REE production along the entire value chain, accounting for 69% of the global production of rare earth oxides (REOs) (USGS 2024)[1], 85% of the purified metal and alloys (IEA 2021) and 85–90% of the production of NdFeB magnets (European Commission 2020). According to the EU-funded project SCRREEN (2023), the EU imports 100% of its REEs, including an annual consumption of 4,734 tons/year of rare earth oxides (REO) and 683 tons/year of REE metals and interalloys during the period 2016–2018. It is forecasted that the global demand for NdFeB magnets by 2035 will increase at a compound annual growth rate (CAGR) of 8.6%, boosted by the growth of the EV and wind-power sectors. Over the same period, the global production of magnet REEs is expected to collectively increase at a slower CAGR of just 5.4%, as the supply side of the market increasingly struggles to keep up with the rapidly growing demand (Adamas Intelligence 2022).

[1] https://pubs.usgs.gov/periodicals/mcs2024/mcs2024-rare-earths.pdf

1.3 REE resources in the Nordics

The Nordic countries, here specifically Greenland, Norway, Sweden and Finland, are considered to have significant mineral resources and potential for REEs due to their long and complex geological evolution and related bedrock affinities (e.g., Goodenough et al. 2016, Jonsson et al. 2023, and references therein). The REE-enriched mineralization types in the Nordic countries mainly comprise primary ore deposits, which occur in different types of rocks and geological environments (Fig. 2). One of the most important primary deposit types with both relatively high grades and tonnages is typically associated with alkaline–peralkaline igneous rocks and carbonatites that formed in particular plate tectonic settings, specifically in so-called intracontinental rift environments (e.g., Chakmouradian and Zaitsev 2012, Goodenough et al. 2016). These vary in age from Paleoproterozoic to Paleozoic in the Fennoscandian shield and Greenland (e.g., Norra Kärr in Sweden, Kringlerne in Greenland). Carbonatites are rare rocks that characteristically occur in continental extensional or rift settings and may contain significant concentrations of REEs, beside other commodities such as niobium (Nb) and industrial minerals, as well as other metals. The Sarfartoq carbonatite complex in Greenland, the Sokli intrusion in Finland and the Fen complex in Norway are examples of such carbonatite-hosted deposits with variable but overall high potential for REE minerals. Magnetite–(hematite)–apatite ores of the Kiruna type in northern and south-central Sweden, primarily mined for their iron contents, contain high grades of REEs, which are hosted by primary fluorapatite, often remobilised into later-formed monazite, allanite and xenotime (e.g., Harlov et al. 2002, Jonsson et al. 2016, and references therein). The Kiruna/Per Geijer, Malmberget and Grängesberg deposits are examples of this REE mineral deposit type. It is also notable that stockpiled tailings from earlier mining in some cases contain appreciable amounts of REE-bearing fluorapatite and associated REE-enriched minerals. Hydrothermal skarn-type mineral deposits occur in the Bergslagen ore province in south-central Sweden, and this type of deposit (so-called Bastnäs-type deposits) has locally very significant contents of REEs but is of low volume. Some alkaline to granite-associated and numerous granitic pegmatite fields in the crystalline bedrock of the Nordic countries show locally high REE concentrations (e.g., Evje-Iveland in southern Norway, numerous pegmatites in central Sweden; Goodenough et al. 2016, Jonsson et al. 2019, Sadeghi et al. 2020), while the granite-associated hydrothermal Olserum-Djupedal REE deposits in southern Sweden seemingly have good near-future potential (e.g., Jonsson et al. 2023, and references therein). Several REE mineral deposits in the Nordic countries are thus also listed among the more advanced REE projects globally. Of these, the Kringlerne deposit in Greenland is one of the largest known untapped REE mineral resources in the world, whereas the Norra Kärr deposit in Sweden has high proportions of HREEs, as does Olserum, while Sokli in Finland has great mineral potential for both REEs and P in part of the complexes, and finally the Fen deposit in Norway has recently been ranked as Europe's largest known deposit of rare earth elements[2].

[2] https://www.ngu.no/en/nyheter/norway-hosts-largest-known-deposit-rare-earth-elements-europe

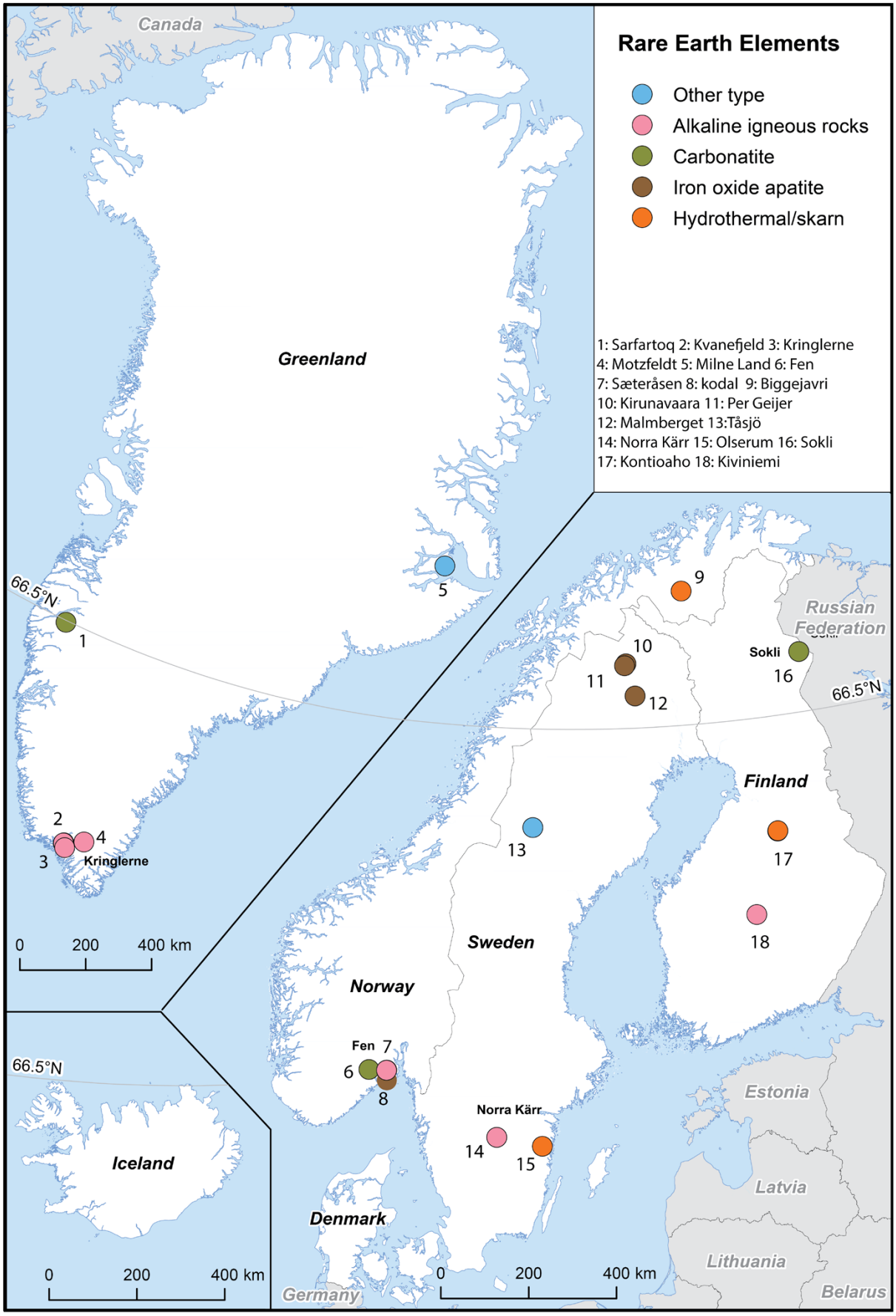


Figure 2. Location of very large to medium-sized deposits of REE resources in the Nordic countries. Case study deposits in this project are mentioned on the map.

1.4 Existing traceability approaches

Traceability applications, commonly used techniques in many supply chains such as the food and forestry industries, are designed to increase transparency, ensure good practice, and thus build trust in the entire supply chain. The mineral and metal industry, one of the most important economic sectors for the global economy, unfortunately does not have a reliable traceability system (Van Den Brink et al. 2019). In the present mineral and metal market, end-product suppliers, such as electronics and automotive companies, cannot provide information beyond their immediate suppliers[3] and are constantly facing management risks (UN Global Compact Report 2014). These downstream companies are increasingly demanding information from the lower-tier suppliers. Overall, the provenance, i.e., the geographic origin (mine), of minerals and metals that are contained in their products is the most concerning information (RCS Global and ICMM 2017). Mineral and metal supply chains are often the focal point of scrutiny and regulation from external stakeholders (the general public, governments, international organizations and non-government groups) in the ever-growing demand for verifiable transparency and better performance (Fig. 3). Consequently, supply-chain participants, downstream companies in particular, are desperately searching for solutions to determine metal provenance[4]. Likewise, having a good traceability technique in place may bring many benefits to the supply-chain stakeholders, for instance, in the development of reputation, supplier selection, risk control, operation efficiency and process consistency (UN Global Compact Report 2014).

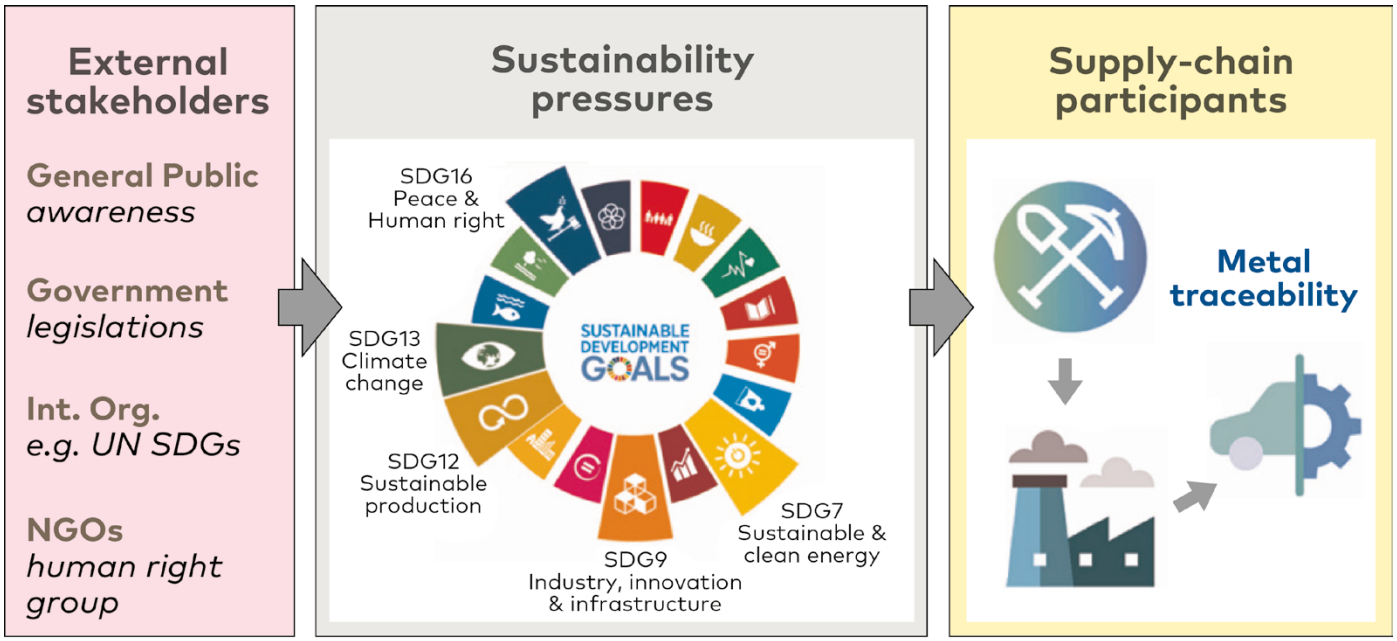


Figure 3. A schematic diagram showing that external stakeholders, including the general public, governments, international organizations and non-government organizations, are exerting pressure on supply chain participants for transparency, which can only be achieved using traceability techniques.

[3] Traceability and labelling of sustainable metals and minerals. 13 February 2019: https://www.tillvaxtanalys.se/in-english/publications/pm/pm/2019-02-13-traceability-and-labelling-of-sustainable-metals-and-minerals----efforts-to-increase-transparency- credibility-and-demand.html.

[4] Traceability of sustainable metals – a blockchain-based solution. May 2019. https://www.sipstrim.se/wp-content/uploads/2018/09/sparbarhet-2019-enkelsidor-1.pdf.

Although there is mounting evidence that the partial shut-down of the global economy had positive effects on the environment during the COVID-19 pandemic, this is by no means a viable strategy for sustainable development. Instead, a prosperous, fair and green economy should be the centre of efforts. For metal industries, establishing effective and efficient traceability systems constitutes an important part of such efforts by maximizing supply-chain transparency. To date, traceability strategies for metals and minerals are still in their infancy. Two broad categories are in practice, i.e. "document-based" approaches, which prove the intentional sourcing in the supply chain, as well as the transaction of the product, and "sample-based" ("geo-bas©ed") approaches, which analyse the product in order to quantify its composition or trace its origin (Desaulty et al. 2022). Different analytical techniques can be used to extract different types of information (Fig. 4).

Proof of intention

A code of conduct and supply chain statements are the most common approaches used to ensure supply chain compliance. These declarations are assuring claims from the supplier, i.e., proof of good intentions, but are not a guarantee, for instance, of the origin of the product. The legitimacy of the statements can be strengthened by allowing a third party to document the claims and/or by introducing an audit process. A code of conduct and due diligence provides the lowest level of proof for the origin (Tables 1, 2).

Proof of transaction

Chain of custody (CoC) systems track minerals from the mine to the final product, ensuring that each step in the supply chain is documented and verified. Examples include iTSCi (the ITRI Tin Supply Chain Initiative), which tracks tin, tantalum and tungsten from mine to smelter, providing data and risk assessments. The chain of custody system is composed of features such as automated product ID registration, a blockchain to log the ID registrations, automated data analysis, GPS tracking and on-site inspection of the ID. Chain of custody systems can be further strengthened by means of inspection, either by performing a visual inspection or introducing non-penetrative analytical methods such as hyperspectral cameras, magnetic analysis, 3D scanning and X-ray analysis, such as XRF and XRT. Sometimes, sample analysis is carried out as part of an inspection, usually as a non-representative grab sample with a qualitative result. All in all, documenting the transactions throughout the supply chain does not prove the origin of the product, even with qualitative inspections in place, but it can provide circumstantial evidence of the product origin.

Proof of origin

Quality assurance and control (QA/QC) are two aspects of quality management important for ensuring that the product or service adheres to a defined set of quality criteria. In ore handling, QA/QC control inspections assess whether the concentration and purity of the ore is within an acceptable quality limit (AQL). Because these analyses are both quantitative and statistically representative, they are often capable of ruling out certain origins for high quality products such as mineral ores. In rare cases, the occurrence of a certain mineral in the ore is unique to its locality, and a QA/QC is in fact able to prove the origin of the ore. An example of a unique mineral is the blue mineral nevadaite, which is only known from two locations: Eureka County,

Nevada, and a copper mine in Kyrgyzstan. Another example is the gemstones kayawthuite and painite, which have only been found in Myanmar. The no-longer-mined mineral cryolite from Ivittuut in South Greenland has only been found in Ivittuut. It was mined during 1854–1987 and was primarily used in the aluminium industry.

Geochemical fingerprinting involves analysing the unique chemical and isotopic signatures of minerals to determine their geographic origin by statistically comparing them with a database of references. This was the main topic of this project and is further explored in the next chapter.

Table 1. A general overview of supply chain traceability approaches ranked according to their ability to prove the origin of the ore. Different approaches can supplement each other.

Proof level	Approach	Method + add-ons to the method
Proof of origin	Geochemical fingerprinting & statistical validation	+ Tracer added + Unmixing w. algorithm (necessary for mixed materials with different origins) **Product origin assessment**
	Quality assurance (QA) & Quality control (QC) (rarely proves the origin)	+ Performance test (chemical, physical) + Dimensioning, microstructures + Purity, concentration **Product analysis (quantitative, statistical)**
Proof of transaction	Inspection, check & monitoring	+ Sample analysis (single parameter) + Automated non-penetrative analysis + Hand-held non-penetrative analysis + Visual inspection Quick product examination (qualitative)
	Chain of custody (CoC) systems (what, when, where, how, by whom?)	+ audit/inspection of ID + GPS tracking + data-log analysis + data logging (e.g., blockchain) + automated ID validation **Product ID control**
Proof of intention (claim of origin)	Due diligence	+ Audit + Third party **Supply chain assessment**
	Code of Conduct	+ Tier "n" supplier + Tier 1 supplier **Supply chain policy**

Ability to prove the origin



Analysis of product (sample based)



Declaration of product (document based)

Table 2. A general overview of examples of traceability schemes and projects ranked according to their ability to prove the origin of the ore.

Proof level	Approach	Examples	
		Certification Schemes	Projects (commodity or technology)
Proof of origin	Geochemical fingerprinting & statistical validation	**CIP** (PGEs)	**CERA 4in1** (all) **Geoforensic Passport** (Au) **TRACE** (Co) **BATTRACE** (Co, Li, C)
	Quality assurance (QA) & Quality control (QC) (rarely proves the origin)	Various certification schemes (ISO 9001 series, AS9100)	
Proof of transaction	Inspection, check & monitoring	**Harmonization of Fertilizer Sampling and Methods of Analysis** (P) **Various guidelines & standards (e.g., ISO, AS)**	**X-MINE** (XRF, XRT, 3D/ Zn–Pb–Ag–Au, Cu–Au, Au)
	Chain of custody (CoC) systems (what, when, where, how, by whom?)	**Certificate of Origin and Packaging** **Chain of Custody Standard for Responsibly Mined Materials (IRMA)** **RJC Chain of Custody Certification** (Au, Ag, PGEs) **ASI Chain of Custody Standard** (Al)	**CSyARES** (REEs) **TraceMet** (Cu+Fe) **Minespider** (blockchain) **GS1 GDSN** (ID)
Proof of intention (claim of origin)	Due diligence	**Responsible Minerals Assurance Process (RMAP)** **OECD Due Diligence Guidance for Responsible Supply Chains of Minerals from Conflict-Affected and High-Risk Areas** **GS1 Global Traceability Compliance Criteria Standard** **Kimberley Process Certification Scheme (KPCS)** (diamonds) **Tin Supply Chain Initiative** (Sn)	**LMEpassport** (Al, Co, Pb, Ni, Sn, Zn) **GBA Battery Passport** (Co, Li)
	Code of conduct	**EU conflict Mineral Regulation** (Au, Sn, Ta, W) **Extractive Industries Transparency Initiative (EITI)** **German Due Diligence Law** **ASI Performance Standard** (Al)	

1.5 Geo-based traceability methodology

Mineral deposits are "born" with many geological and geochemical signatures. At different scales, these signatures can include the rock type (e.g., host rock, intrusion), ore structure, mineral assemblage (e.g., hydrothermal alteration), mineral texture, ore and gangue mineral chemistry (e.g., major, minor, and trace elements and their ratios), as well as the isotopic composition in ore and gangue minerals (e.g., present-day isotope ratios, isotope ages, and sources of magma, fluid, and ore materials) (Fig. 5a). All these pieces of information have been exclusively used by economic geologists and geochemists to understand the genesis and origin of mineral deposits (Deb & Sarkar 2017). Nevertheless, not all of them are important or, to be precise, equally important in identifying a specific deposit and tracing metals that derived from the deposit through their lifetime along the value chain. The main reasons are that most of the signatures might be variable across the deposit, and most of them are lost during mineral processing, metal refining and manufacturing (Fig. 5a). Even if a signature is constant and conservative, it might not be unique to the deposit when compared to others, especially those that are formed in similar geological conditions.

A simple, although not scientifically sound, analogy to understand this is the human body. Humans are born with many biological signatures, such as skin colour, hair colour, muscle density, blood type and so on. To identify a person, the most reliable evidence a biologist would want to collect is DNA. The reason is that DNA is, for one thing, almost the same in all tissues and cells. In comparison, other signatures such as skin colour might not be the same in different parts of the body. In other words, DNA is relatively more representative of a human body. For another, DNA remains largely constant throughout the entire lifetime of a human and is less susceptible and more resistant to variations in external conditions. Lastly, as is well known to all, DNA is unique to a specific human. All these three characteristics together enable DNA to be employed as a fingerprinting technique (Giardina 2013).

Following a similar logic to DNA fingerprinting as described above, a theoretical framework has been developed in the Nordic Sustainable Minerals project for searching for the "DNA" of a mineral deposit. This can be used to identify and trace the derivative minerals and metals, which is, in its essence, traceability. This framework sets out to investigate the geochemical and isotopic variability of a signature in both space and time (homogeneity), characterize and quantify potential changes in the signature along the value chain (conservativity), and determine whether the signature is unique among global counterparts (uniqueness) (Fig. 5b).

We name this geochemically and isotopically based fingerprinting technique "geo-fingerprinting". Ideally, geo-fingerprinting can be utilised for two purposes, i.e., for differentiating a deposit of interest and tracing the derived minerals and metals downstream along the value chain, which is named "geo-certification", and for identifying the geographic origin of metals back upstream, which is named "geo-forensics".

For both purposes, holistic analyses of ore minerals (i.e., monazite in the case of rare earth deposits) and processed/devised materials (rare earth metals and Nd magnets, for instance) in terms of petrography, mineralogy, major, minor and trace elements, and isotopes are required (Fig. 5c).

We selected analytical methods based on the analytical instruments available at the Nordic geological surveys, considering the cost, processing time and accuracy of the methods (Fig. 4).

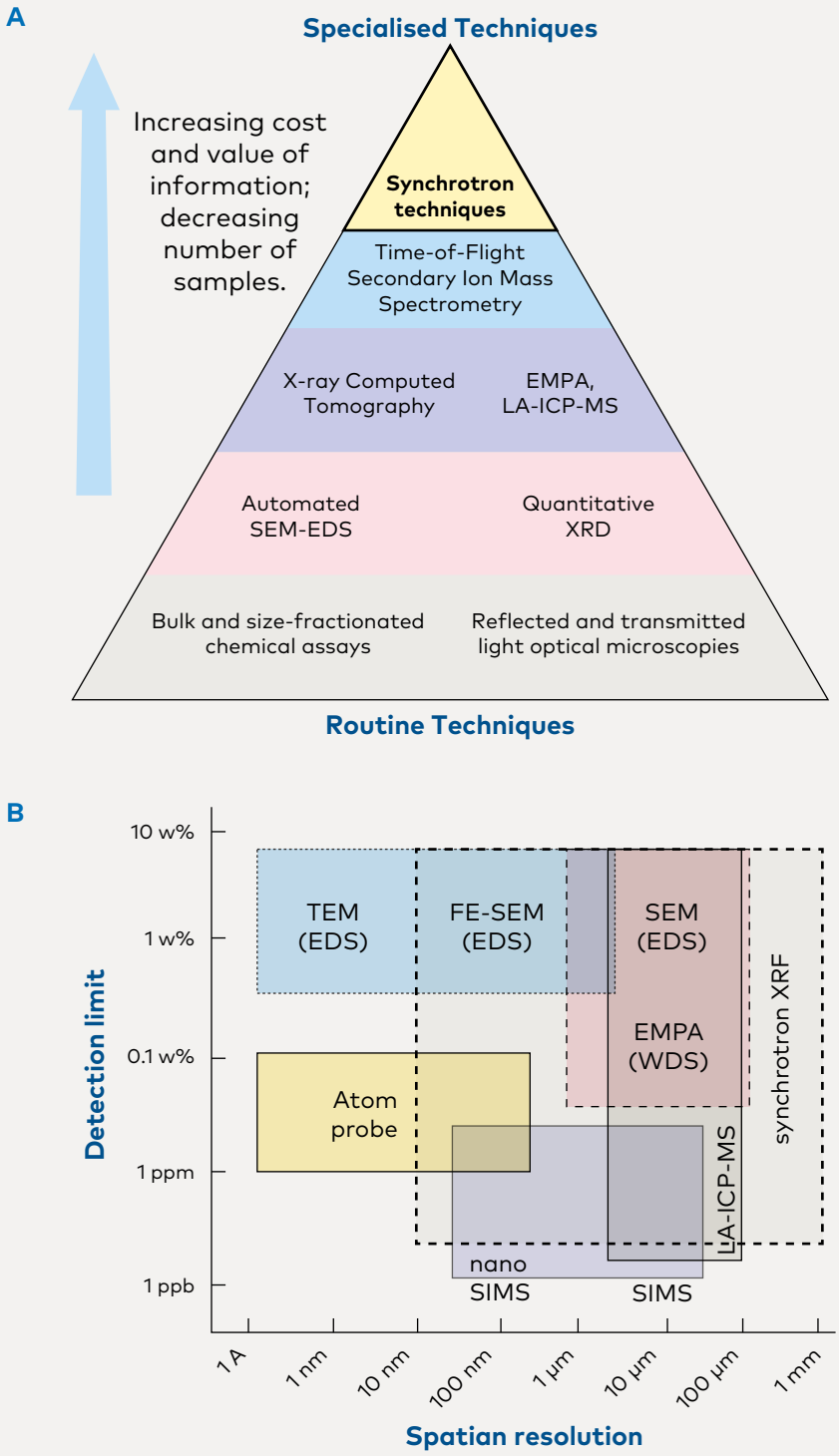


Figure 4. Geo-chemical analysis techniques ranked according to their cost and value information (a) and their spatial resolution and detection limit (b). Figures from von der Heyden et al. (2020), originally adapted, respectively, from Becker et al. (2016) and from Reich et al. (2017) and Stromberg et al. (2019).

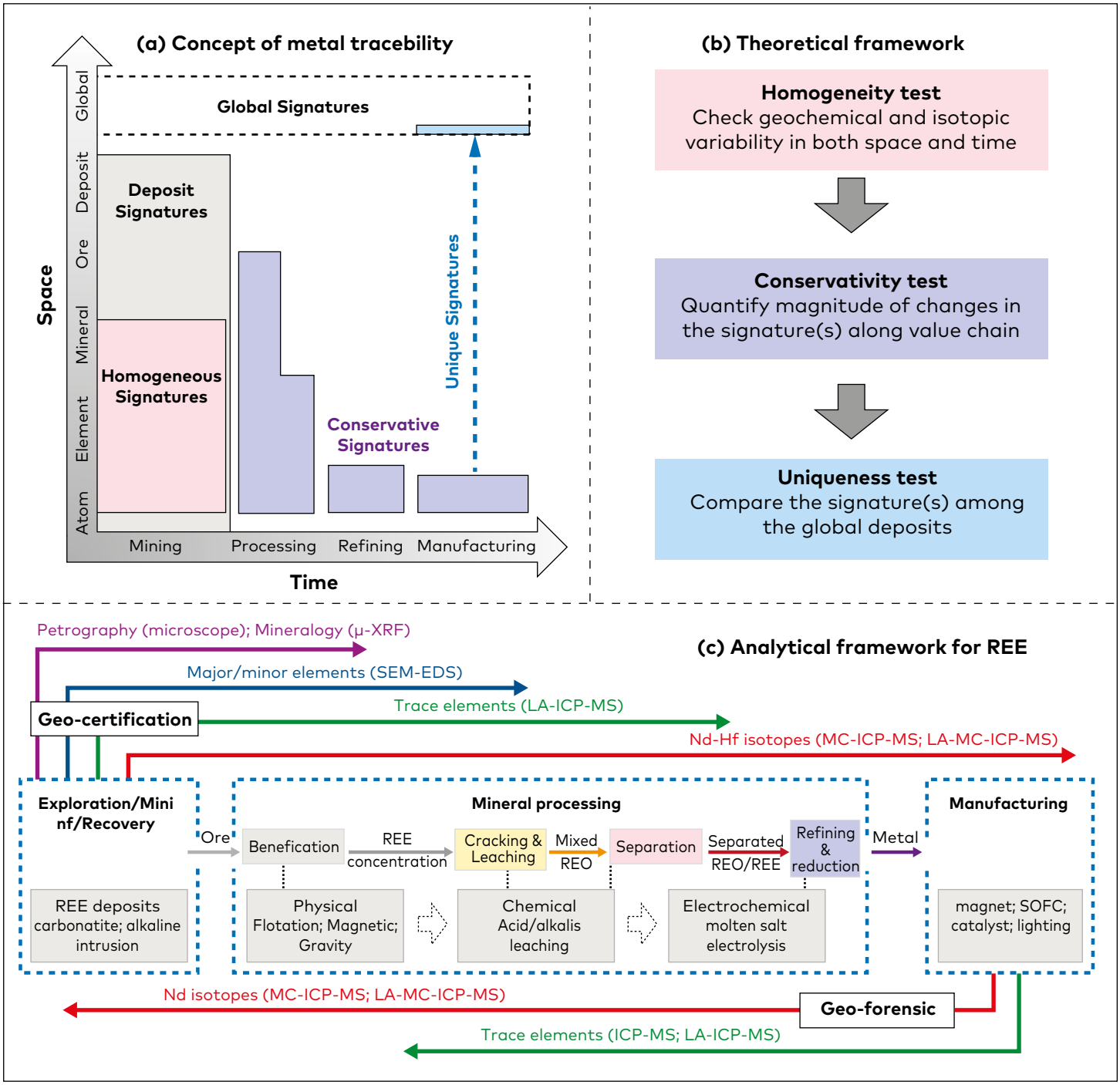


Figure 5. Schematic diagrams showing the general concept of metal traceability (a), a theoretical framework for performing the proof of concept (b), and an analytical framework for rare earth elements in the Nordic Sustainable Minerals project (c).

In (a), the time axis shows part of the lifetime of metals, starting from mining, which extracts ore minerals from a deposit, through mineral processing to concentrate ore minerals and refining to separate and purify the metal, to the use of the metal for manufacturing a part of a product. The space axis shows different scales that encompass a mineral deposit, from a single atom, an element (sub-nanometer, 10-9 m), through a mineral (microns to centimetres, 10-6 to 10-2 m), to an ore and deposit (centimetres to metres, 10-2 to 100 m). The boxes represent signatures existing in the materials at each stage of the value chain. Note that only a fraction of the total signatures might be homogeneous at (sub)mineral scales in a deposit. Furthermore, the number of signatures dramatically decreases as the ores and minerals undergo processing and refining. Ultimately, there might be even fewer signatures that can be used as a traceability signature when compared to other deposits globally. In (c), a part of the REE value chain is presented together with geological and geochemical signatures that can be obtained using various analytical instruments. μ-XRF: micro-beam X-ray fluorescence spectroscopy; SEM-EDS: scanning electron microscopy–energy dispersive spectroscopy; LA-MC-ICP-MS: laser ablation–multicollector–inductively coupled plasma–mass spectrometry.

2. Main results

2.1 NSM REE traceability methodology

To test the concepts of geo-certification and geo-forensics, we designed a methodological setup based on the analytical expertise hosted by the Nordic geological surveys and tested the methodologies on Nordic REE ore concentrates and Nd magnets.

The geo-certification methodology was applied to REE ore, as illustrated in detail in Figure 6. The geo-certification methodology consists of three tests for understanding the homogeneity, conservativity and uniqueness of the signatures. In the homogeneity test, the key component was the sampling strategy, which should maximize the spatial and temporal coverage to include samples from different alteration and mineralization zones, as well as different ore-forming stages. The ore minerals in the selected samples were then analysed for the mineral texture, assemblage and paragenetic sequence, as well as elemental and isotopic compositions. In the conservativity test, lab-scale experiments were conducted to produce mineral concentrates through a physical separation method, REE compounds through chemical leaching and individual Nd metal through molten salt electrolysis. Ideally, the flowsheet should be consecutive, starting with the same feed materials. However, due to the unavailability of large amounts of REE mineral concentrates (several tens of kilos) and the limited budget and time, the feed materials (eudialyte from Kringlerne) were only used until chemical purification. The feed materials for electrolysis were Nd oxides purchased online with an unknown origin. A detailed description of the materials used is provided in the following sections. Samples from each part of the flowsheet were obtained and analysed to evaluate the magnitude of change of the aforementioned geochemical signatures. In the uniqueness test, a geochemical database of REE deposits in the Nordic countries was constructed, which was used to evaluate whether the target geo-signatures were unique to the target deposit.

The geo-forensic pilot study was designed to investigate whether Nd magnets were chemically different and the likelihood of tracing them back to a potential geographic origin by using geo-fingerprinting.

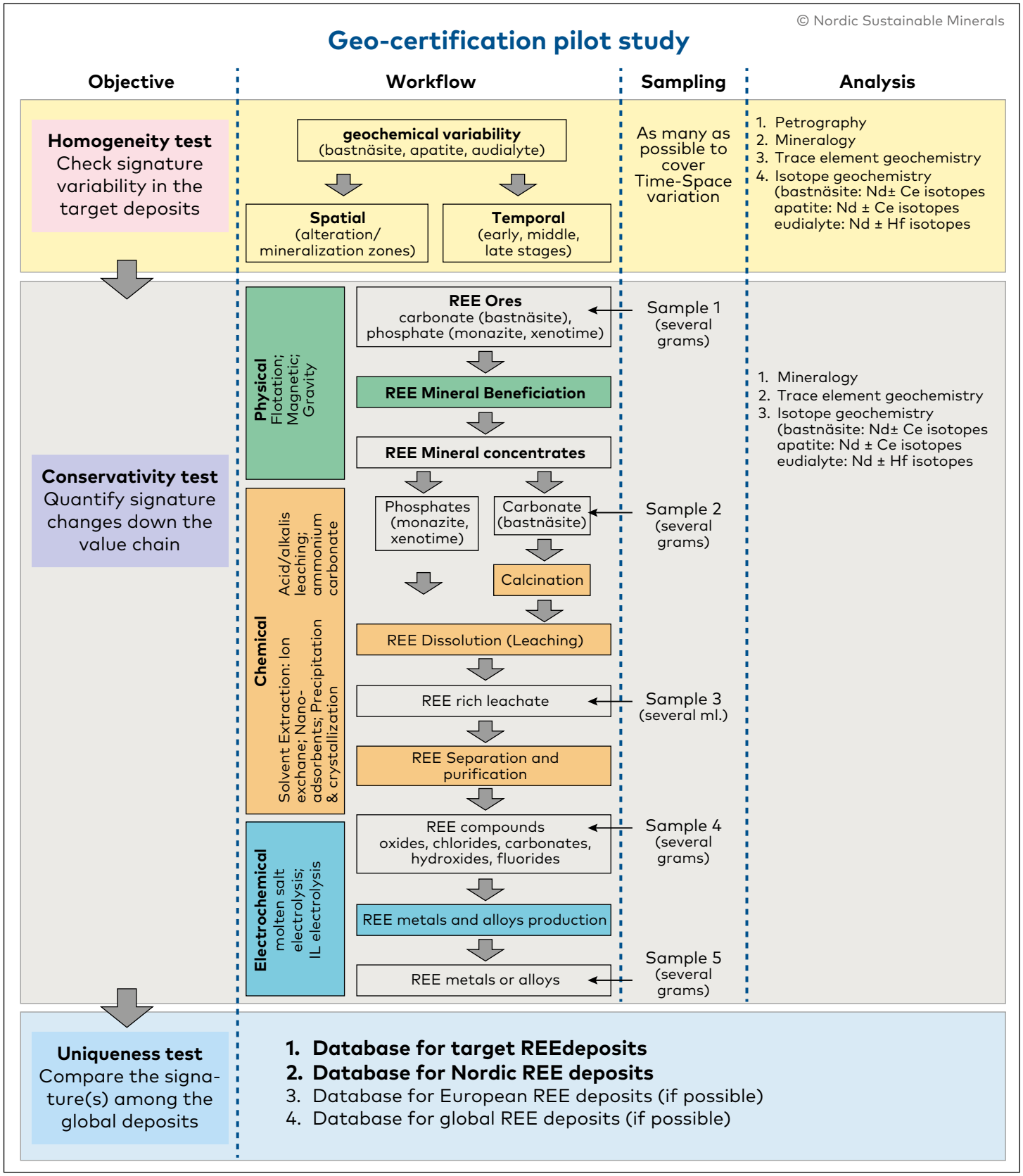


Figure 6. A diagram of the geo-certification methodology for the Nordic Sustainable Minerals project, illustrating the workflow for producing a lab-scale REE value chain, the sampling strategy and the analytical measurements in relation to the three traceability requirements. See the text for details.

Target material

In the geo-certification pilot study, four Nordic REE mineralisation targets were selected, including Kringlerne (Greenland), Norra Kärr (Sweden), Fen (Norway) and Sokli (Finland).

All four targets are mineral occurrences that have the potential for near-future REE mining. Kringlerne and Norra Kärr are magmatic REE deposits associated with alkaline intrusions, whereas Fen and Sokli are magmatic–hydrothermal REE deposits associated with carbonatite. These two types of deposits represent the major sources of REEs around the world (Liu et al. 2023). The main ore minerals are eudialyte for Kringlerne and Norra Kärr, monazite and bastnäsite for Fen and apatite for Sokli. The location and geology of the targets are described in detail in section 2.2.1.

In the geo-forensic pilot study, 61 neodymium magnets were tested. Known and unknown magnets were purchased, including Nd magnets with a known production year (1999 to 2023) and scrap Nd magnets without any information.

Overall, the NSM methodology covers traceability from mining to processing and magnet use, as illustrated in Figure 7, and it should be noted that the rest of the value chain currently lacks traceability.

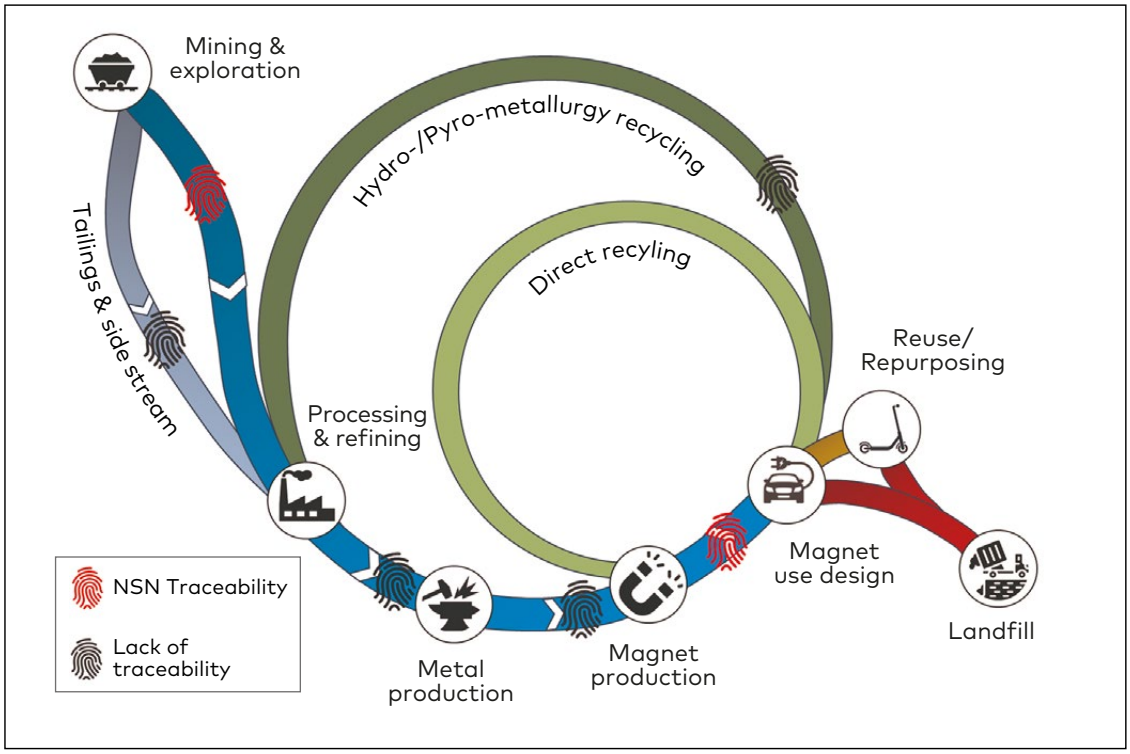


Figure 7. A schematic diagram showing the primary value chain (in blue) from mineral exploration to magnet use design, the secondary chain for tailings and side streams (in dark blue), the re-use/repurposing chain (in brown), the recycling chains (in green) and the waste chain (in red). In this project, the NSM traceability methodology (highlighted with red fingerprints) was applied at the mining stage (REE ore) and to finished magnets and scrap magnets.

2.2 Geo-fingerprinting pilot study: REE minerals

2.2.1 Homogeneity test

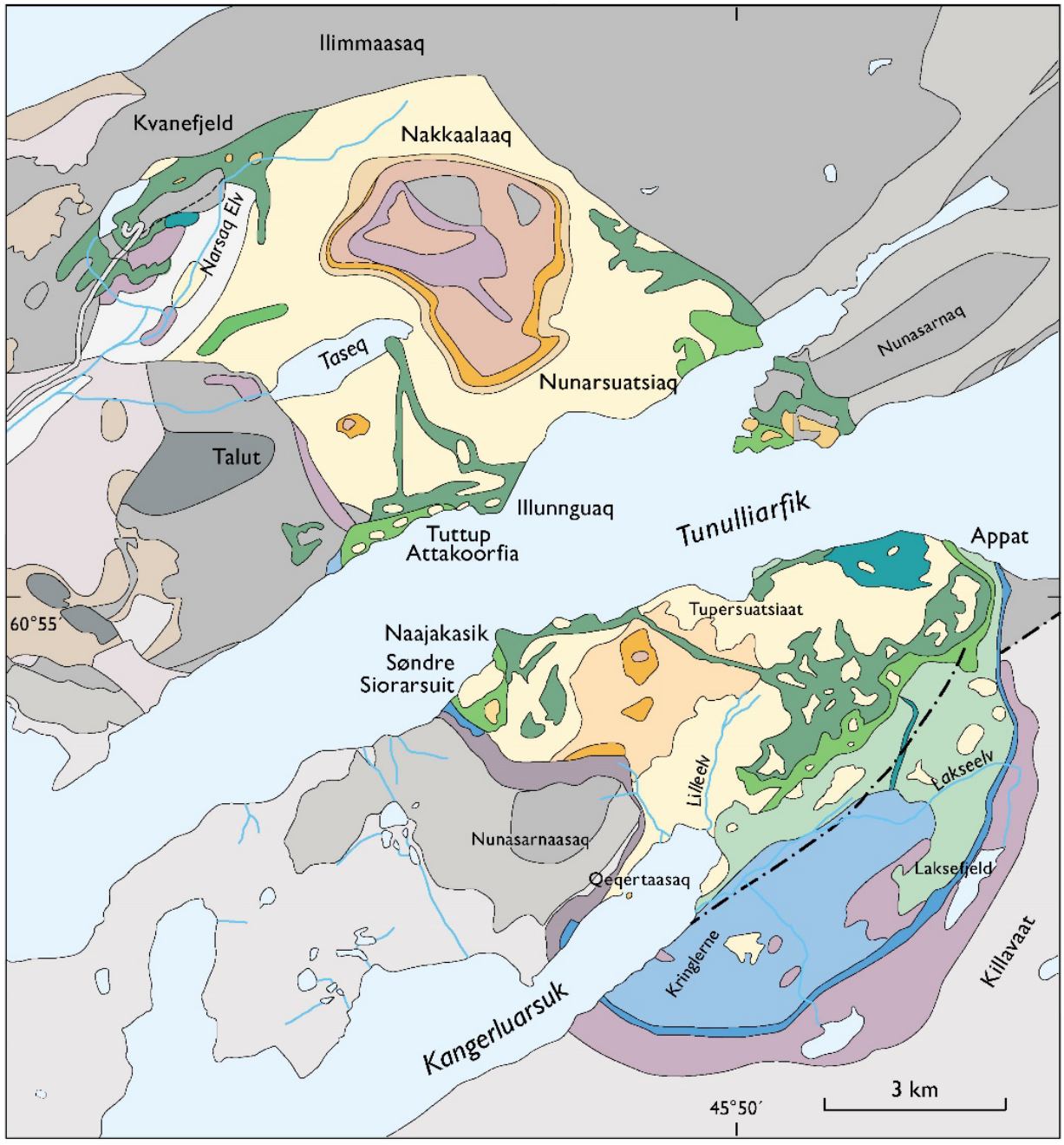
2.2.1.1 The Kringlerne (Killavaat Alunnguat) deposit, South Greenland

General geology

The Ilímaussaq Complex is an oval-shaped (17 km by 8 km) alkaline intrusive complex, which is a part of the Mesoproterozoic Gardar Province in South Greenland (Fig. 8). The Gardar Province is related to two rifting episodes between 1.3 and 1.1 Ga and consists of a volcanic-sedimentary sequence, dyke swarms and several alkaline to peralkaline central intrusive complexes (Upton 2013). The Ilímaussaq Complex has been dated repeatedly by single-crystal $^{40}Ar/^{39}Ar$ step heating of amphibole and yielded plateau ages of 1160 ± 5 Ma (Krumrei et al. 2006) and 1156 ± 1.4 Ma (Borst et al. 2019), and is part of the younger Gardar rifting episode.

Within the Ilímaussaq intrusion, the floor sequence of the agpaitic nepheline syenite, designated as kakortokite, represents an accumulation of the zirconium-rich mineral. The layered kakortokite (29 cyclic layers) contains repetitive banding of black, red and white layers in which the varying concentrations of the main constituents arfvedsonite, eudialyte and alkali feldspar result in the banded appearance (Bohse et al. 1971, Johnsen et al. 2001, Sørensen 2001, Pfaff et al. 2008). The red layers are composed of eudialyte, with lesser amounts of arfvedsonite, alkali feldspar and nepheline, whereas the white layers are composed of alkali feldspar and nepheline, with lesser amounts of arfvedsonite and eudialyte. The black layer is dominated by arfvedsonitic amphibole. Locally, sodalite occurs as a significant mineral phase, especially in the white and red kakortokite (Borst et al. 2018).

A total of 29 units have been distinguished, equivalent to a thickness of 212 m. Of these, 17 occur above and 11 below the reference unit and are labelled +1 to +17 and -1 to -11, respectively (Bohse et al. 1971). A subdivision of kakortokite above unit +17 into a rock series with inconspicuous layering and a transitional layered series was proposed by Bohse and Andersen (1981). This led to the following stratigraphy of the kakortokite (Bohse & Andersen 1981): 1. lower layered kakortokite (LLK), 210 m thick, followed by 2. slightly layered kakortokite (SLK), 35 m thick, and overlain by 3. transitional layered kakortokite (TLK) with a thickness of 40 m.



Gravel road

Quaternary
- Surficial deposits

Ilímaussaq intrusion
- Augite syenite
- Alkali granite and quartz syenite
- Pulaskite, foyaite

Agpatitic nepheline syenites
- Sodalite foyaite
- Naujaite
- Medium- to coarse-grained lujavrite
- Lujavrite transition zone
- Arfvedsonite lujavrite
- Aegirine lujavrite
- Kakortokite
- Marginal pegmatite

Other Gardar intrusions
- Narssaq syenite
- Narssaq alkali granite
- YGDC intrusive sheet

Eriksfjord Formation
- Lavas
- Sandstone

Ketilidian orogen
- Julianehåb batholith

Figure 8. A geological map of the Ilímaussaq Complex showing the location of the Kringlerne deposit to the south. From Upton (2013).

The texture of the kakortokite is idiomorphic granular with euhedral alkali feldspar laths (~1 cm in length), equant grains of eudialyte (~1 mm in diameter) and nepheline (~1 mm in diameter). Alkali feldspar constitutes between 30 and 50 vol.% of the rock. Nepheline is often square-shaped and generally rich in inclusions, especially of arfvedsonite. Arfvedsonite is the main interstitial mineral and can locally occur as oikocrysts enclosing eudialyte and nepheline chadacrysts. Sodalite is interstitial and constitutes a smaller part of the rock together with aegirine; the latter occurs as small laths and as a fibrous alteration product of arfvedsonite. Alkali feldspar shows perthite textures. A eudialyte-rich syenite occurs, which has fine-grained sacchoroidal textures generally 0.2–1 m thick. Besides eudialyte, this rock is composed of aegirine, analcime and a minor amount of coarse-grained microcline and/or nepheline (Schønwandt et al. 2023a, b).

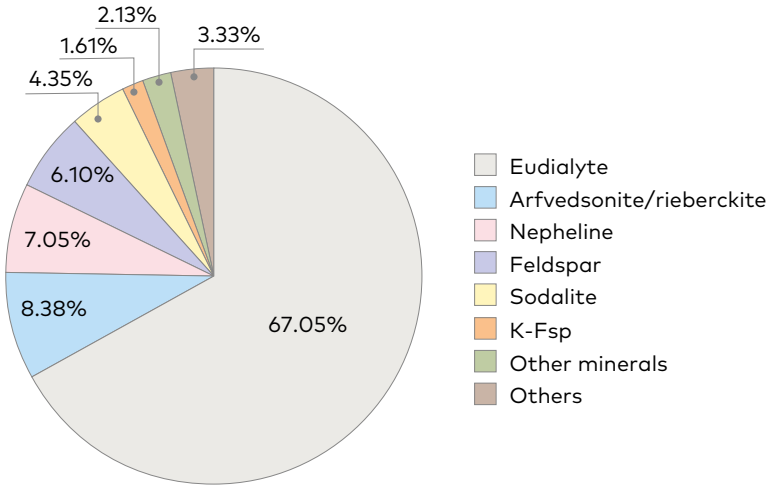


Figure 9. Composition of the eudialyte concentrate – EURARE project (Ma et al. 2019).

The red layers of the transitional layered kakortokite are formed by assimilation and metasomatism of naujaite autoliths detached from the naujaite roof. Several petrographic features (poikilitic texture, grain size, feldspar petrography and geochemistry of eudialyte and amphiboles) suggest that naujaite was the precursor of red layers A–D (Schønwandt et al. 2023a).

The mineral eudialyte is enriched in Zr–REE–Nb, and the red kakortokite layers are the main exploration targets for REEs. Until recently, TANBREEZ Mining Greenland A/S was the license holder of the concession, but in June 2024, the Critical Metals Corporation acquired a controlling role in the company [5]. Tanbreez estimated the resource to be not less than 4,300 Mt grading 0.65% REO, 1.9% ZrO2, 0.2% Nb2O5 and 0.025% Ta2O5 (Rosa et al. 2023), with HREEs (including Y) reported to comprise 27% of the REEs (Fig. 9). The deposit ranks as one of the world's largest REE deposits, and the project has been granted an exploitation license and may come into production in the near future if financing is secured and final permitting granted.

[5] https://ir.criticalmetalscorp.com/news-releases/news-release-details/critical-metals-corp-acquire-tanbreez-one-worlds-largest-known.

Pfaff et al. (2008) studied the chemical variation in eudialyte and amphibole through the kakortokite series and parts of the overlying lujavrites of the Ilimaussaq intrusion. Surprisingly little variation in chemical composition was found within the kakortokite. The slight change in chemical composition of the eudialyte solid solution towards kentbrooksite, indicated by an evolution from a Ca- and Fe-dominated composition to a composition slightly richer in Mn and REEs, is insignificant regarding practical magnetic processing of the Tanbreez ore (Schønwandt et al. 2016).

Geo-signatures and homogeneity

The two studies by Borst et al. (2016) and Borst et al. (2018) provided a thorough examination of the variability in the eudialyte group minerals (EGM) assemblage within the Kringlerne intrusion. Although the overall chemical variations are relatively subtle, they are distinct and reflect both primary magmatic differentiation and hydrothermal alteration. The work by Borst and coworkers revealed that the EGM crystals exhibit complex internal zoning patterns, including sector and oscillatory zoning within the crystal cores (Fig. 10). Their patterns reflect the magmatic history and processes within the intrusion linked to variations in temperature, pressure and magma composition.

Stratigraphic fractionation trends in EGM cores display a systematic decrease in elements such as Ca, Fe Ti, Nb and Cl, while elements such as Mn and REEs increase upwards through the layered sequence. This suggests a continuous differentiation process of a single agpaitic bulk melt in a closed magmatic system.

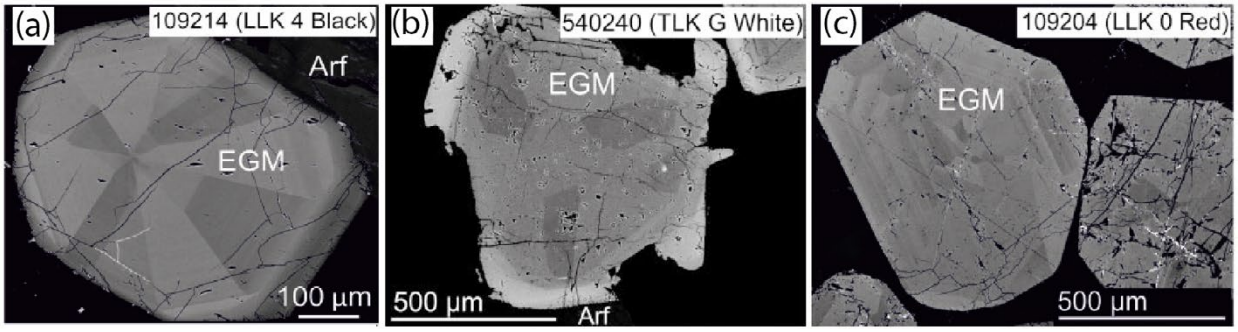


Figure 10. Backscattered electron (BSE) images of eudialyte studied by Borst et al. (2018) displaying various types of typical zonation in the ore mineral from the Kringlerne deposit. a) A sector-zoned eudialyte crystal with overgrowth at the rim of the crystal, sample from the black kakortokite sublayer; b) Subhedral eudialyte with a sector-zoned core, sample from the white kakortokite sublayer; c) Complex sector and oscillatory zonation, sample from the red kakortokite sublayer. Abbreviations: Arf = arfvedsonite, EGM = eudialyte group mineral. Figure modified from Borst et al. (2018).

Subhedral EGM overgrowths are compositionally distinct from the cores and show systematic variations across the stratigraphic sequence, which exceed overall the stratigraphic changes in the EGM cores. These overgrowths have been interpreted to represent *in situ* fractionation trends of intercumulus mush melts that have been somewhat isolated from the main bulk magma. Schønwandt et al. (2023a) suggested that the uppermost four eudialyte-rich horizons were strongly influenced by metasomatic processes caused by a mineral melt reaction and were not simply the result of conventional igneous magmatic cumulate formation, as has been inferred for the underlying kakortokite layered units. Recognition of a significant metasomatic process has an

important bearing on the distribution of minerals with specific elements, such as REEs in eudialyte, from both a petrological and an economic perspective.

A eudialyte concentrate was obtained from the Eurare project, which was provided by Tanbreez. A brief description of the concentrate production method is given in Appendix 1. This eudialyte concentrate sample was investigated with scanning electron microscopy (SEM)–automated quantitative minerology (AQM)/–energy dispersive spectroscopy (EDS) for its homogeneity. All the investigated grains were derived from the same sample, and inter-sample homogeneity was not therefore reinvestigated in this study.

The SEM-AQM and SEM-EDS analyses revealed that a major part of the studied sample is a Ce-poor (less than 1 wt% Ce) Ca-bearing eudialyte with a rather consistent eudialyte composition of 37% O, 25% Si, 12% Na, 10% Ca, 8%, Zr, 6% Fe, 1% Cl and ca. 0.05% Ce. It should be noted that our sample displayed lower Ce contents compared to literature data. The sample consisted of approximately 93% of this Ca eudialyte, with inclusions of 3% low-Ce eudialyte, 1% canasite/combeite, 1% rinkite, 0.5% sodalite, 0.2% kalsilite and 0.1% aegirine (Fig. 11). The internal homogeneity of the eudialyte grains is illustrated with a backscattered electron (BSE) image in Figure 12 and by element mapping of the major cations in the sample, Na, Ca, Zr and Si (Fig. 13). The grains are homogeneous for all these elements, as was also observed with BSE imaging (Fig. 12), without evidence of internal zonation (Fig. 10) or alteration rims, as described in the literature.

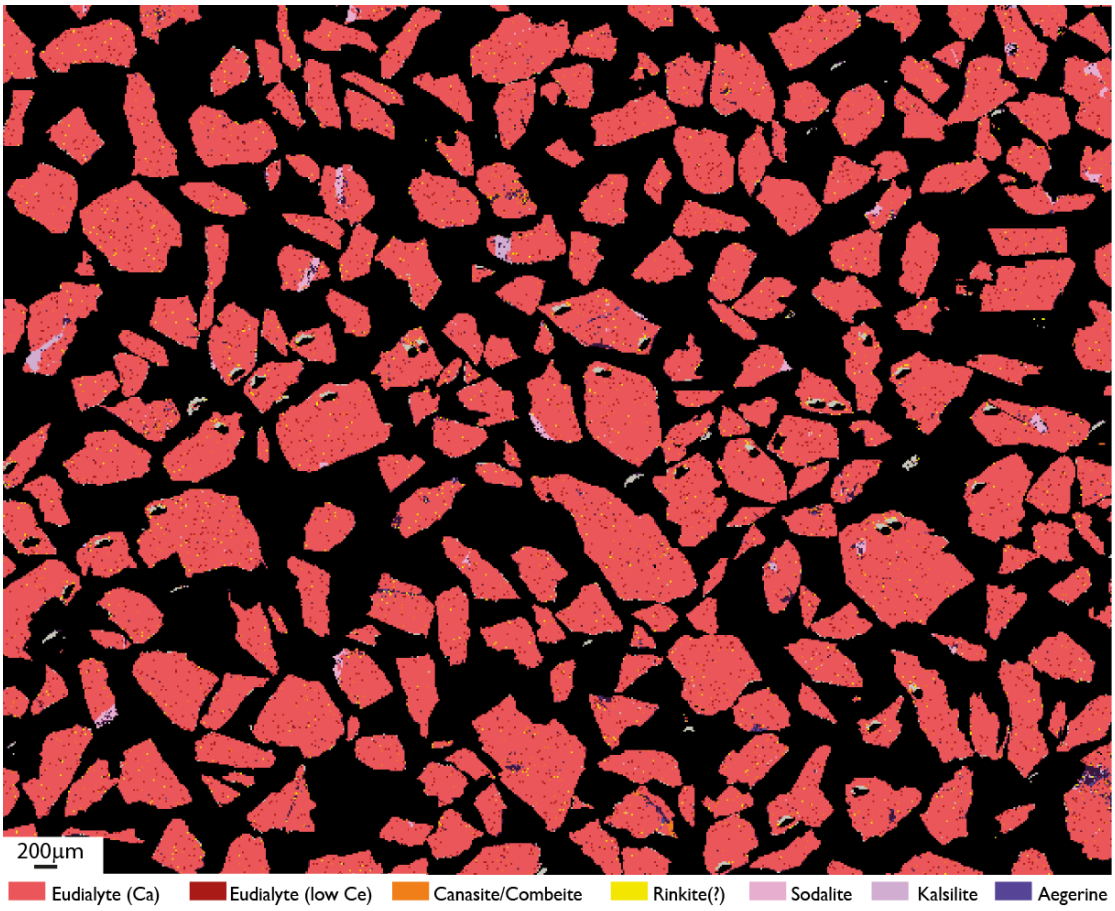


Figure 11. SEM-AQM mineral map of the Kringlerne eudialyte concentrate. 93% of the sample consists of Ca eudialyte.

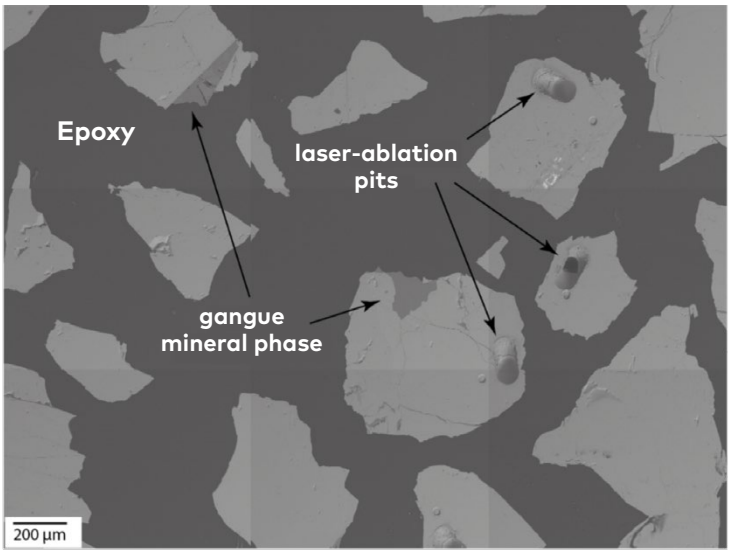


Figure 12. Backscattered electron (BSE) image of the studied eudialyte concentrate from Kringlerne (sample ID 202202193).

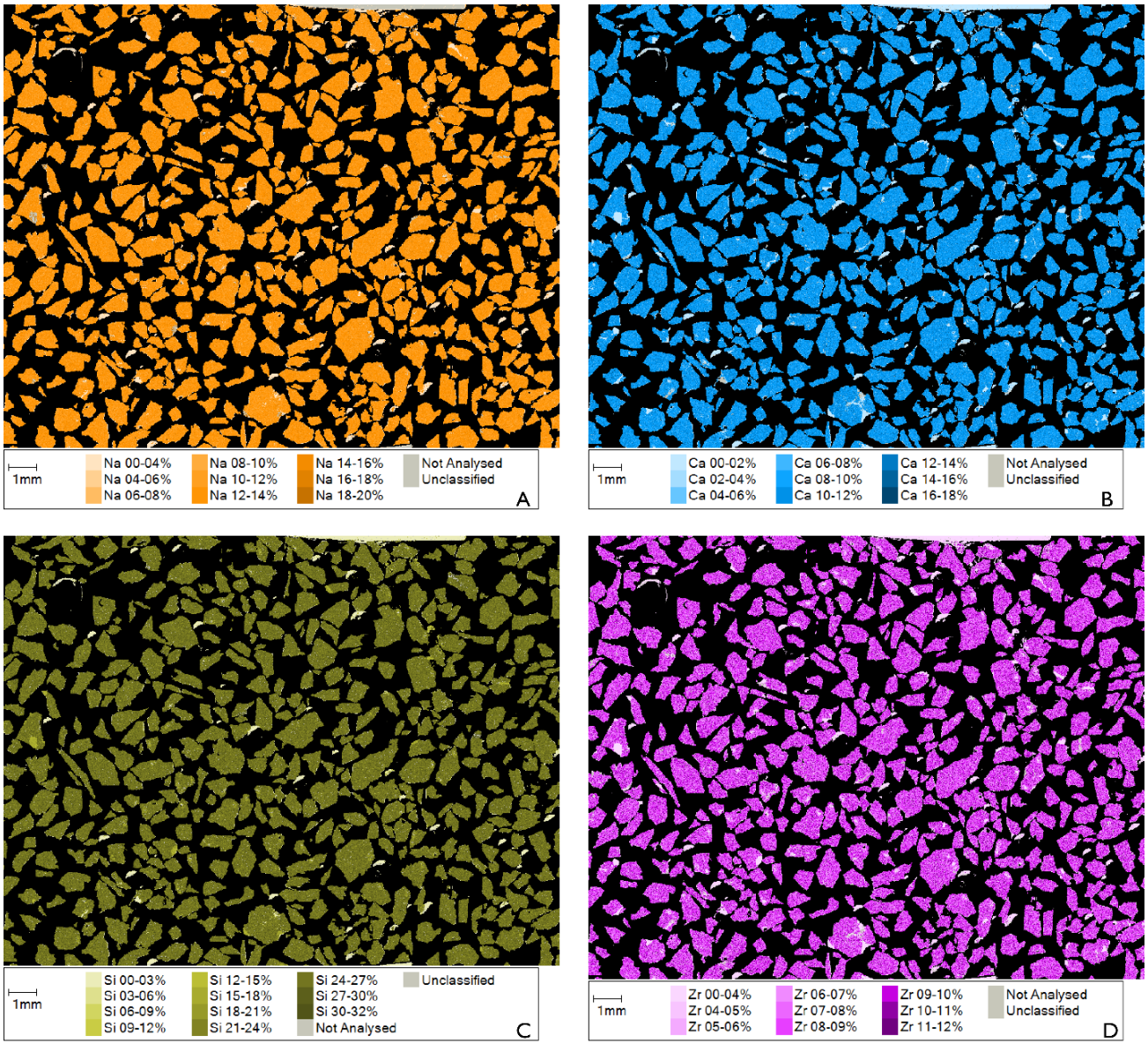


Figure 13. SEM-AQM element map of the Kringlerne eudialyte concentrate. Eudialyte grains are internally homogeneous for their major cations, a) Na, b) Ca, c) Si and d) Zr.

Complementary to the SEM analysis, trace elemental laser ablation inductively coupled plasma mass spectrometry (LA-ICP-MS) experiments were conducted on selected grains. The elements analysed included Li, Be, Mg, Al, Si, Ca, Sc, Ti, V, Mn, Fe, Zn, Ga, Rb, Sr, Y, Zr, Nb, Sn, Sb, La, Ce, Pr, Nd, Sm, Eu, Gd, Tb, Dy, Ho, Er, Tm, Yb, Lu, Hf, Ta, W, Pb, Th and U. Variation plots are presented compared to data available in the literature from the karkortokites. Although the chemical variation in the eudialyte grains can assigned to zoning and overgrowth, selected grains show differences, particularly in commonly investigated features such as the Eu* and Ce* contents. Figure 11 presents the mineral content variations in the analysis performed on grains from the mineral concentrate compared with literature data from Borst et al. (2018).

These subtle variations within sample grains may reflect the redistribution of HREEs compared to LREEs (e.g., Borst et al. 2018). For instance, Borst et al. (2018) described how the eudialyte group mineral overgrowths along the rims display a change in REE patterns. Figure 14 presents a summary of samples from Kringlerne, where positive and negative correlations could be associated with whether the analyses are conducted near the rim of the crystals.

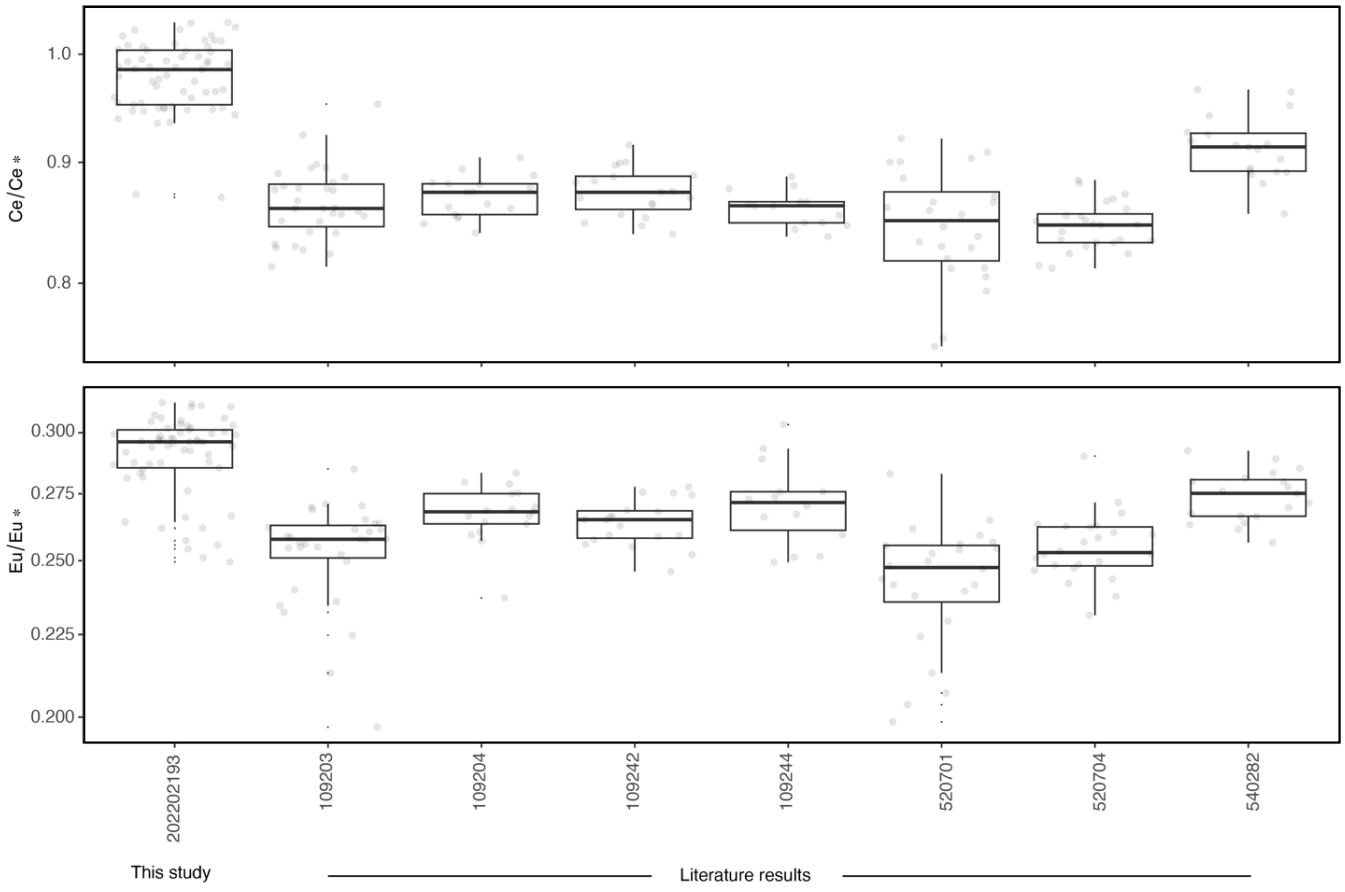


Figure 14. Boxplot showing a comparison between the mineral concentrate analysed and literature results from Kringlerne (Borst et al. 2018). Normalising values are the chondritic values of McDonough and Sun (1995), whereas the anomalies are calculated using the neighbouring elements, namely and , where the subscript N indicates normalisation to chondritic values.

The above observed variations can be used to further evaluate the formation of eudialyte in terms of the stratigraphic position in the layered sequence. Chemical variations in eudialyte have previously been observed (e.g., Pfaff et al. 2008) from the base of the lower layered kakortokites through the transitional layered kakortokites and the aegirine–lujavrite to the augen–lujavrite. The provided eudialyte grains have been plotted using the Ta_N/La_N, La_N/Sm_N and Gd_N/Lu_N ratios and compared with the results of Pfaff et al. (2008). The sample analysed here shows lower values overall for the Ta_N/La_N ratio, although with a small overlap, higher La_N/Sm_N ratios overall and scatter but higher Gd_N/Lu_N ratios, as illustrated in Figures 15, 16.

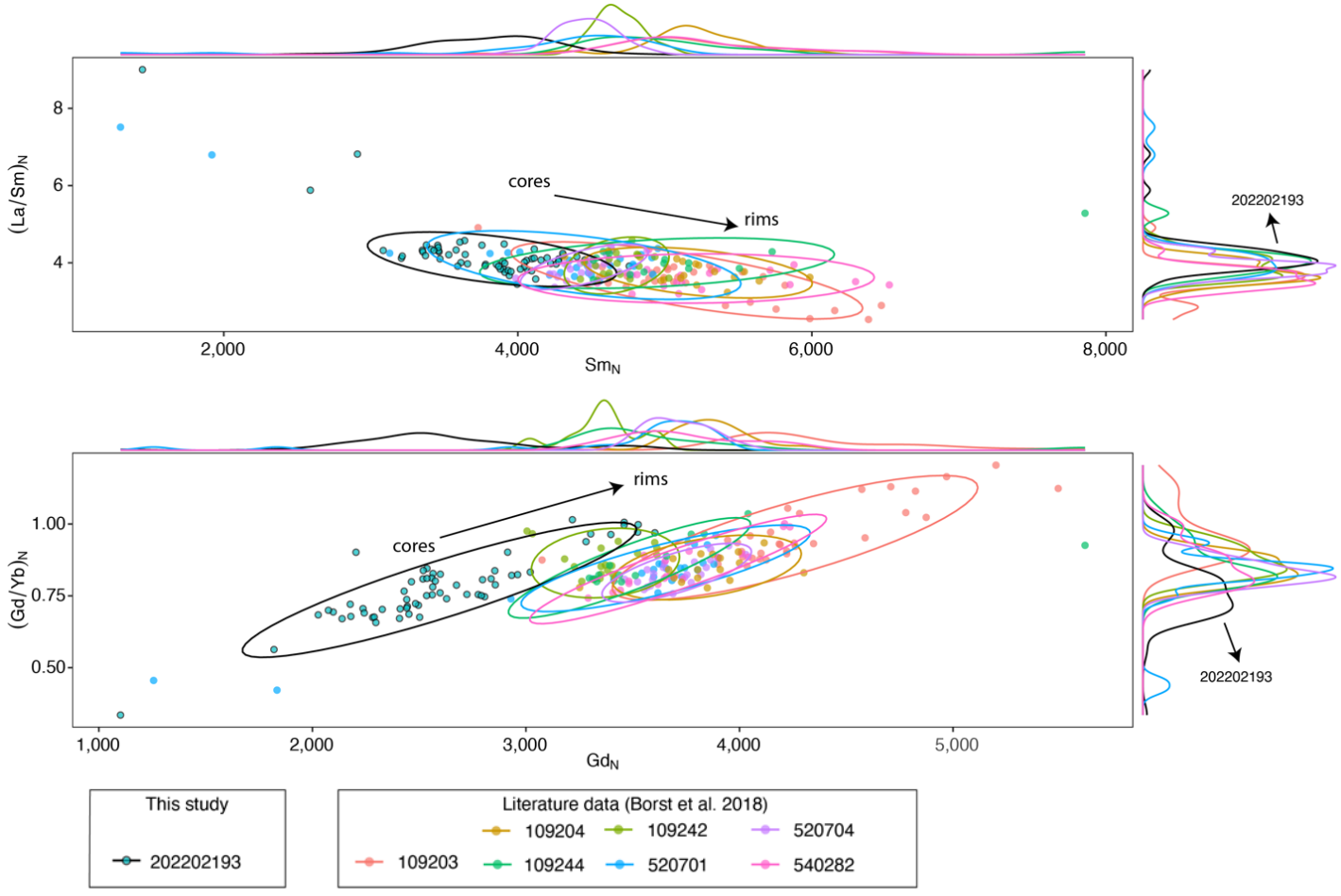


Figure 15. Rare element fractionation trends as suggested by Borst et al. (2018). Sample ID 202202193 also displays a positive and negative trend, possibly related to the position of the analysis during the laser ablation experiment. Density plots illustrate subtle variation in the and ratios. Normalising values are the chondritic values of McDonough and Sun (1995).

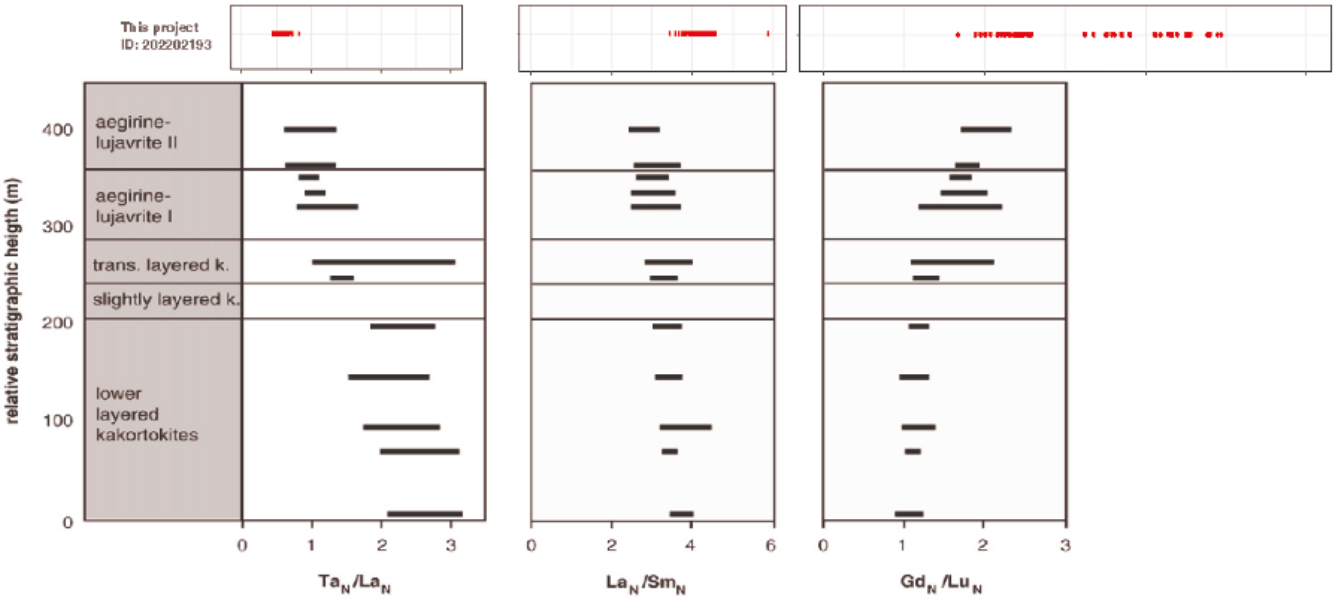


Figure 16. Variation in the ratios Ta_N/La_N, La_N/Sm_N and Gd_N/Lu_N through the kakortokite–lujavrite sequence compared to the data of Pfaff et al. (2008).

Sm and Nd isotopes for the eudialyte concentrate were acquired at the Geological Survey of Finland by laser ablation MC-ICP-MS. Results are presented in Figure 17. The present-day $^{143}Nd/^{144}Nd$ ratios were 0.511775 ± 14 (2σ). The initial $^{143}Nd/^{144}Nd$ ratio (denoted as εNd(i) as compared to the Chondrite Uniform Reservoir, CHUR) in published data for eudialyte has been reported with a considerable spread of values ranging from +0.4 to -5.7 (e.g., Borst et al. 2019). The regression line for the sample analysed in the pilot study provided an initial $^{143}Nd/^{144}Nd$ ratio of 0.51077 ± 0.00065, which is considerably lower than the published values determined using TIMS instrumentation (initial $^{143}Nd/^{144}Nd$ = 0.51110 ± 0.0002). Although inter-instrumental comparison can be difficult to account for, internal reproducibility can be achieved by repeating experiments using the laser ablation technique. Figure 17 presents the laser ablation data from a session acquiring Sm–Nd isotopic data. Epsilon values are compared with literature data for eudialyte from the lower layered kakortokites and other eudialyte localities. Furthermore, computed initial Nd isotopes have been plotted to examine the internal reproducibility.



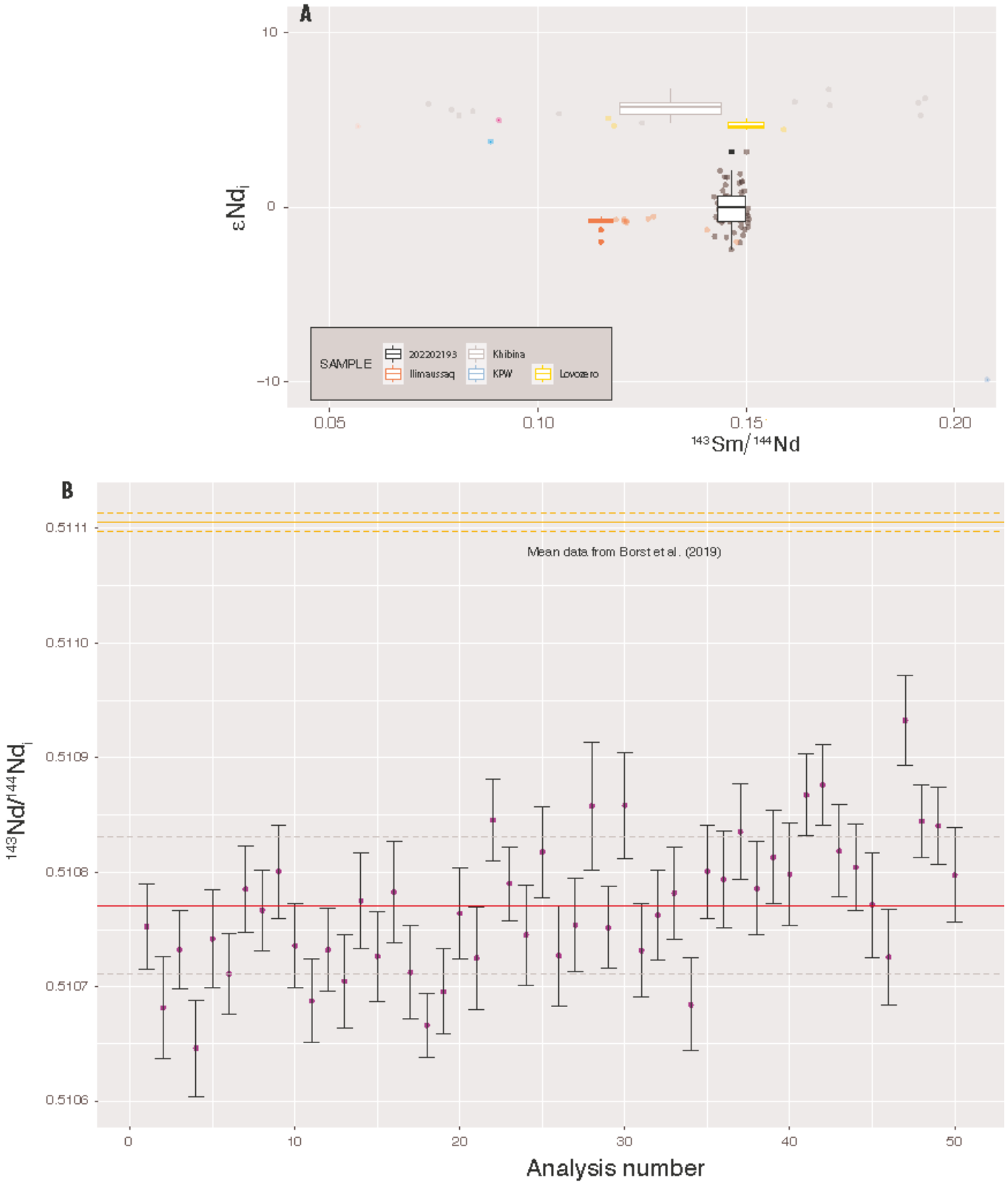


Figure 17. A) Initial εNd values compared to literature data for the layered kakortokites. Khibina and Lovozero have also been plotted for comparison. B) Reproducibility of analysis by laser ablation MC-ICP-MS. Mean data from Borst et al. (2019) are also presented to allow comparison between TIMS and laser data.

2.2.1.2 The Norra Kärr deposit, southern Sweden

General geology

The "exotic£ rocks occurring at Norra Kärr were originally discovered during regional bedrock mapping by the Geological Survey of Sweden and first described by Törnebohm in 1906. The Norra Kärr alkaline rocks occur in the form of a small, complex, zoned and deformed intrusion of agpaitic nepheline syenite rocks located east of Lake Vättern in southern Sweden (Fig. 18). Its crystallization age has been inferred as 1489 ± 8 Ma, and whole rock Rb/Sr age dating yielded an age of 1545 ± 61 Ma (e.g., Sjöqvist 2021, and references therein). The complex intruded into 1791 ± 8 Ma granite of the so-called Växjö type belonging to the Transscandinavian Igneous Belt (TIB) (e.g., Sjöqvist 2021, Högdahl et al. 2004). Significantly post-dating the primary crystallization of the alkaline complex, it was subjected to metamorphism and deformation that included folding and partial melting of the alkaline rocks due to the early effects of the Sveconorwegian orogeny, as shown by the dating of eudialyte growth in an undeformed pegmatoid vein at 1144 ± 53 Ma (e.g., Sjöqvist 2021, and references therein).

Four main rock types (note that these are generally historical "local" names and not IUGS approved) make up the Norra Kärr alkaline complex: grennaite, kaxtorpite, lakarpite and pulaskite. Their modal mineralogy is summarized in Table 3. As described, for example, by Sjöqvist et al. (2013b), grennaite is the main rock unit at Norra Kärr (earlier called catapleiite syenite; Törnebohm 1906) and is a mesocratic fine-grained nepheline syenite in which the major minerals are nepheline, microcline, albite, aegirine and variable catapleiite and eudialyte-group minerals (the latter are the main, economic REE hosts in the deposit). Of several varieties, a specific subtype of grennaite variably contains abundant pegmatitic or pegmatoid veins that are interpreted as having a migmatitic origin (e.g., Sjöqvist 2021, and references therein). This has been termed "PGT" or pegmatitic grennaite in the terminology of Tasman Metals and subsequent resource statements (e.g., Short et al. 2015, Bowell et al. 2021; cf. also Fig. 18 and Table 3), despite the fact that the veins are not true pegmatites, but rather are pegmatoid in nature. Other varieties are "migmatitic grennaite" and "catapleiite grennaite" (e.g., Sjöqvist et al 2013b; Table 3). During the exploration work, the pegmatitic or pegmatoid-bearing (PGT-type) grennaite was in turn subdivided into 7 subclasses or types based on the relative contents of pegmatoid material in them (5–10, 10–30, 30–50, 50–70, 70–90, >90%, and a recrystallized variety). However, the average PGT grennaite composition should be representative of the bulk composition of the overall PGT domain (Sjöqvist 2021). Kaxtorpite is a melanocratic nepheline syenite, which is foliated and folded and occurs in the central part of the complex. Lakarpite occurs in the northern part and is dominated by albite, arfvedsonite and nepheline, together with accessory minerals such as apatite, titanite and fluorite. Pulaskite is an alkali feldspar syenite with minor nepheline. Based on trace element geochemical data from these rocks, it was inferred that they are directly interrelated through magmatic evolution, as seen, for example, in similar Eu/Eu* values, increased Zr, Hf and Sn, and strong depletion of Pb, Sr, P, Ti, Cu, Sc and Ni (Sjöqvist 2021). The latter author suggested that the pegmatoid-bearing grennaite is the most evolved rock type in the complex, not least indicated by its high concentration of incompatible elements, including REEs, Zr and Hf, while the pulaskitic rocks were deemed as the most primitive and earliest crystallized.

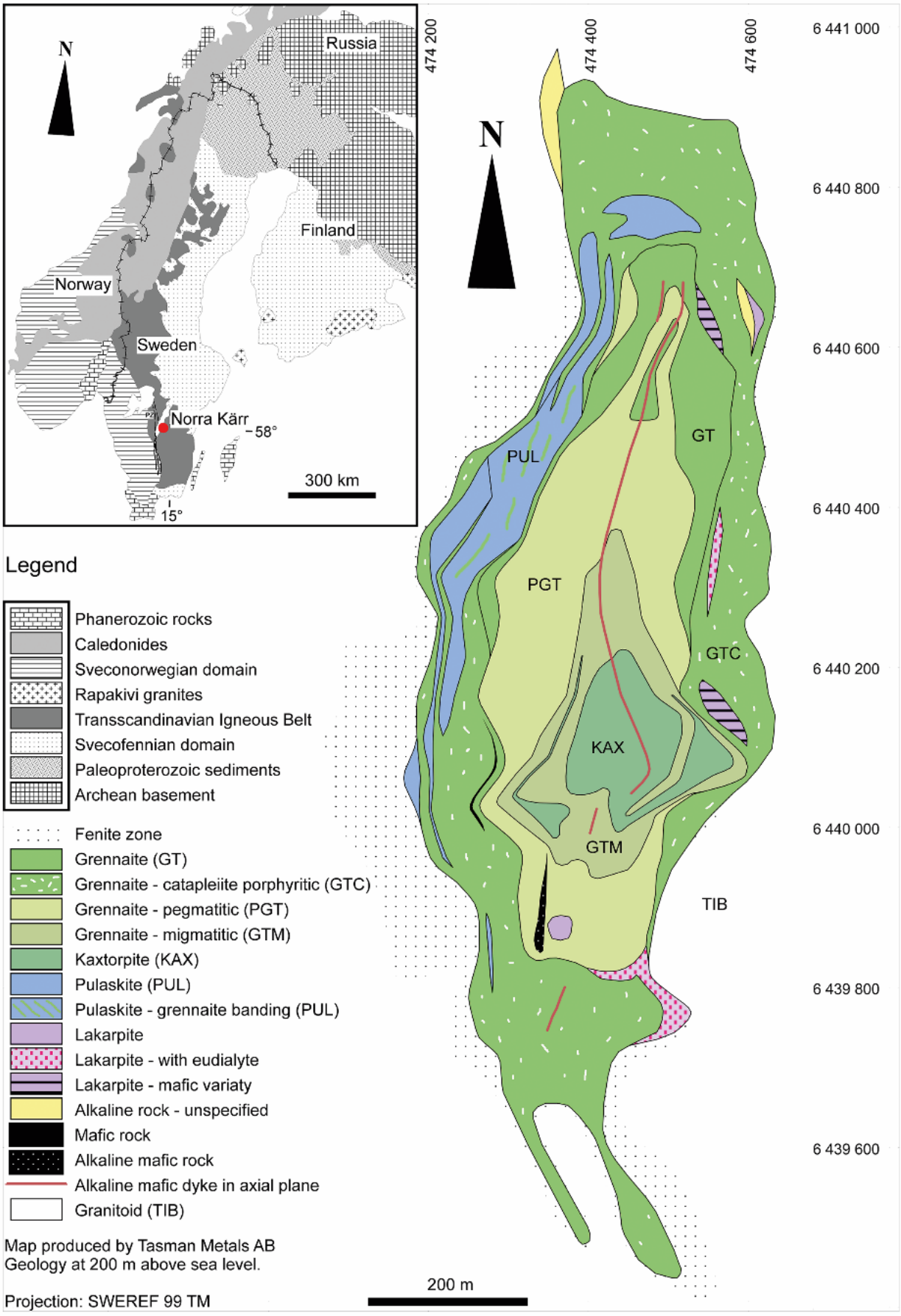


Figure 18. Geological map of Norra Kärr. (Source: Saxon et al. 2015)

The overall ore mineralogy of the Norra Kärr deposit is defined by the abundance of eudialyte-group minerals present in the host rock, combined with their specific TREO contents together with HREO/TREO ratios, despite the fact that eudialyte does not itself have any essential REEs in its ideal formula. As can be seen in resource statements (cf. below; the latest update is Bowell et al. 2021), the defined resource has quite good average contents at 0.5 wt% TREO, and HREO proportions are typically >50% of TREO. The eudialyte-group minerals are very complex and have a multitude of structural sites that can accommodate different cations as well as anions and anionic groups. The presently accepted generalized structural chemical formula for the eudialyte-group minerals is $N_{15}[M(1)]_6[M(2)]_3[M(3)][M(4)]Z_3(Si_{24}O_{72})O'_4X_2$, in which N = Na, Ca, K, Sr, REE, Ba, Mn, H_3O^+; M(1) = Ca, Mn, REE, Na, Sr, Fe; M(2) = Fe, Mn, Na, Zr, Ta, Ti, K, Ba, H_3O^+; M(3, 4) = Si, Nb, Ti, W, Na; Z = Zr, Ti, Nb; O′ = O, OH^-, H_2O, and X = H_2O, Cl^-, F^-, OH^-, CO_3^{2-}, SO_4^{2-}, SiO_4^{4-} (Johnsen et al. 2003). Thus, REEs can be hosted in two different positions, N and M(1), which may potentially lead to some fractionation effects, depending on the preferred site. Analytical characterization of the eudialyte-group minerals in the Norra Kärr complex was performed by Sjöqvist et al. (2013a), utilising electron beam energy-dispersive (SEM-EDS) and wavelength-dispersive (WDS-EMP) X-ray microanalysis, complemented by whole-rock analyses. Their whole-rock datasets clearly demonstrated that the pegmatoid-bearing grennaite (PGT) type had the highest overall REE contents and a high proportion of HREEs over TREEs, with a comparatively flat chondrite-normalised spider diagram pattern. Among the specific REEs, the span for Nd contents in the whole-rock dataset ranged between a low 87 ppm in a kaxtorpite to the highest, 1140 ppm Nd, in a pegmatoid-bearing grennaite, while Hf contents ranged from 16 ppm to a high 349 ppm Hf, also from a pegmatoid-bearing grennaite. From their mineral-chemical analyses, specifically those from WDS-EMP, Nd_2O_3 contents in the eudialytes ranged from below the detection limit to 1.38 wt%, while HfO_2 contents ranged from 0.19 to 0.37 wt%. Based on their entire mineral-chemical dataset, Sjöqvist et al. (2013a) could separate three distinct groups of eudialyte-group minerals in the Norra Kärr rocks: 1) an Fe-rich, REE-poor, pink eudialyte from the lakarpite, 2) an Fe–Mn-bisected, HREE-rich eudialyte from "pegmatitic" grennaite, and 3) a Mn-rich, LREE-rich eudialyte from "migmatitic" grennaite. They could thus observe that, utilizing terminology based on eudialyte-group end members, there is an evolutionary trend at Norra Kärr, going from a true eudialyte, via a Ca-poor Fe–Mn-bearing eudialyte–ferrokentbrooksite, to a Ca-poor eudialyte–kentbrooksite. Of the groups, the most relevant one from an economic (REE mining) perspective is the HREE-rich one from the pegmatitic or pegmatoid-bearing grennaite (PGT). Overall, based on Sjöqvist et al. (2013a, b), there appears to be relatively sparse alteration of the eudialyte-group minerals, particularly so in the coarsest types hosted by the pegmatoid-bearing grennaite.

Mining and ESG aspect

Norra Kärr is one of the contentious mine projects identified in Sweden by Fjellborg et al. (2022). It is also found as a dispute case within the Environmental Justice Atlas[6] (EJAtlas; Temper et al. 2015). It has been opposed by the local community and environmental non-governmental organizations (ENGOs) because of a fear of environmental impacts of a mine on Lake Vättern. The Norra Kärr-Motala Bay movement was formed in opposition to mining projects in the region. According to Fjellborg et al. (2022), a high activity period was from 2009 to 2019, involving civil disobedience by anarchists (Colonies Network). The movement is supported by NGOs, as well as left and Green parties. As second homeowners along the lake shore are involved, the dispute can be referred to as typical trans-local resistance of the "not in my leisure area" (NIMLA) type, which is a common phenomenon in Finland (Eerola 2022). The municipalities have also been against the project. There has been demand for more local influence for municipalities and landowners. The movement has faced internal controversy regarding the mode of action, i.e., non-confrontational vs. direct action, and according to Fjellborg et al. (2022), its future has been uncertain, but the resistance is still active (Fjellborg pers. comm. 2023). However, it seems that the whole Swedish mining-skeptical movement is losing its impetus (K. Lax, pers. comm. 2023).

Ore minerals and primary host rocks

In summary, the ore mineralogy of the Norra Kärr deposit is entirely based on eudialyte-group minerals ("eudialytes", essentially eudialyte *sensu stricto* – kentbrooksite – ferrokentbrooksite; Sjöqvist et al. 2013a), and specifically the particular chemical types in the different parts of the delineated ore zone that makes up the present resource (cf. Bowell et al. 2021). It is apparent that the chemical variability of Norra Kärr eudialytes depends on variation in local chemistry, which is in part primary magmatic, but also reflects the migmatisation of the complex, a process that significantly post-dates primary crystallization and led to the crystallization of at least the pegmatoid "ore" eudialytes (e.g., Sjöqvist 2021). According to Sjöqvist et al. (2013a, b), eudialyte-group minerals at Norra Kärr can be divided into three types: A) an Fe-rich, REE-poor, pink eudialyte, B) an Fe–Mn, HREE-rich eudialyte from pegmatitic grennaite and C) a Mn-rich, LREE-rich eudialyte from migmatitic grennaite. The eudialyte-group minerals at Norra Kärr display a trend from low to high Mn/(Fe+Mn) ratios with a corresponding increase in the absolute and relative LREE content. This trend was interpreted by Sjöqvist et al. (2013a) to be a result of magmatic evolution based on the increasing Mn/(Fe+Mn) ratio, while the εHf signature of the Norra Kärr rocks implies a non-crustal source for this complex. However, the eudialyte-group minerals that form the pegmatitic or pegmatoid-bearing grennaite type of "ore" at Norra Kärr, dated at ca. 1.14 Ga, are essentially interpreted as formed through later migmatisation of the complex through effects of the Sveconorwegian orogeny, and their formation post-dates primary crystallization by some
350 Ma (e.g., Sjöqvist 2021). Hence, they are relatively sparsely altered, as was reported by Sjöqvist et al. (2013a), and should be relatively easy to process using methods under development. This type of host rock and eudialyte-type is the one with the most favourable total REE contents, as well as the highest HREO/TREO ratios. Additionally, the relatively coarse general grain size, from millimetres to centimetres+, of this eudialyte-type makes it more amenable to separation prior to extractive chemistry.

[6] https://ejatlas.org/conflict/norra-karr-norra-karr-sweden-mining-conflict

Geo-signatures and homogeneity

Modal mineralogy studies on the different grennaite domains (Table 3) have demonstrated that the highest eudialyte (*sensu lato*) concentrations are in the pegmatitic or pegmatoid-bearing type of grennaite, which is closely correlated with what has been described above and with previously reported analytical data, specifically the whole-rock geochemistry data of Sjöqvist et al (2013a). However, it should be noted that the absolutely best REE "ore grades" (i.e., highest TREO and highest HREO/TREO) of eudialyte depend on its type and chemistry, as also noted above. Yet, they characteristically seem to be primarily hosted by the pegmatitic or pegmatoid-bearing grennaite (PGT).

Table 3. Major and accessory minerals in the different types of grennaite rock from mineral liberation analysis (MLA) (source: Leading Edge Materials; cf. also Sjöqvist et al. 2013b)

Mineral	Pegmatitic grennaite (%)	Migmatitic grennaite (%)	Catapleiite grennaite (%)
Eudialyte (*s.l.*)	7.8	6.7	4.2
Catapleiite	3.8	2.4	3.1
Microcline	15.7	18.1	14.8
Albite	17.6	19.9	28.2
Aegirine	22.2	20.4	16.5
Nepheline	30.7	28.6	31.8
Plagioclase	0.7	1.5	0.6
Alkali–Amphibole	0.53	1.31	0.8
REE–Y–Accessories	0.10	0.12	
PF–Accessories	0.09	0.08	
Fe–Ti–Ca–Accessories	0.05	0.05	
Zircon	0.03	0.06	



According to the latest inferred mineral resource statement (Bowell et al. 2021), at Norra Kärr, a resource of 110 Mt @ 0.5% TREO, 1.7% ZrO_2 and 0.05% Nb_2O_5 is reported. Light REO as a proportion of total REO is 0.48%, and for the heavy REO is 0.52%. There are two historical trenches in the Norra Kärr complex, the so-called north trench and south trench, originally excavated by the Boliden company (cf. Sjöqvist et al. 2013b). Recent sampling and analysis of samples from the trenches have revealed 1.92% zirconium oxide and 0.37% TREO in the north trench and 1.51% ZrO_2 and 0.50% TREO in the south trench (Bowell et al. 2021).

Notably, the only presently defined Hf resource within the Fennoscandian Shield is the Norra Kärr deposit. Short et al. (2015) reported 23.57 Mt of ore at a grade of 0.0286% Hf. Surprisingly however, Hf was not included in the later overall resource (Bowell et al. 2021).

Polished sections of seven rock samples were prepared and analysed for trace elements in eudialyte. These samples belong to PGT, GTC and a late eudialyte-rich pegmatitic vein. Results are presented in Figure 19. In addition to the major elements Na, Ca, Mn, Fe, Y, and Zr, many elements occurred at appreciable contents (>1 ppm), and surprisingly, most of them were quite homogeneous between sample types, as seen from the relative standard deviation (RSD) of a group of analyses. These elements include Cu (RSD: 0.06), REEs (RSD: 0.09-0.32), Mg (RSD: 0.22), P (RSD: 0.13), Sc (RSD: 0.16), Zn (RSD: 0.34), Ge (RSD: 0.26), Sr (RSD: 0.25), Nb (RSD: 0.38), Sn (RSD: 0.31) and Ba (RSD: 0.36). Less homogeneous elements include Al Cu (RSD: 0.59), K Cu (RSD: 1.15), Ti (RSD: 0.43), Ga (RSD: 0.59), Ta (RSD: 0.54), W (RSD: 0.57), Pb (RSD: 0.39), Th (RSD: 0.49) and U (RSD: 0.47).

Some element ratios display homogeneity better than other ratios. It is observed that Nb shows a roughly positive correlation with Ta (Ta/Nb ratio 0.06 ± 0.02), W (W/Nb ratio 0.04 ± 0.02) and La (La/Nb ratio 1.56 ± 0.55) (Figs 20a, b, c), while Nd shows a very good linear correlation with Pr (Pr/Nd ratio 0.21 ± 0.02) and Sm (0.32 ± 0.04). Interestingly, Nd displays a positive correlation with La, Ce and Pr, whereas the correlation gradually becomes a negative one with Lu and Y (Figs 20d, e, f). The slight fractionation in REEs might indicate changes in the source of materials, which is worth further attention with respect to heterogeneity in the material source and mineralization process.

Solution analyses of two grounded wet ores by Neoma MS/MS MC-ICP-MS yielded $^{143}Nd/^{144}Nd$ ratios of 0.512237 ± 5 (2σ) and 0.512235 ± 5 (2σ). Sm–Nd isotope analyses with a laser ablation Neoma MS/MS MC-ICP-MS revealed that the Norra Kärr eudialyte has a very consistent $^{143}Nd/^{144}Nd$ ratio of 0.512950 ± 0.000210 (1σ, n = 18, RSD = 0.0004), corresponding to present-day εNd values of 6.1 ± 4.1. Our result is slightly higher than that of Sjöqvist et al. (2020) (0.51242 ± 0.00010, 1σ, n = 6), determined by thermal ionization mass spectrometry (TIMS). The $^{147}Sm/^{144}Nd$ ratio revealed in this study was 0.2177 ± 0.0102 (1σ, n = 18), a little higher compared to 0.1666 ± 0.0148 (1σ, n = 6, Sjöqvist et al. 2020). It should be pointed out that the discrepancy might be due to the common offset between ICP-MS and TIMS, or due to poor tuning on the Neoma instrument, since it was installed only recently.

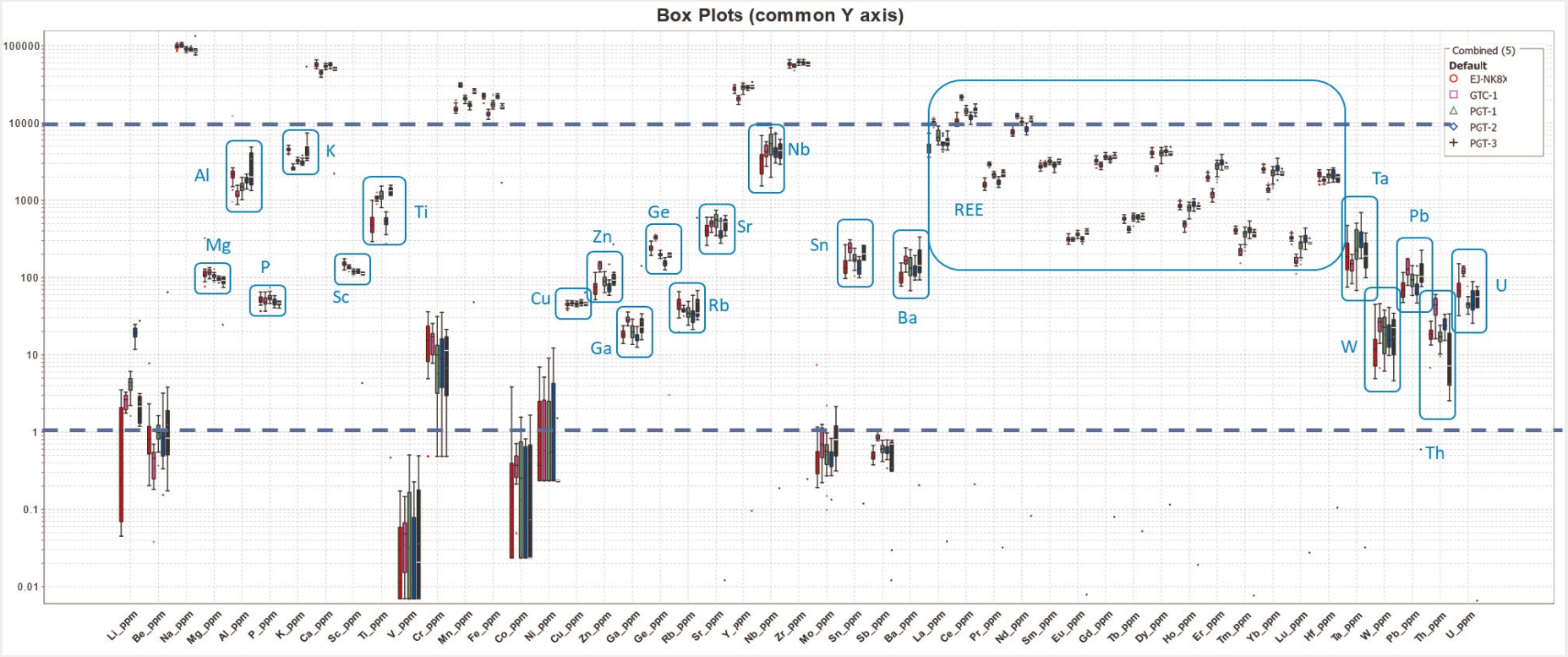


Figure 19. A box & whisker plot of all elements analysed by LA-ICP-MS. The x-axis and y-axis present the element and concentration in ppm, respectively. The colour of the box corresponds to the colour of the symbol in the legend.

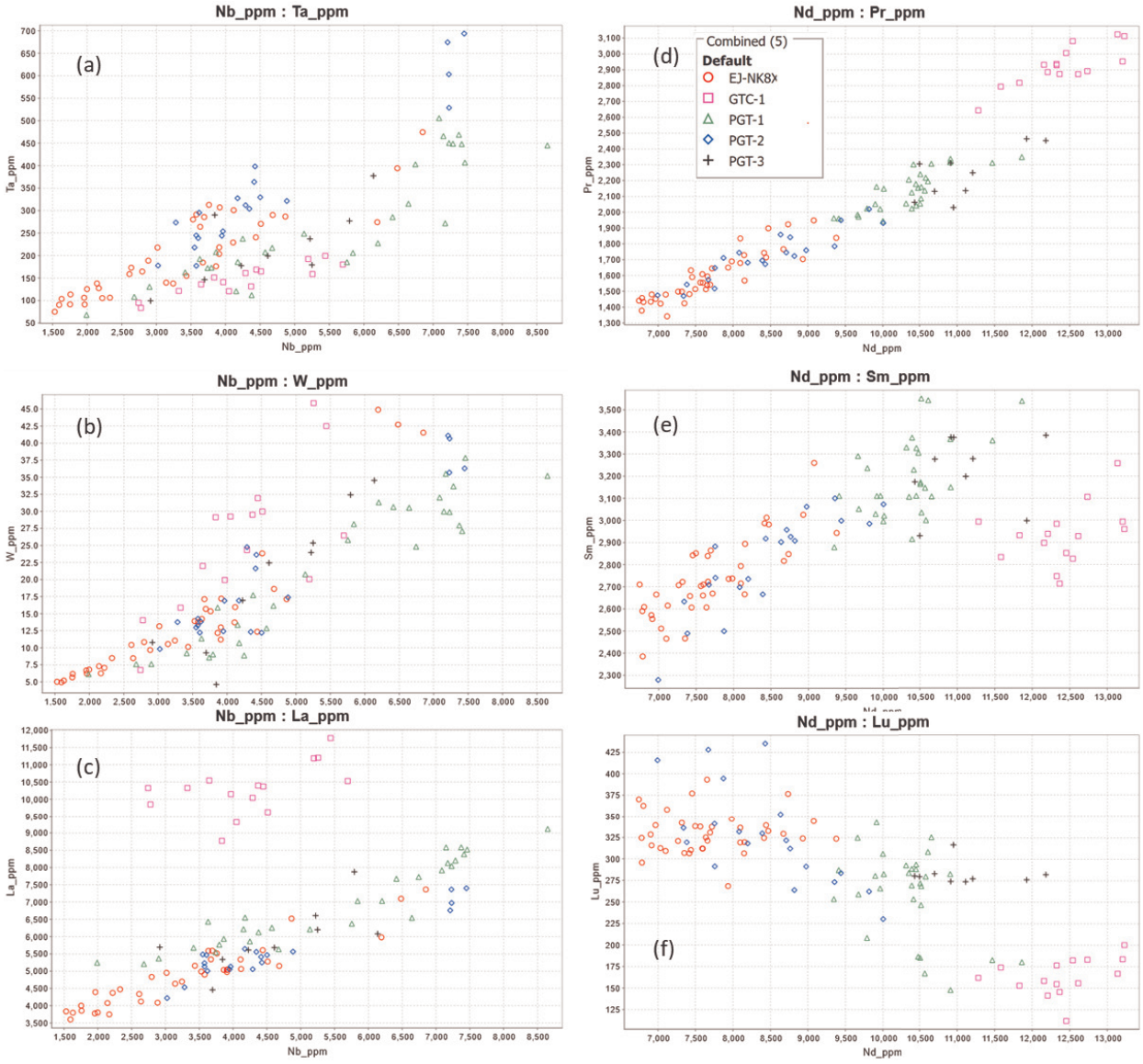


Figure 20. Selected homogeneous trace element bi-variate plots for eudialyte of the Norra Kärr deposit

2.2.1.3 The Fen deposit, Norway

General geology

The Fen alkaline and carbonatite complex, located in the municipality of Nome, SW Norway, is a significant REE deposit undergoing exploration by REE Minerals AS (CIM Inferred 95 Mt @1.28% TREO) and Rare Earths Norway AS (JORC-compliant inferred resources of 559 Mt of ore with an average grade of 1.57 wt% TREO (8.8 Mt TREO)[7]). Local community relations with Rare Earth Norway AS are reportedly positive (Watne 2023). The latter also collaborated with local authorities by delivering necessary input to their municipal master plan process.

The Fen Complex gained scientific prominence in 1921, when C. Broegger proposed a magmatic origin for carbonatite. Historically, the site was the object of various mining activities, notably the Fen iron mines (1657–1927) and the Soeve niobium mine (1953–1965).

[7] https://rareearthsnorway.com/europes-largest-deposit-of-rare-earth-elements-discovered-at-fen-norway

The Fen carbonatite complex (Fig. 21) is a deep-seated subvertical volcanic pipe emplaced around 580 Ma into older 1190 Ma Telemark gneisses (Dahlgren et al. 1990, Sæther 1957). Subsequent erosion exposed the 2–3-km-deep volcanic root system. The first magmatic activity is represented by alkaline rocks (ijolite–melteigite series), a calcite carbonatite (søvite) and a dolomite carbonatite (rauhaugite I) (Bergstøl & Svinndal 1960, Andersen 1988). At this point, large amounts of fluids were released, leading to the fenitisation of the host rock (Fig. 21) (Brøgger 1921, Andersen 1989, Elliott et al. 2018). Later, magmatism resumed with the emplacement of an iron–dolomite carbonatite (rauhaugite II or ferrocarbonatite) and the hematization of some of the units, forming the "rødberg", a calcite hematite rock (Andersen 1984). Ultramafic lamprophyre, called damtjernite, cuts across all units.

Geo-signatures and homogeneity

In this study, we focused on the REE-bearing iron–dolomite carbonatite (rauhaugite II). In Fen, LREEs (lanthanum to europium) are dominant, as opposed to alkaline complexes such as Norra Kärr in Sweden or Kringlerne in Greenland (sections 2.2.1.1 and 2.2.1.2), where HREEs constitute the main resource.

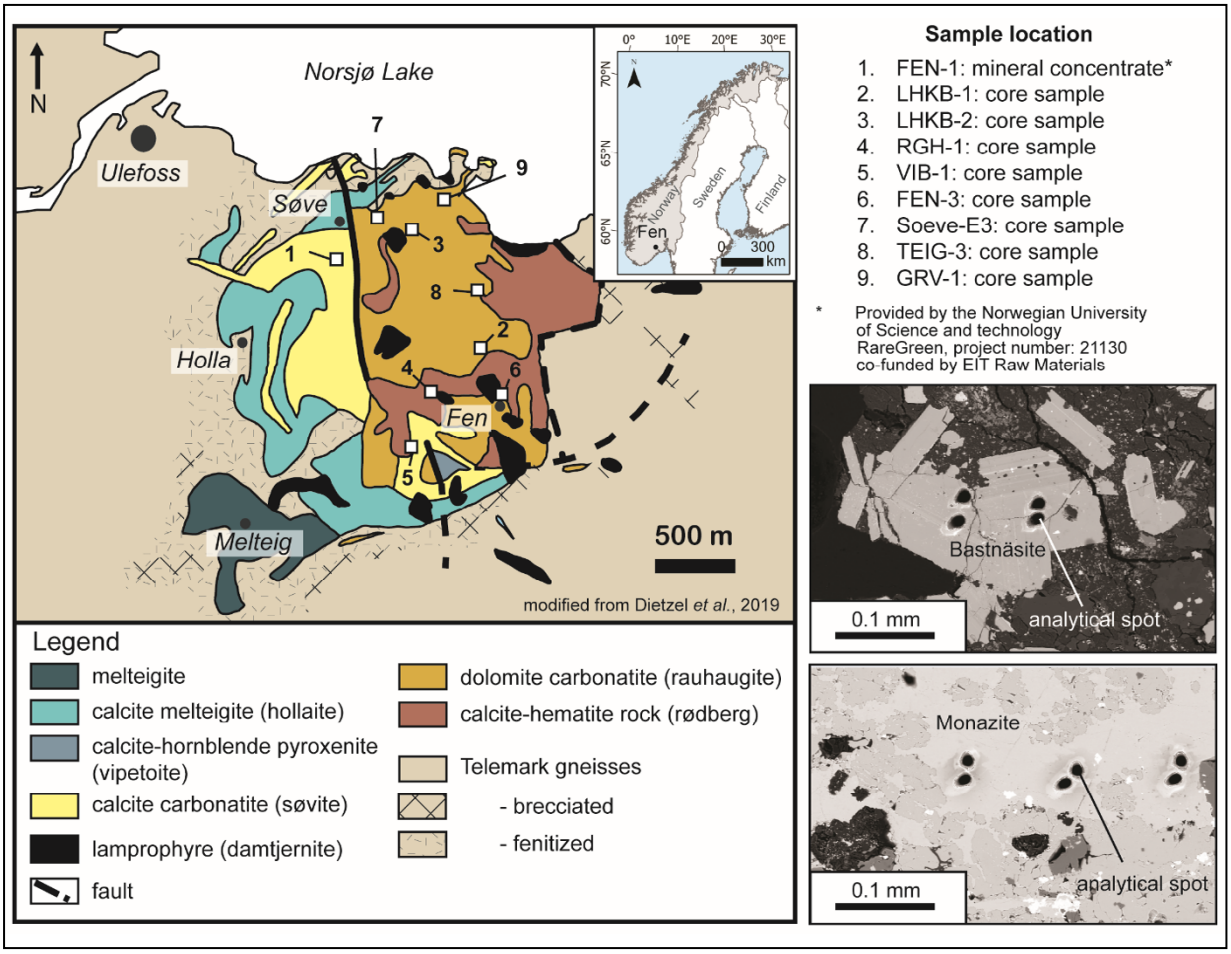


Figure 21. Simplified geological map of the Fen complex, showing the location of the samples used in this study and examples of the REE-bearing minerals analysed.

The studied samples, spread across the unit of interest to test the concept of homogeneity (Fig. 21), consist of rock fragments from drill cores and of a mineral concentrate provided by the University of Science and Technology in Trondheim, Norway.

Automated mineralogy conducted by the Geological Survey of Finland (GTK) on nine core samples indicated that REEs in this carbonatite are primarily hosted in rare earth element fluorocarbonates (hereafter REE-F-carbonates: 0–16 modal%), with minor occurrences of monazite (up to 5%). REE-bearing minerals form mm-scale clusters and are intergrown with baryte, Fe oxides, sparse pyrochlore (Niobium oxide), sulphides (pyrite, galena, sphalerite), chlorite, apatite, quartz, albite and hornblende (Table 4) in a matrix dominated by iron-rich dolomite, minor dolomite, calcite and sparse ankerite.

Table 4. Modal mineralogy of the samples considered in this study.

	Main carbonates					REE-minerals				Oxides, sulfides,...			
Sample	Cc	Dol	Fe-Dol	Ank	Sd	Bst	Prs	Mnz-Rhb	Ap	Brt	Pcl	FeOx	Py
FEN197920	8.8		53.2	3.4				5.6	0.1	14.1		3	5.4
FEN193407a	0.4	3.1	57.7	1.5	0.2	4.6	1.0	5.5	7.8	12.0		3.2	1.2
FEN093461	0.9	4	57.5	0.1	0.1	14.8	1.6	0.3	0.1	11.7		0.1	0.4
FEN193412a	2.8	3.6	29.9	1.1		0.6	7.5		1.2	9.9		0.3	43
FEN093463	8.3	9	65.6			2.7	5.6	0.1	3.7	0.4		0.1	
FEN093466	0.1	11.5	57.4	0.1	0.1	1	8.5	0.3	1.9	12.4	0.1	0.4	4.7
FEN093454		36.2	59.5		0.1	0.4	2.9		0.1	0.1		0.1	0.5
FEN093456	0.1	7.5	65.3	0.1		0.5	11.6	0.2	1	7.7	0.2		0.5
FEN093458	84.6	0.7	6.5			1.4	4.7	1.6					

	... sulfates		Silicates										
Sample	Sp	Fe-sulfate	Ab	Qz	Chl	Mg-Bt/Phl	Ms	Ba-Al silicate	Zrn	Crd	Hd	Mg-Hbl	Total
FEN197920	0.3		0.4	1.9	0.4			3.3			0.1		100.0
FEN193407a	0.9		0.5	0.4	0.2								100.1
FEN093461				7	0.5	1							100.1
FEN193412a		0.1		0.1									100.1
FEN093463				4		0.6			0.1				100.2
FEN093466				0.6	0.2					0.1		0.5	99.9
FEN093454				0.1									100.0
FEN093456				0.4	3.8		0.2						99.1
FEN093458				0.1			0.1			0.2			99.9

Cc: calcite, Dol:dolomite, Ank: ankerite, Sd: siderite, Bst: bastnäsite, Prs: parisite,
Mnz-Rhb: monazite, rhabdophane undifferenciated, Ap: apatite, Brt: baryte, Pcl: pyrochlore
FeOx: iron oxides, Py: pyrite, Sp: sphalerite, Fe sulfate: iron sulfate, Ab: albite
Qz: quartz, Chl: chlorite, Mg-Bt-Phl: magnesium-rich biotite - phlogopite, Ms: muscovite,
Ba-Al silicate: barium alumino silicate, Zrn: zircon, Crd, cordierite,
Hd: hedenbergite, Mg-Hbl: magnesium-rich hornblende

For each sample, we analysed the chemical composition of the minerals of interest and their neodymium (Nd) isotopic signature, an element used to manufacture permanent magnets. The analytical methods are presented in Appendix 1. The main challenge encountered in Fen was related to grain size, with REE-F-carbonates only being tens of microns in size and often intergrown. As a result, the trace element data presented below display a range of expected concentrations for endmember minerals. Nevertheless, these data can be used to assess chemical variations associated with the Fen complex.

The current lack of active mines at Fen limited access to the larger material quantities necessary to perform processing experiments.

Rare earth elements are a major constituent in monazite and the REE-F-carbonate mineral family, which encompasses bastnäsite, parasite, roentgenite and synchysite. These elements are therefore poor discriminants, as their concentration depends on the nature of the mineral rather than geological processes.

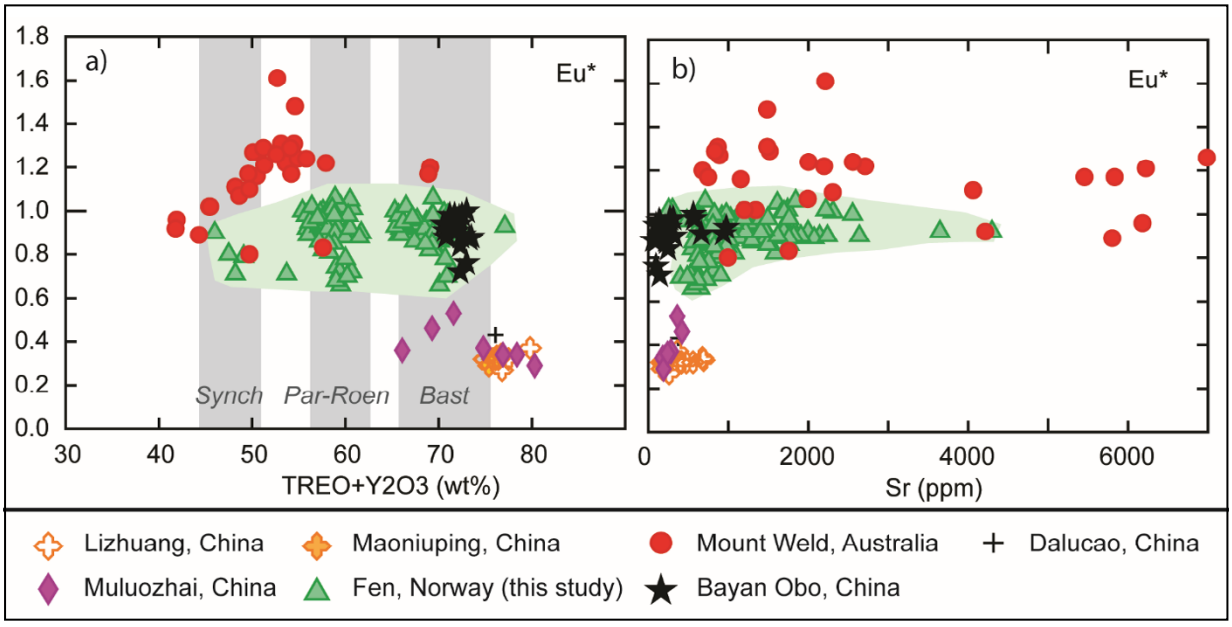


Figure 22. Compositional variation in REE-F-carbonates. a) TREO+Y_2O_3 versus Eu anomaly. b) Strontium versus Eu anomaly.

Chemical analyses of REE-F-carbonates revealed that trace elements such as strontium and europium anomaly (Eu*), a parameter tracking the oxidation state and a common criterion used to track the geological processes, can discriminate between different REE deposits (Fig. 22). Strontium concentrations in REE-F-carbonates from Fen range widely but are generally lower than those of Mount Weld (Australia) and comparable to those of Bayan Obo. The europium anomaly ranges from 0.6 to 1 in Fen, in contrast to Mount Weld, where the anomaly is positive, and Bayan Obo, which shows a strong negative anomaly.

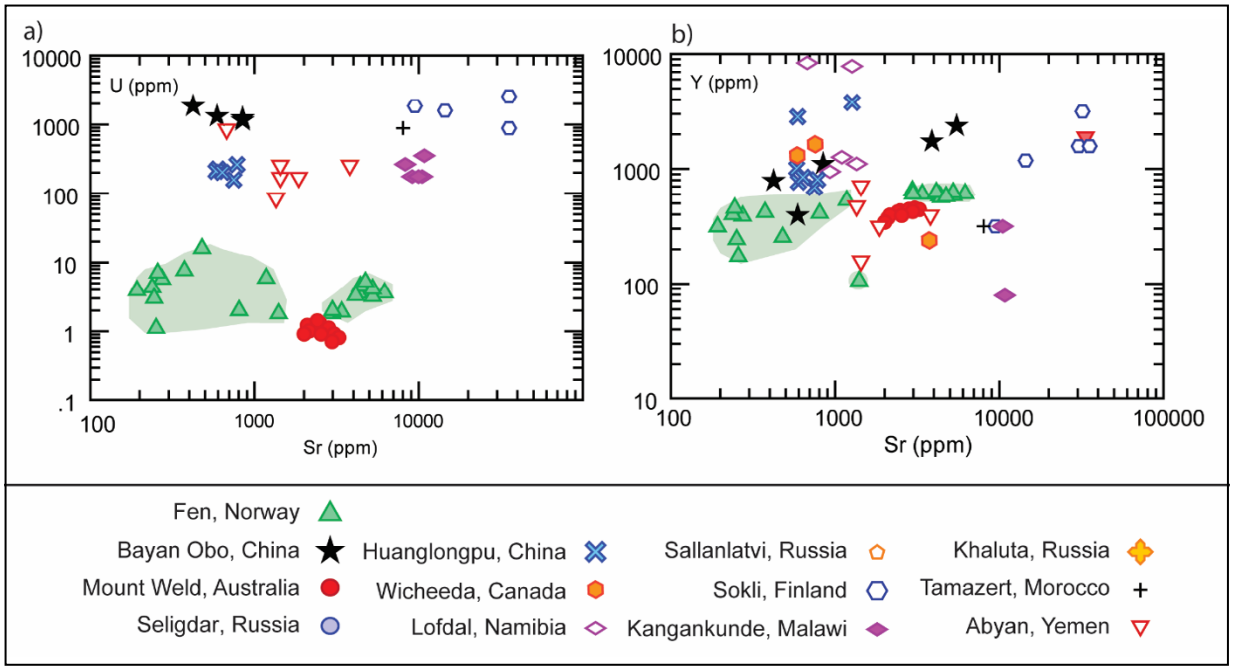


Figure 23. Monazite compositional variations. a) Strontium versus uranium concentrations. b) Strontium versus yttrium.

Monazite and potential rhabdophane, a hydrous LREE phosphate, from Fen contain low uranium concentrations (Fig. 23), partially overlapping with monazite from Mount Weld, unlike other REE deposits, where monazite is strongly enriched in uranium. Additionally, when rhabdophane is inferred in Fen, it is enriched in yttrium and strontium but remains low in uranium.

The present-day neodymium isotopic signature $\varepsilon(Nd)_0$ carried by the minerals is only affected by geological processes that occur over a long period of time under high temperature and pressure conditions. This signature is therefore difficult to modify and one of the criteria that is most likely to be preserved during processing of the ore, where the structure of the minerals is destroyed to liberate individual elements.

In the Fen complex, $Eps(Nd)_0$ varies between 1 and -15.2, with monazite showing slightly lower values than REE-F-carbonates. The distribution of the average $Eps(Nd)_0$ is relatively homogeneous throughout the mineralized unit, except for one sample that has less negative values and a higher $^{147}Sm/^{144}Nd$ ratio (Fig. 24). The $^{147}Sm/^{144}Nd$ ratio varies widely and depends on the crystallographic structure of the minerals, illustrating the diversity of crystallographic structures of REE-F-carbonates.

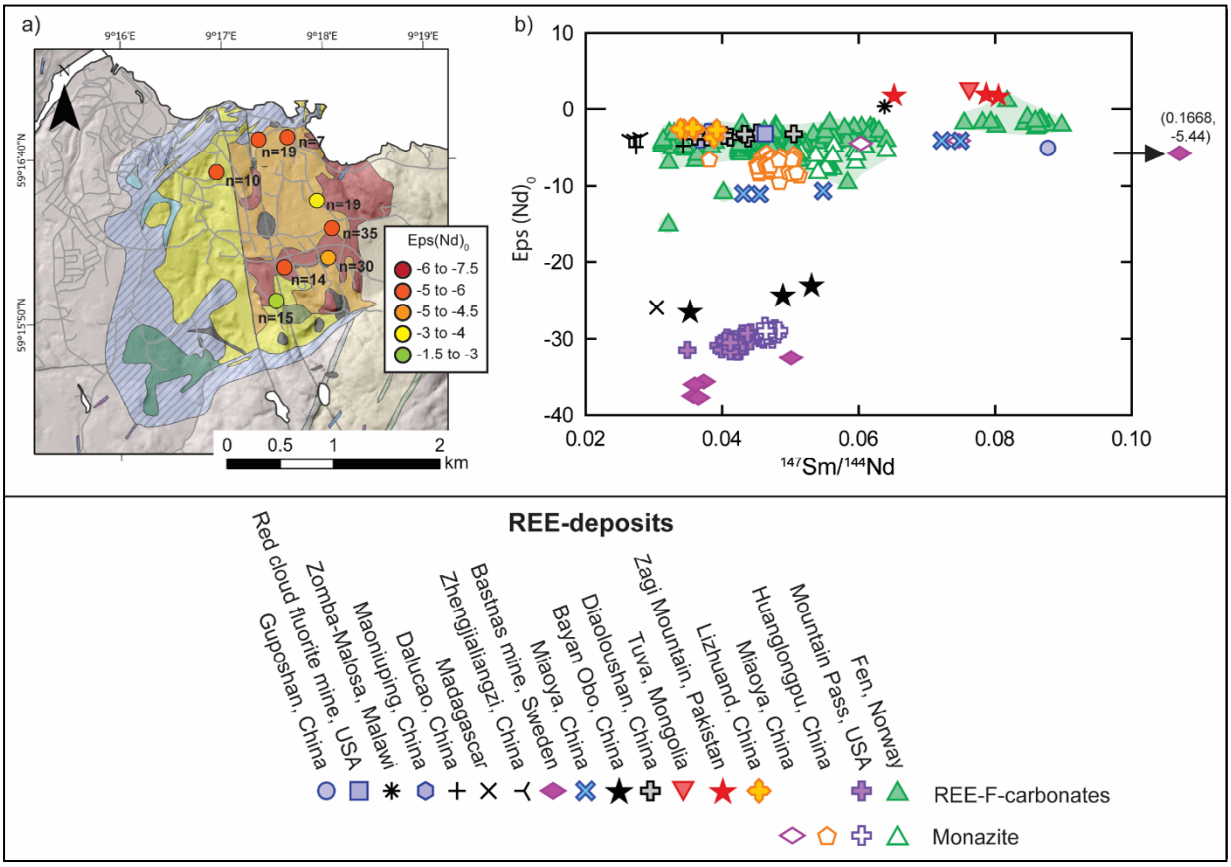


Figure 24. a) Average epsilon neodymium value for REE-F-carbonates in the Fen Fe-dolomite carbonatite. n = number of analyses. b) Neodymium isotopic composition of REE-F-carbonate and monazite from various REE deposits around the world.

While the present-day Nd isotopic signature of the REE-bearing mineral of Fen overlaps with several REE deposits around the world, it is distinct from those of the largest deposits, such as Bayan Obo (China) and Mountain Pass (USA).

Despite mineralogical complexities and the grain size, REE-bearing minerals from Fen were successfully analysed. Strontium, europium anomaly, uranium and to a lesser extent yttrium are elements that show restricted variation throughout the iron–dolomite carbonatite at Fen and can be used as potential tracers for REE minerals, although datasets can overlap. Neodymium isotopes vary throughout the unit, but no systematic geographical variation has been identified. However, the present-day neodymium isotopic signature of Fen remains distinct from the largest REE deposits, such as Bayan Obo and Mountain Pass.

Datasets gathered with similar types of instrumentation over REE-F-carbonates and monazite need to be acquired systematically to further test our preliminary results presented in this report. Additionally, uranium–lead dating of the REE-bearing minerals could help identify the source of the minerals.

2.2.1.4 The Sokli deposit, northeastern Finland

General geology

The carbonatite complex and associated P–REE–Nb mineralization at Sokli is located in eastern Finnish Lapland, near to the Finnish–Russian border. It belongs to the Devonian Kola alkaline province (KAP), which consists of 22 alkaline–carbonatite complexes (O'Brien & Hyvönen 2015). The carbonatite complex shows an oval shape on the plan, measuring about 18 km^2 on the surface and possibly representing the largest carbonatite in the world (Fig. 25).

The general geology of the deposit has been extensively studied since its discovery in 1967 by geological mapping, drilling and geophysical surveys (e.g., Vartiainen & Woolley 1976, Vartiainen & Paarma 1979, Vartiainen 1980, O'Brien & Hyvönen 2015; references therein). The Sokli complex intruded into the Precambrian basement rocks of tonalitic migmatite and amphibolite at around 380–360 Ma (Kramm et al. 1993). The deposit principally comprises a fenite aureole and a carbonatite (an igneous rock dominated by carbonate minerals) complex, which is composed of three concentric zones: a central calcite-dominant carbonatite (sövite) and phoscorite (carbonate–olivine–magnetite–apatite) surrounded by semicontinuous rings of metasomatic carbonatites, which are enveloped by an even more heterogeneous zone of phlogopite-rich carbonated ultramafic silicate rocks (Vartiainen 1980) (Fig. 25). The complex displays a concentrically zoned, funnel-like body with a younger, plug-like carbonatite magmatic core measuring 2.5 km in width at the surface and 1 km in width at 5 km depth, as indicated by deep seismic soundings (O'Brien & Hyvönen 2015). Based on detailed petrographic observation, Vartiainen (1980) established that a paragenetic sequence of rocks occurs at Sokli, which include, from early to late, emplacement of ultramafites (magnetite olivenite, olivenite rock and pyroxenite), succeeded by fenite and meta-ultramafites (phlogopite and amphibole rocks) formed through alkali metasomatism, which are then followed by metasomatic carbonatite and metasomatic phoscorite produced by carbonatizing agents from magmatic carbonatite. The magmatic carbonatite was believed to have formed in five stages, from early to late, including three paired phoscorite–carbonatite (P1C1, P2C2, P3C3), crystallization of banded and massive sövite, silicosövite and beforsite (dolomite carbonatite) (D4) and carbonatite veins (D5) (Vartiainen 1980, Lee et al. 2004). The carbonatite complex has undergone intense surficial weathering.

As noted by Vartiainen and Paarma (1979), economically viable mineral resources of the Sokli complex may come from two main ore types, i.e., the lateritic ores (the so-called soft ores) in the western and eastern glacial overburden and weathered crust, and pyrochlore and phoscorite ores (the so-called hard ores) in the deeper part of the complex. Phosphorus (P) in the lateritic ores was the main commodity for historical mining in the 1970s to 1980s, and in recent years, the utilization of REEs and niobium (Nb) in both lateritic and phoscorite ores has been under revived development by Finnish Minerals[3]. According to the results of Finnish Minerals Group's scoping study, Sokli could produce at least 10% of the amount of REE needed annually in Europe to make permanent magnets. Until recently, studies on REE mineralization have mainly focused on locations where REEs are evidently enriched, namely areas such as Jammi (Al Ani & Sarapää 2009) and Kaulus (Al Ani et al. 2011, Al Ani & Sarapää 2013). These studies have discovered abundant REE minerals, such as apatite, monazite, francolite, bastnäsite, ancylite and parasite, in the

fenite aureole and D5 carbonatite veins. Due to the limited time and resources in the Nordic Sustainable Minerals project, research has primarily focused on apatite, leaving other REE minerals to future projects.

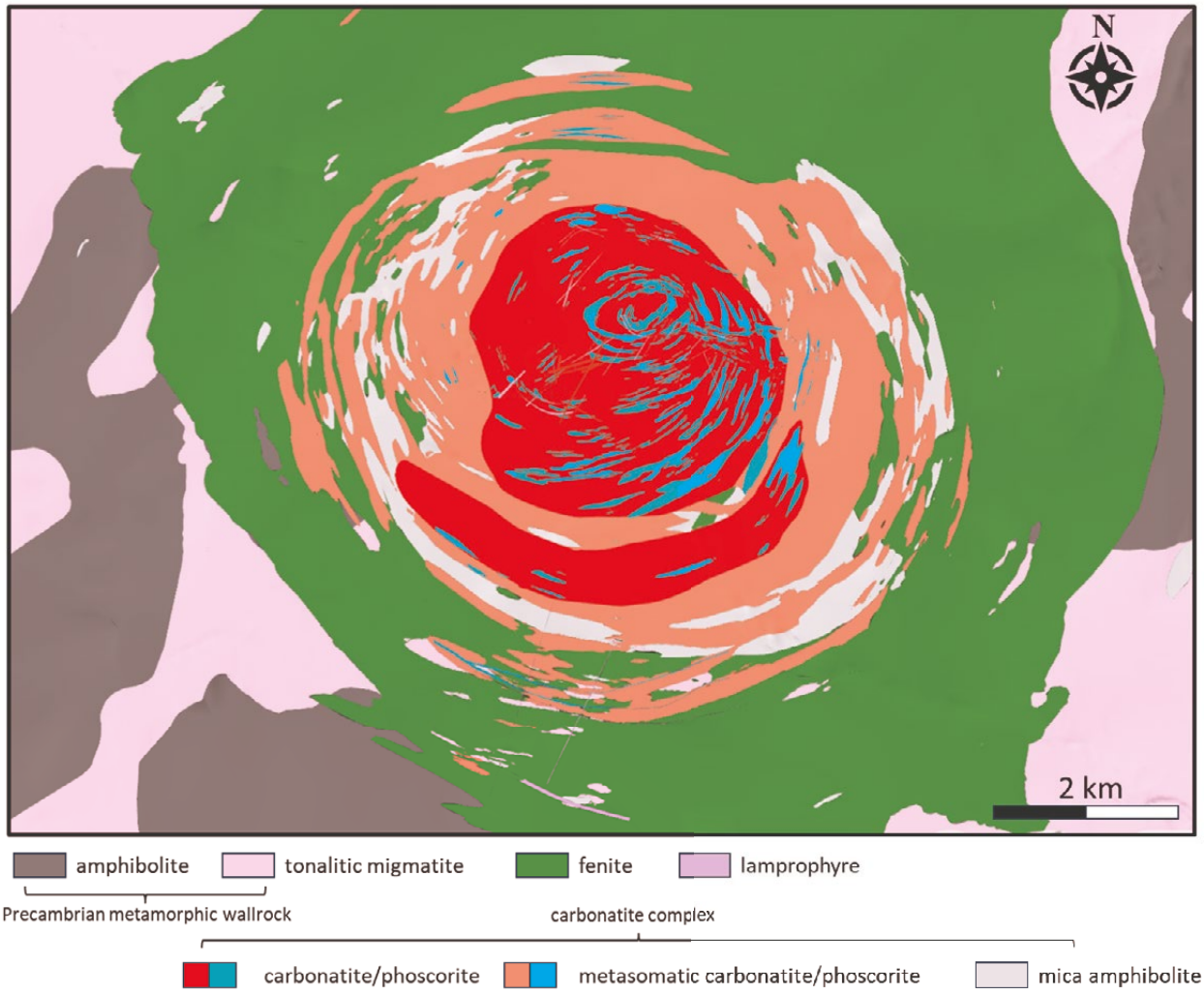


Figure 25. A geological map of the Sokli P–REE–Nb deposit (modified from the data of the Finnish Minerals Group [8])

Mining and ESG aspect

The Sokli carbonatite deposit was found in 1967 by the Finnish state-owned company Rautaruukki. It was owned by the Finnish fertilizer producer Kemira GrowHow until 2007, when it sold it to the Norwegian fertilizer producer Yara. During its long history, there have been several attempts to turn the deposit into a mine, but its remote location and lack of infrastructure have prevented this so far because of its unfeasibility. Yara looked into multiple options to process the ore in Russia or Canada, but after years of feasibility studies, it sold the project to the Finnish state-owned Finnish Minerals Group in 2021, which is now developing the deposit into a mine. Because Yara's environmental permit application was rejected by a Supreme Court ruling, Finnish Minerals Group needs to elaborate a new environmental impact assessment (EIA) and apply for the permit again.

[8] https://vrify.com/decks/12910

Eerola (2022) identified Sokli as one of the contentious mine projects in Finland. It is also found as a dispute case within the EJAtlas. Since the deposit was acquired by the Norwegian company Yara in 2007, the mine project has been opposed by local reindeer herders and ENGOs. This coincided with the national uranium debate since 2005, when all projects associated with uranium started to be opposed (Eerola 2022). Therefore, Sokli is among the oldest mining disputes in Finland. The reasons for opposition are the association with uranium and the environmental and social impacts of the mine. The deposit is located in a watershed area, which is also a habitat for fish. Furthermore, the mine project's area is surrounded by protected areas, which are among the sensitive contexts prone to mining and mineral exploration disputes in Finland (Fig. 26). Another reason for opposition was the foreign origin of Yara, which was due to resource nationalism. However, even though the project is now again held by a national state-owned company, this has apparently not reduced opposition. Therefore, it seems that the involvement of Finnish companies in mining and mineral exploration disputes may reduce the importance of resource nationalism as one of the reasons for disputes in Finland. In an attempt to block the project, activists have proposed the connection of surrounding protected areas. However, the project has largely been approved by the local population and decision makers, although repeated unsuccessful attempts to turn the deposit into a mine have also caused frustration. The company has practiced active stakeholder engagement and communication with the local community, and also its opposers. In fact, the project is seen to support the local economy and development plans of Eastern Lapland, which has suffered from high unemployment, migration to cities and an aging population, which is common in the Finnish countryside.

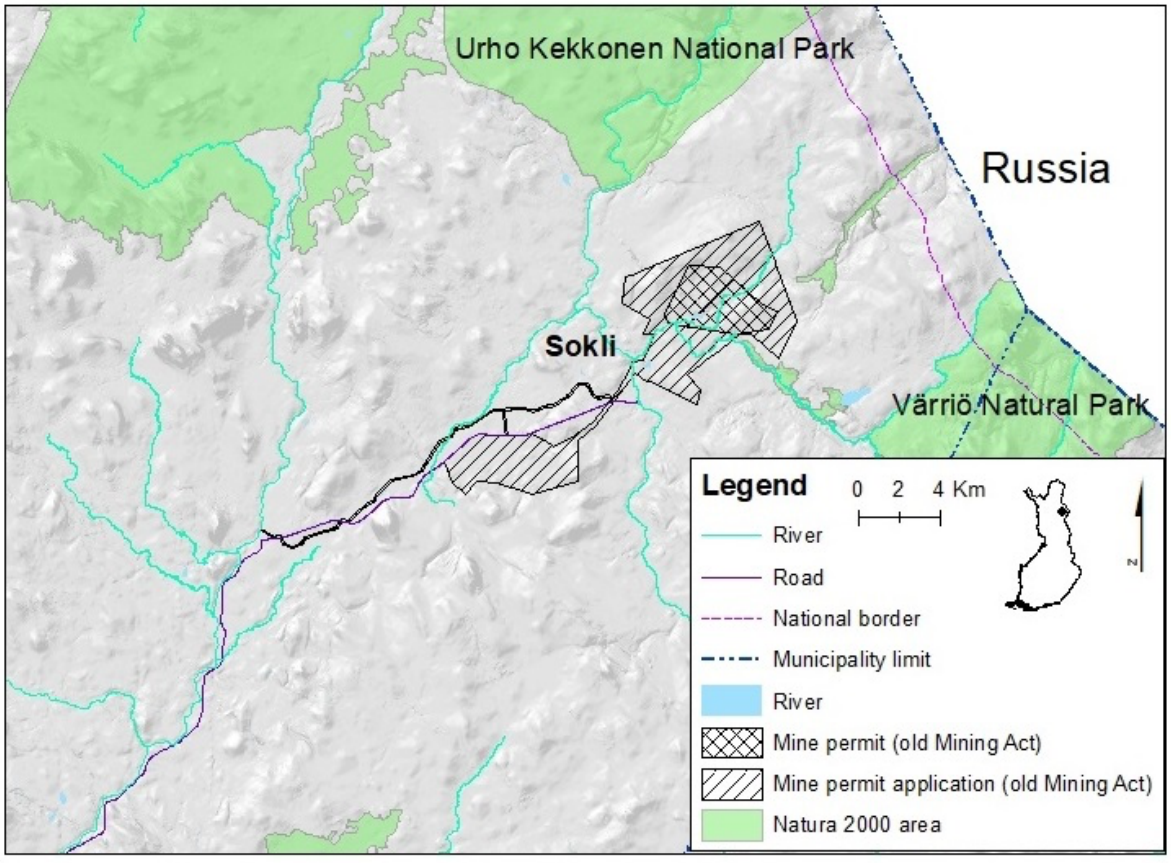


Figure 26. The Sokli mine project and surrounding protected areas in Savukoski, Eastern Lapland.

In any case, its contentious situation may compromise or constrain the benefit of traceability of the Sokli REE ore, as ENGOs can appeal regarding the potential impacts of a mine on reindeer herding and the environment. In this sense, they can claim that production would be unsustainable.

Geo-signature and homogeneity

In relevance to the differentiation and thus the traceability of Sokli apatite, a brief description of the mineral assemblage and mineral textures is presented below on the basis of a literature review and a petrography study conducted in this project. The objective is not to understand the genesis of apatite but rather to evaluate the homogeneity of the mineralogical and textural features in relation to traceability.

Apatite occurs in nearly all rock types of the Sokli carbonatite complex with a variable modal composition ranging from up to 50% in some of the phoscorites down to tens of percent in the late dolomite carbonatites (O'Brien & Hyvönen 2015). It also displays a large variety of mineral associations depending on the rock types. According to Vartiainen (1980), apatite commonly occurs with magnetite, baddeleyite, perovskite, diopside, calcite and dolomite in the early-phase unaltered olivenite and pyroxenite, whereas it occurs with alkali metasomatic minerals such as aegirine, amphibole, richterite, albite, iddingsite, serpentine, phlogopite, ferriphlogopite and zircon in the metasomatic ultramafites. In the intermediate stage of metasomatic rocks, apatite occurs with various metasomatic silicates, carbonates and sulphides, while in the late-phase magmatic carbonatite, apatite intergrows with magnetite, baddeleyite, phlogopite, calcite, pyrochlore and sulphides. In the lateritic ores, apatite commonly intergrows with francolite, goethite, Mn oxide, hematite and rhabdophane.

To briefly summarise, at the rock scale, the ore type, modal minerology and mineral association exhibit large variation and none appear to be representative of the entire deposit. In other words, these rock-scale signatures can only represent a part of the deposit in a specific space and time, beyond which the signatures are no longer representative.

Moving down to the mineral scale, Sokli apatite appears to have a variable grain size, which varies from millimetres to micrometres, as well as a variable textural morphology, ranging from complete euhedral crystals to anhedral grains (O'Brien & Hyvönen 2015). Under backscattered electron (BSE) imaging, apatite in most of the deposit, regardless of the rock type, retains a very similar response due to relatively homogeneous major to minor elemental compositions. Only in a few areas, particularly in the late carbonatite veins, may primary apatite have been hydrothermally altered to Sr- and REE-rich apatite varieties (Al Ani & Sarapää 2009). In these cases, the primary apatite (grey BSE) may contain numerous solid and fluid inclusions in the core, which is typically coated with Sr apatite (bright BSE), and intergrows with monazite, bastnasite, allanite, brabantite (Th apatite), Sr–Ce apatite, ancylite, columbite and belovite (Al Ani & Sarapää 2009, Al Ani & Sarapää 2013).

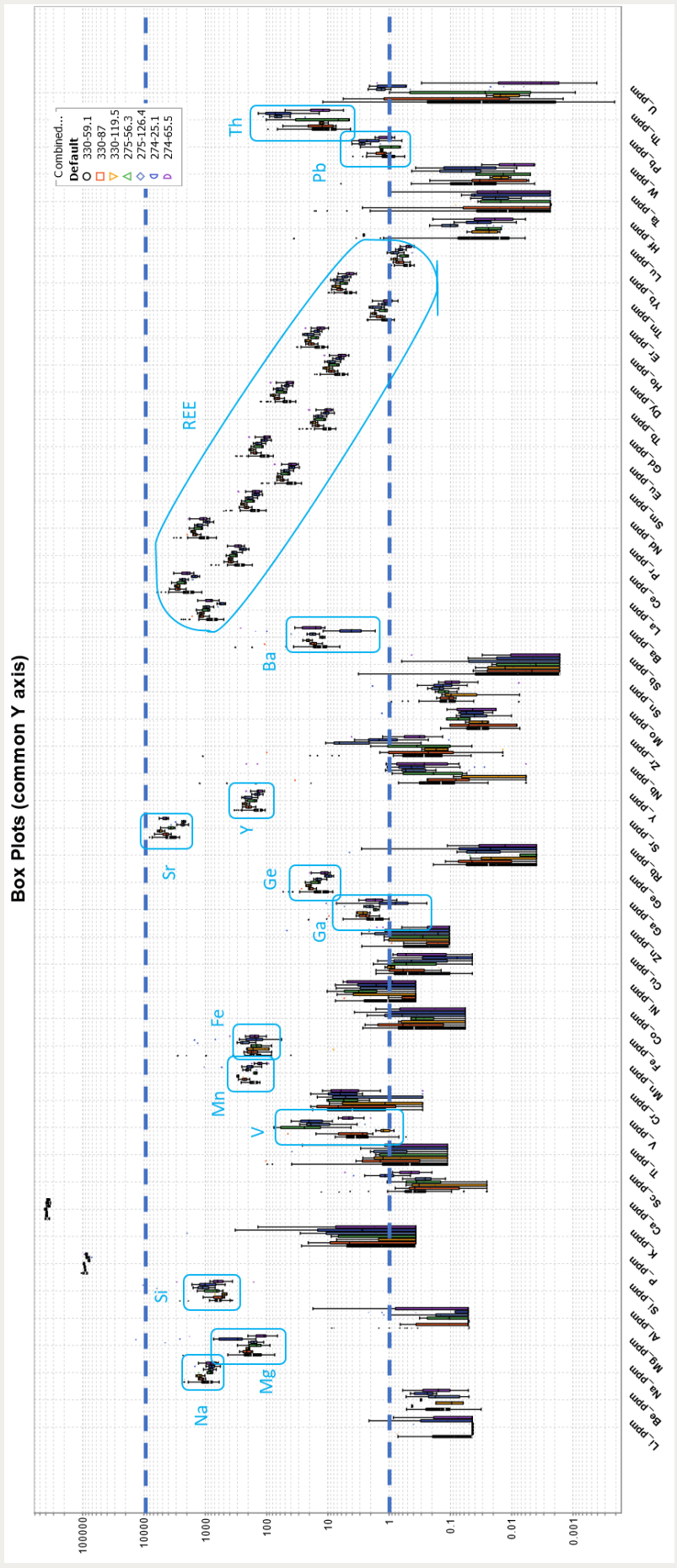


Figure 27. A box plot of trace elements in apatite of the Sokli deposit

Further down to mineral chemistry, little work has been conducted on Sokli apatite. Limited electron microprobe analyses on apatite from the carbonatite vein and fenite in the southern part of the deposit (Jammi) revealed different compositional varieties of apatite, which was attributed to the isomorphic substitution of Ca by Sr, LREEs, Na, Th and Y (Al Ani & Sarapää 2009). Different apatite varieties may differ in SiO_2 (0.04–0.8 wt%), FeO (0.3–1.39wt%), MnO (0.1–1.35 wt%), CaO (8–35 wt%), Na_2O (B.D.–3.7 wt%), SrO (2–14 wt%), P_2O_5 (25–35 wt%) and Ce_2O_3 (0.8–22 wt%).

Few trace element analyses on Sokli apatite have been reported in the literature. Within the Nordic Sustainable Minerals project, we collected rock samples from drill holes and analysed trace elements in apatite using LA-ICP-MS. The results of 126 analyses of 8 ore samples suggest that Sokli apatite contains the following trace elements with appreciable concentrations: Na, Mg, Si, V, Cr, Mn, Fe, Ga, Ge, Sr, Ba, REY (rare earth and yttrium), Pb and Th. Among all these elements, the Na, Si, Ge, Mn, Sr, Ba and REE contents had RSD values of <0.3 (Fig. 27). The remaining elements display considerable variation, but it has been noted that the REE inter-ratios (e.g., Th/Pb, Sm/Nd, Pr/Nd) are quite homogeneous, with RSD typically being <0.1. There are two distinctive Sr/REE ratios corresponding to Sr-poor apatite and Sr-rich apatite (Fig. 28).

Compared to trace elements, isotopic ratios are believed to be more consistent due to resistance to mass-dependent fractionation (White 2020). Sm–Nd isotope analyses with a laser ablation Neoma MS/MS multicollector (MC)-ICP-MS revealed that the Sokli apatite has a consistent $^{143}Nd/^{144}Nd$ ratio of 0.512671 ± 0.000255 (1σ, n = 15, RSD = 0.0005), corresponding to present-day εNd values of 0.6 ± 5.1. It should be pointed out that these data were preliminary and shall be further validated due to potentially poor tuning on the Neoma instrument, since it was installed only recently.

In summary, rock-scale signatures (ore type, modal mineralogy and mineral association) are heterogeneous across the space and time dimensions, and are not therefore representative of the deposit. At the mineral scale, apatite shows relatively homogeneous BSE intensity and, locally, exhibits special associations with REE minerals. At major to minor element scales, Sokli apatite shows large chemical variabilities, for instance in Ca, P, Sr and rare earths. At minor to trace element scales, elements and ratios such as Si, Ga, Ge, Mn, Fe, La/Nd, Th/Pb and Sr/REEs display good homogeneity.

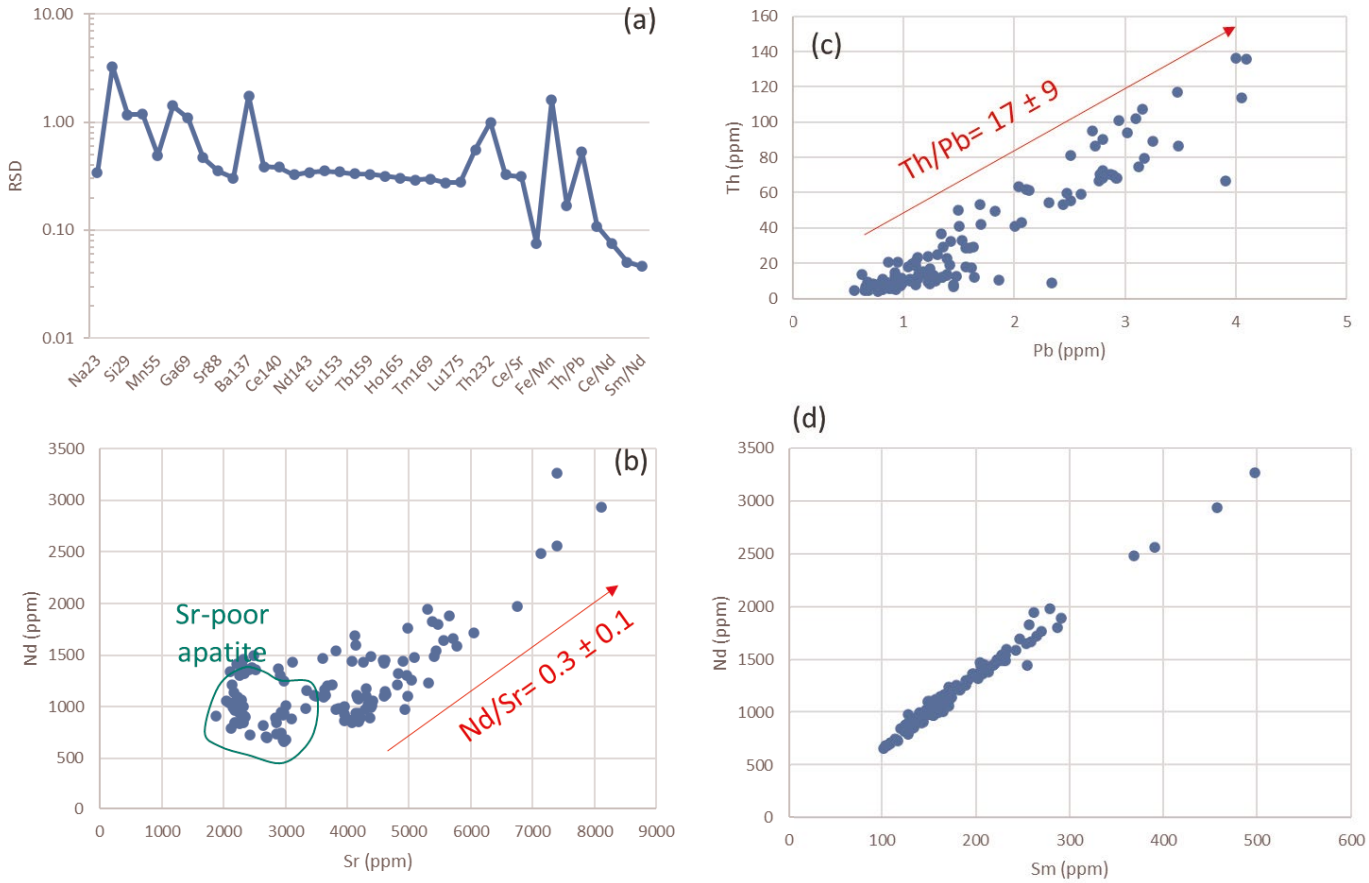
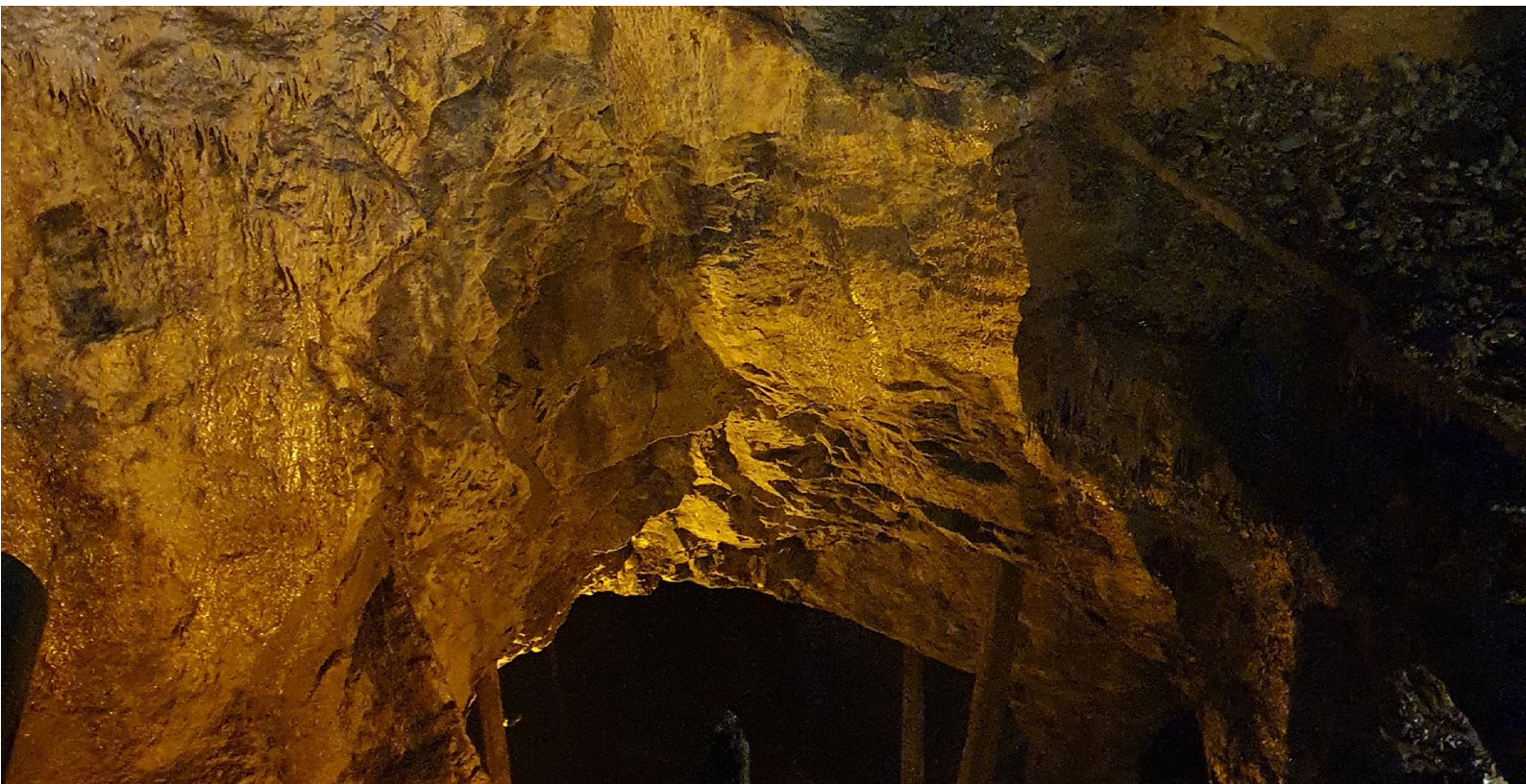


Figure 28. Trace elements and ratios of the Sokli apatite analysed by LA-ICP-MS



2.2.1.5 The basalt fibre, Iceland

General aspects

Fibre reinforced plastics (FRPs) are used in a wide range of industries, such as space, automotive, marine and construction-related industries, because of their weight savings, reliable mechanical properties and cost effectiveness (Shunga 2012). As such, it will help these sectors in supporting the UN and EU mission on global warming and improve the well-being of all citizens (e.g., Jóhannesson et al. 2016).

Lightweight FRPs exhibit excellent mechanical performance and are typically associated with low CO_2 emissions during their use phase. However, the production of carbon FRPs and glass FRPs is associated with a rather large carbon footprint due to their energy-intensive manufacturing process (from burning coal, gas and oil) and inefficient waste recovery in their end-of-life phase (e.g., Jóhannesson et al. 2016). In addition, glass fibres can result in hazardous health effects. Hence, in order to promote positive environmental impacts, it is important to minimize the CO_2 emission in each phase within the life cycle of FRPs. Mafic volcanic rocks, especially basalt and basaltic andesite, are present in abundance in Iceland, and are hence a bountiful resource for the production of reinforcing basalt-based fibres. Such fibres will be produced by using 100% renewable energy in the melt-spinning production process, as opposed to the fossil-based electrical energy used in most of the current production countries (e.g., Jóhannesson et al. 2016), reducing the production-associated CO_2 emissions by ~30%. Regarding mechanical performance, basalt fibres bridge the gap between glass and carbon fibres, and in contrast to glass fibres, natural basalt fibres are non-toxic and display remarkably low LCA values for human-terrestrial and aquatic toxicity (e.g., Fort et al. 2021). Hence, as such, they would have a unique positive environmental impact.

General geology

The stratigraphical unit of interest belongs to the Flank Series of the Brekkufjall Phase within the extinct, 3.5–5.5 Ma Hafnarfjall-Skarðsheiði central volcano situated in a Neogene volcanic succession in West Iceland and largely confined to the lowlands of the Andakíll district (Fig. 29; Fransson 1978).

The Brekkufjall Phase volcanic sequence is ~900–1000 m thick and represents some of the earliest constructs of the central volcano, and was followed by the Hafnarfjall, Skarðsheiði and Heiðarhorn Phases (Franson 1978). The Brekkufjall Phase features mafic lavas of the lower Hvanneyri Tholeiite Series (~250 m thick) and the felsic lavas and pyroclastic units of the Brekkufjall Acid Series (≤700 m thick). The latter phase represents a voluminous but brief eruption episode that culminated in the formation of a caldera. It consists of two structurally distinct formations: i) the Brekkufjall Caldera Series (not considered further) and ii) the Flank Series, which, as the name implies, flanks the Brekkufjall caldera and features the stratigraphical unit of interest. The Flank Series comprises a sequence of andesite lavas up to 700 m thick, outcropping in the lowlands between Andakílsa and Grímsá and thus very accessible (Figs 29, 30), and thinning out to the north over a distance of 10 km, i.e., just north of Grímsá (Fig. 30). It is divided into two sequences, where the lower sequence consists of seven xenolith-free andesite lava units with normal polarity and a collective maximum thickness of 300–400 m (strike NE–SW, dip ca. 17° SE) and thinning out northward over 1.5 km. The upper sequence consists of

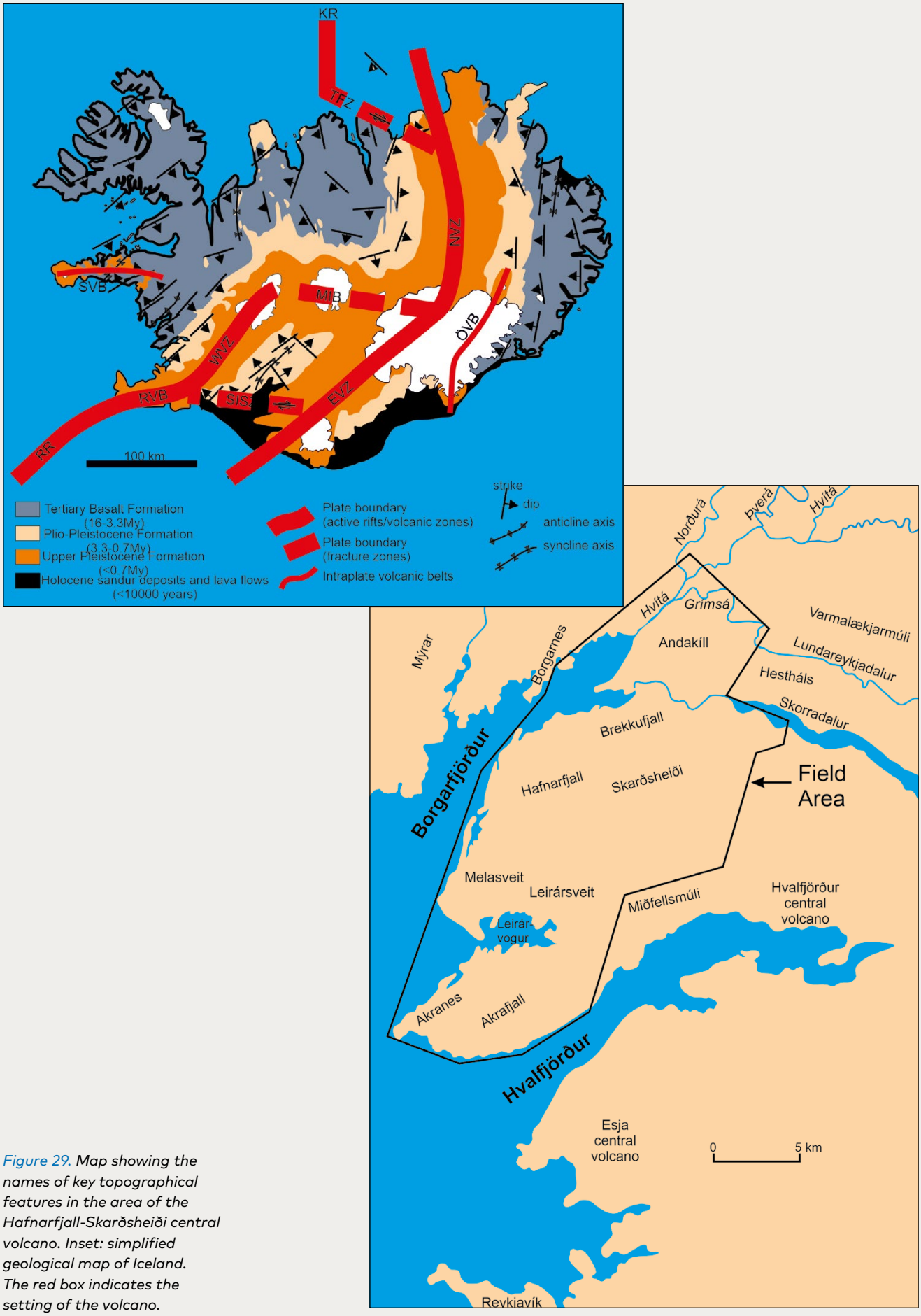


Figure 29. Map showing the names of key topographical features in the area of the Hafnarfjall-Skarðsheiði central volcano. Inset: simplified geological map of Iceland. The red box indicates the setting of the volcano.

several xenolith (rhyolite)-bearing intermediate units (dominantly andesite; range is basaltic andesite to dacite) dipping ca. 15° E–SE. The sequence maintains a ~300–400 m thickness over ~8 km, or within 1 km from Grímsá, where it rapidly thins out and disappears (Fig. 30). The lavas of the upper sequence are thinner, in some instances only a few meters thick, and are distinguished from the lower sequence lavas by their xenolithic nature and their erratic magnetic polarities.

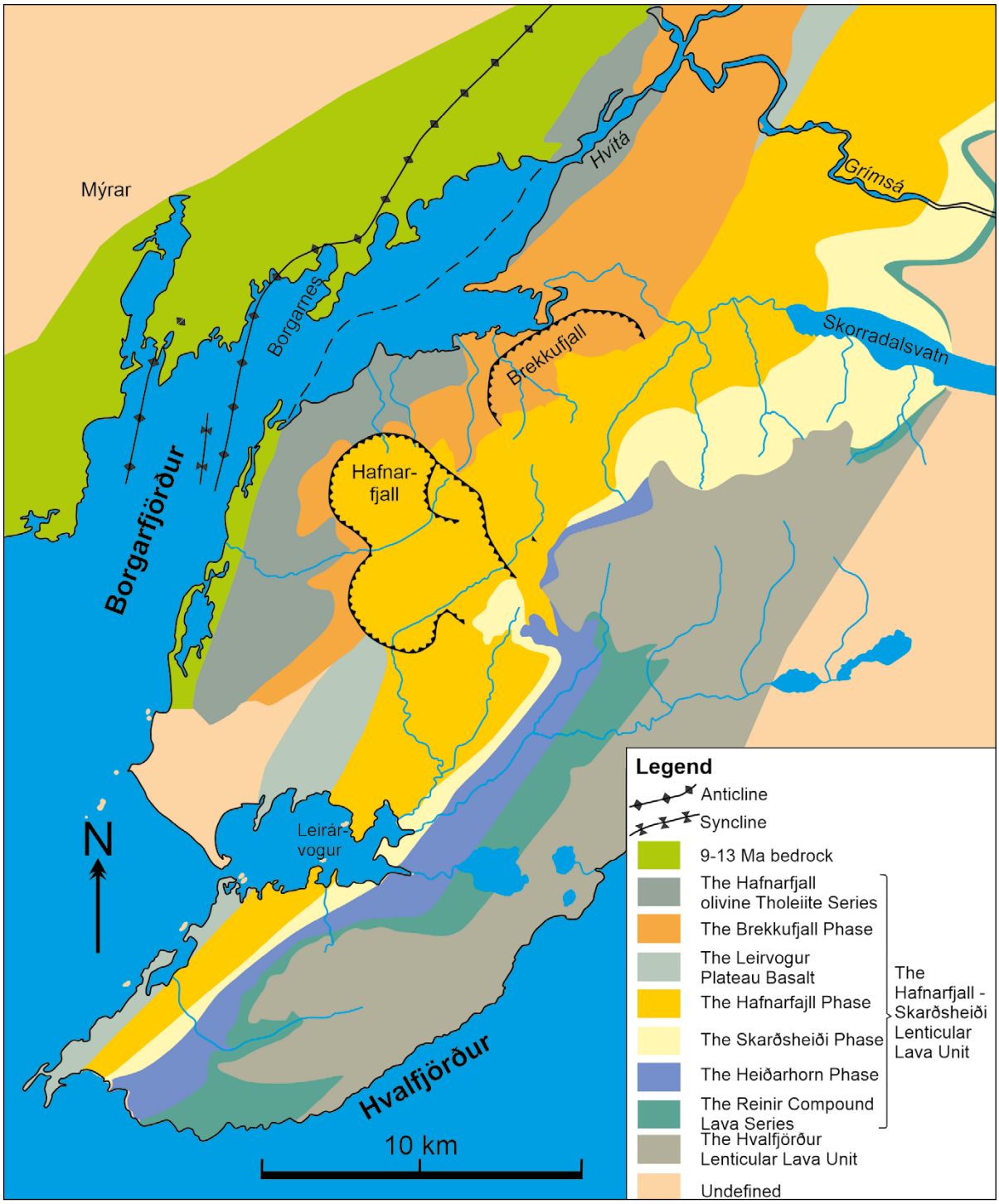


Figure 30. Simplified geological map of the Hafnarfjall-Skarðsheiði central volcano showing the extent of main eruptive phases. Note the Brekkufjall phase. The black box indicates the approximate location of the stratigraphical unit of interest.

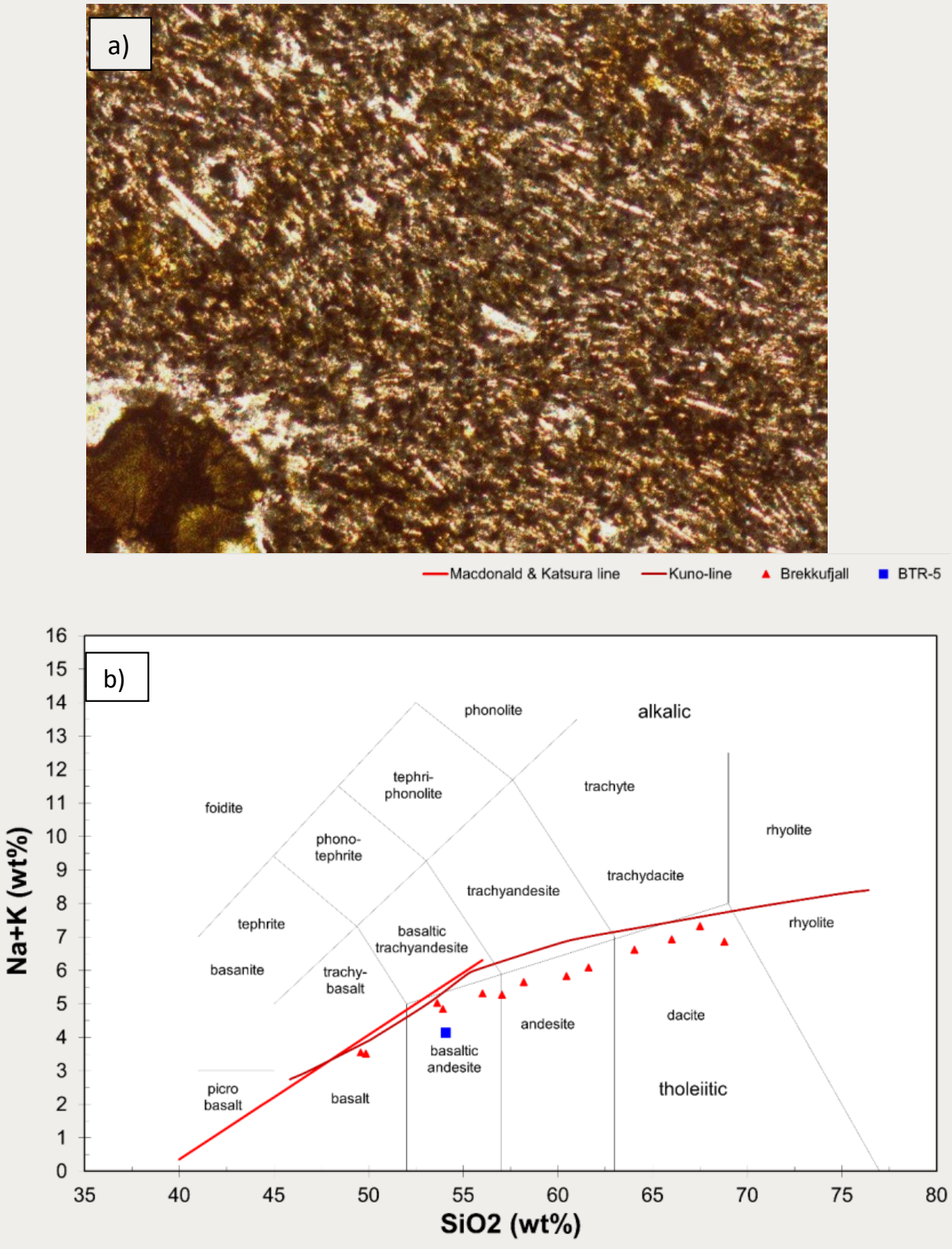


Figure 31. (a) Sample BTR-5. Photomicrograph showing a fine-grained andesite with flow-aligned groundmass and microcrystic plagioclase laths in plane polarized light. The black dots show the interspersed opaque minerals and the brownish grains are pyroxene. A vesicle filling in lower left corner with quartz and clay (probably mixed layer clay). (b) TAS classification plot showing the compositional variation within the Brekkufjall Phase of the Hafnarfjall-Skarðsheiði central volcano. The blue square denotes the basaltic andesite of BTR-5.

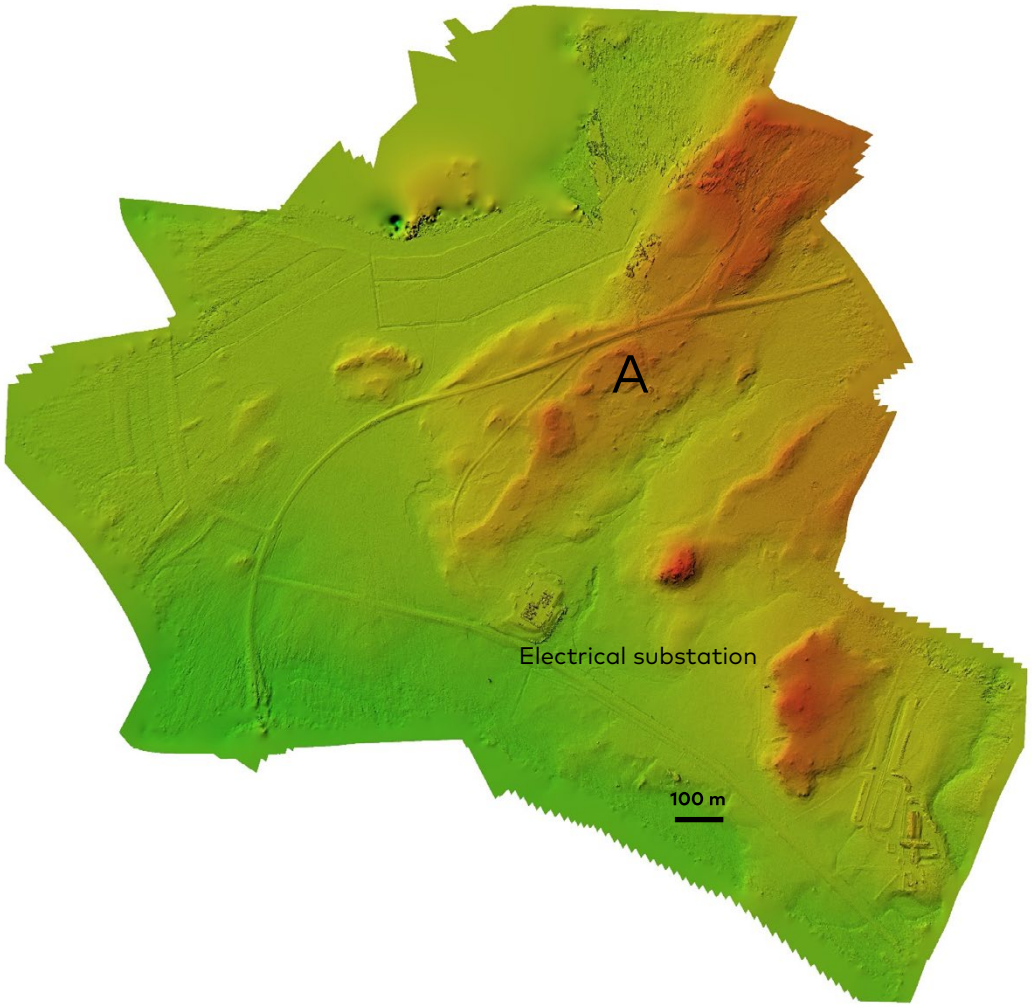


Figure 32. A 3D relative elevation map of the southern half of the stratigraphical unit of interest (A). Also shown is the location of the electrical substation.

Apparently, the xenolith-free lower sequence lavas are well suited to basalt fibre production, while the upper sequence lavas are not due to their silicic enclaves. The sample (BTR-5; coordinates N64.556: W21.721) used in the rock fibre production comes from a fine-grained, massive basaltic andesite (Fig. 31; Table 5) flow unit near the top of the lower Flank Series lava sequence, outcropping over a 350-m-wide area extending up to 3 km to the NE from the electrical substation (Fig. 32).

Table 5. Major element (whole rock by ICP) composition of the Brekkufjall Flank Series showing that the sequence is comprised of basaltic andesites to dacites. Samples are listed in stratigraphical order and the latitude and longitude of sample sites is given. Also shown is an example of the composition of the underlying and overlying basalt stratigraphical sequences. The basaltic andesite used in basalt fibre production is underlined. From Jóhannesson et al. (2016).

Sample	WGS84_X	WGS84_Y	Technique	Rock Type	Formation
BTR-6	-21.736507	64.569235	ICP - 2014	basalt	Hvanneyri Tholeiite Series
BTR-1	-21.721613	64.560290	ICP - 2014	dacite	Brekkufjall Flank Series
BTR-3	-21.726066	64.560656	ICP - 2014	basaltic andesite	Brekkufjall Flank Series
BTR-2	-21.717124	64.560932	ICP - 2014	dacite	Brekkufjall Flank Series
BTR-4	-21.726441	64.560877	ICP - 2014	dacite	Brekkufjall Flank Series
BTR-5	-21.721705	64.556475	ICP - 2014	basaltic andesite	Brekkufjall Flank Series
BTR-7	-21.677706	64.574294	ICP - 2014	andesite	Brekkufjall Flank Series
BTR-8	-21.676893	64.573792	ICP - 2014	andesite	Brekkufjall Flank Series
BTR-9	-21.674759	64.573324	ICP - 2014	andesite	Brekkufjall Flank Series
BTR-10	-21.668466	64.575686	ICP - 2014	dacite	Brekkufjall Flank Series
BTR-11	-21.665967	64.575400	ICP - 2014	andesite	Brekkufjall Flank Series
BTR-12	-21.658300	64.573833	ICP - 2014	basaltic andesite	Brekkufjall Flank Series
BTR-13	-21.668967	64.560900	ICP - 2014	andesite	Brekkufjall Flank Series
BTR-14	-21.693017	64.530683	ICP - 2014	basalt	Tungukollur Tholeiite Series

Sample	SiO2	TiO2	Al2O3	FeO_T	MnO	MgO	CaO	Na2O	K2O	P2O5	Total
BTR-6	49.58	3.15	13.35	15.27	0.24	5.06	9.25	3.09	0.47	0.38	99.46
BTR-1	67.51	0.60	14.20	6.76	0.14	0.39	2.77	5.12	2.21	0.11	99.68
BTR-3	53.61	2.63	13.72	12.53	0.27	3.41	7.32	3.90	1.13	1.33	98.51
BTR-2	64.04	0.96	13.79	9.04	0.21	0.78	4.07	4.81	1.81	0.29	99.52
BTR-4	68.79	0.57	13.92	6.93	0.20	0.15	2.28	4.69	2.18	0.10	99.70
BTR-5	54.07	2.65	13.92	12.63	0.20	3.41	7.51	3.39	0.75	1.32	98.53
BTR-7	58.19	1.72	13.55	11.77	0.34	1.80	6.10	4.38	1.28	0.67	99.12
BTR-8	57.05	1.82	13.45	12.89	0.32	1.93	6.28	4.10	1.17	0.79	99.01
BTR-9	61.61	1.36	13.46	10.17	0.30	1.21	5.02	4.56	1.53	0.55	99.23
BTR-10	66.01	0.61	14.61	7.44	0.17	0.35	3.55	5.19	1.74	0.11	99.69
BTR-11	60.45	1.48	13.48	11.28	0.27	1.55	4.88	4.37	1.46	0.57	99.22
BTR-12	53.92	2.34	13.57	14.05	0.32	2.90	6.87	3.85	1.00	1.01	98.82
BTR-13	56.01	1.97	13.43	13.04	0.34	2.27	6.56	4.15	1.16	0.87	98.94
BTR-14	49.86	3.26	13.26	14.65	0.25	5.22	9.40	3.04	0.48	0.40	99.43

Geo-signature and homogeneity

Although mafic magmatism in Iceland was initially produced by partial melting of a heterogeneous mantle source, it features remarkably well-constrained geochemical source signatures, such as Nb/Y, Zr/Y and $^{143}Nd/^{144}Nd$ values, that define the Iceland array (Figs 33, 34; e.g., Fitton et al. 1997, Harðarson et al. 1997, Saunders et al. 1997, Thirwall et al. 2004, Harðardóttir et al. 2022). These elements, and element and isotope ratios, are rather insensitive to crustal contamination, and are hence well suited to source identification and use as tracers. In addition, the study of Banik et al. (2018) indicated that the magmatism associated with the Hafnarfjall-Skarðsheiði central volcano is typified by a restricted range of $^{143}Nd/^{144}Nd$ values (i.e., 0.513010–0.513030; εNd + 7.2 to +7.6) and are conformable to the Iceland array (Fig. 34). Similarly, Nb/Y values of 0.65 and Zr/Y values in the range of 5–7 for the Hafnarfjall-Skarðsheiði volcanics agree well with the established Iceland array (e.g., Banik et al. 2018). Hence, in summary, these data are very encouraging for establishing a viable down-the-product-line traceability procedure for Icelandic basalt fibres.



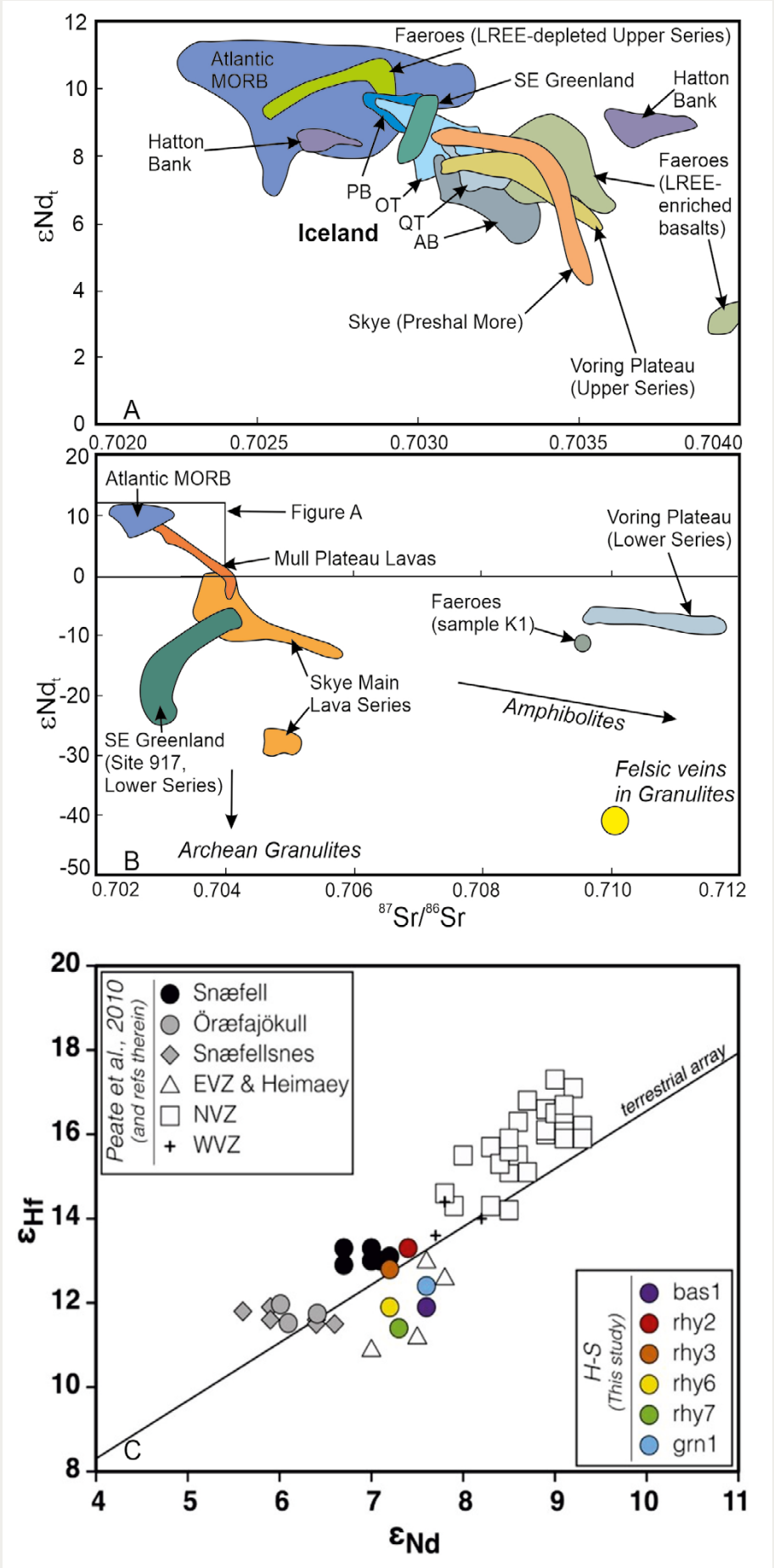


Figure 33. Whole-rock eNd$_t$ versus $^{87}Sr/^{86}Sr$ for basalt and related rocks from the North Atlantic Igneous Province (NAIP) and Iceland. The Iceland array is defined by the compositional domains labelled PB (picrites), OT (olivine tholeiites), QT (quarts tholeiites) and AB (alkali basalt). B. The same as A, but showing the complete range for the NAIP. From Saunders et al. (1997). C. Whole-rock eNd versus eHf in the volcanics from the Hafnarfjall -Skarðsheiði central volcano plotted against the Iceland array (see key for details). Also indicated is the terrestrial array (Banik et al. 2018).

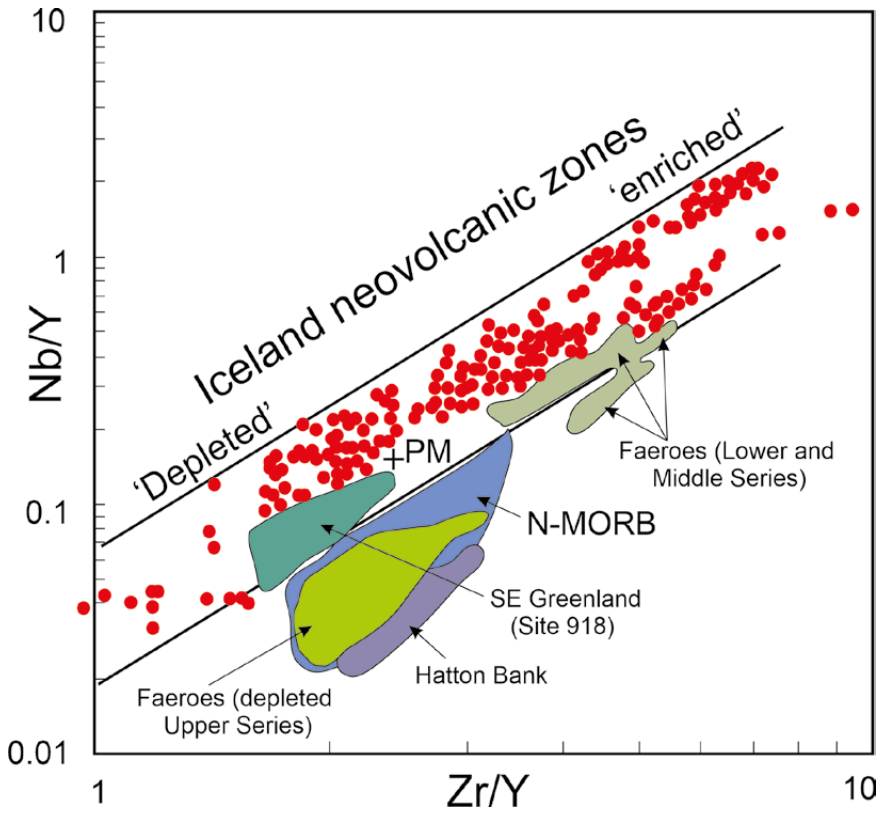


Figure 34. Whole-rock Zr/Y versus Nb/Y from basalts within the neovolcanic zones of Iceland defining the Iceland array. Also shown for comparison are the compositional fields for Zr/Y versus Nb/Y in other parts of the NAIP and MORB.

2.2.2 Conservativity test

In section 2.2.1, the geo-signatures of the deposit and ore minerals are described and their potential variability and homogeneity are evaluated. To qualify as traceability indicators of a deposit, geo-signatures need to be conservative during mineral processing and refining, in addition to being homogeneous and representative of the deposit. Due to limited resources and time, eudialyte ores from the Kringlerne deposit were selected as a demonstration example for evaluating what geo-signatures may be preserved during metallurgical processing.

The feed materials for the hydrometallurgical leaching experiment were eudialyte concentrates from Kringlerne gathered by the EURARE project[9]. The dominant REE-bearing mineral eudialyte has a high liberation degree (80–85%) and coarse grain size, which is able to be beneficiated with dry magnetic separation after crushing. The beneficiation process includes at least two stages of magnetic separation. Firstly, a roughing processing stage is employed at a higher magnetic field intensity and the non-magnetic minerals are removed. Secondly, a cleaning stage is performed at a lower magnetic field intensity and the eudialyte concentrate is obtained by separating eudialyte from the paramagnetic minerals.

[9] https://www.eurare.org/

The modal mineralogy of the ore material was studied by Heino (2013) using mineral liberation analysis (MLA), which revealed the main minerals to be eudialyte (33.36 wt%), nepheline (14.16 wt%), arfvedsonite (13.54 wt%), albite (12.57 wt%) and sodalite (11.71 wt%). After mineral beneficiation, the obtained concentrate consisted of 67.05% eudialyte, 8.38% arfvedsonite/rieberckite, 7.05% nepheline, 6.1% feldspar, 4.35% sodalite, 1.61% K-feldspar and 5.46% other phases according to an MLA study by Ma et al. (2019). It is apparent that modal mineralogy has largely been modified by the mineral beneficiation process, even though the mineral composition and association has not been significantly affected.

A fraction of concentrates was processed by the company 3R-Cycle with their patented green chemistry technology to recover REEs. The process was a one-stage leaching and recovery process that was optimized through multiple test experiments. Due to the protection of commercial secrecy, no more details are revealed in this report. For those who are interested in investment or collaboration, 3R-Cycle can be approached via this project to provide more information under a non-disclosure agreement.

The produced concentrates and some of the raw materials were qualitatively studied for their mineralogy and phase composition at the Research Laboratory of the Geological Survey of Finland. A separate GTK open-file report on the phase characterization of the feeding eudialyte concentrates and leaching products is appended as supplementary materials. Only a brief summary is provided here.

Altogether, 33 samples were characterized during the project, including 2 feed materials, 23 eudialyte concentrates and 8 concentrates of other ores and materials.

Throughout autumn 2023, the 3R-CYCLE leaching and recovery method was tuned for separation of REEs from an eudialyte concentrate. The key outcome of these tests was the production of a high purity REE oxalate separate (sample N12), with Ce, La, Nd, Y, Pr, Dy, Gd and Sm as the detected rare earth metals. In all tests, Nb was typically enriched in the metallic separates, and REE-bearing phases preferred the oxidized and silicic concentrate samples over the metallic ones. Further tests should be focused on verifying the process that led to successful REE separation in sample set 6. In addition, to gain a better idea of the sample purity, bulk ICP-MS analysis, FE-SEM-EDS quantification of the phase composition from a polished sample, and XRD Rietveld modal crystal composition analysis should be considered to quantify the chemical and phase composition of the successful REE separates.

Solution analyses of Nd isotopes with a Neoma MS/MS MC-ICP-MS at GTK's Espoo Research Lab suggested that the eudialyte concentrates (two samples, Nd-195-1 and Nd-195-2) had $^{143}Nd/^{144}Nd$ ratios of 0.512003 ± 5 (2σ) and 0.511997 ± 4 (2σ), which are slightly higher than laser ablation values of 0.511775 ± 14 (2σ) (see section 2.1). Due to the limited amount of REE oxalates, only Nd isotope by solution analysis has been performed. The results for two REE oxalates (N12 and EL1) suggested that the oxalates had a $^{143}Nd/^{144}Nd$ ratio of 0.511997 ± 4 (2σ) and 0.511982 ± 4 (2σ). It is apparent that the hydrometallurgical process did not change the $^{143}Nd/^{144}Nd$ ratios.

Molten salt electrolysis is ongoing at SWERIM, and the results are expected to be released in September 2024. Nd isotope analyses of the obtained Nd metals will follow.

2.2.3 Uniqueness test

The establishment of a comprehensive geochemical database is crucial for the geochemical fingerprinting approach to traceability. Due to limited resources, we have mainly focused on collecting Sm–Nd isotopic data for the world's major REE deposits, including Mountain Pass, Bayan Obo, Gakara, Olympic Dam and Mountain Weld. A more comprehensive database encompassing geochemical analyses from bulk rock compositions and mineral analyses of trace elements analyses and isotopic studies is still ongoing.

A comparison of Sm–Nd isotope data for the REE targets of this project is presented in Figure 35a, and a comparison with the world's major REE deposits is provided in Figure 35b. In Figure 35a, it is clear that Kringlerne, Norra Kärr, Fen and Sokli are reasonably separated based on the present-day εNd values, with overlaps between the latter three. These four targets are best differentiated when an initial εNd value is calculated based on the age of the mineral. Furthermore, the four targets had very distinctive $^{147}Sm/^{144}Nd$ ratios. These features are better shown on a quasi-global scale, as in Figure 35b. Present-day εNd values are not good discriminants for the different deposits, which display quite large overlaps, whereas initial εNd values separate them quite well.

Therefore, it can be inferred that the initial εNd value, calculated from the present-day εNd value, age of the mineral and $^{147}Sm/^{144}Nd$ ratio with a decay equation, is unique for the REE deposits investigated in this project.

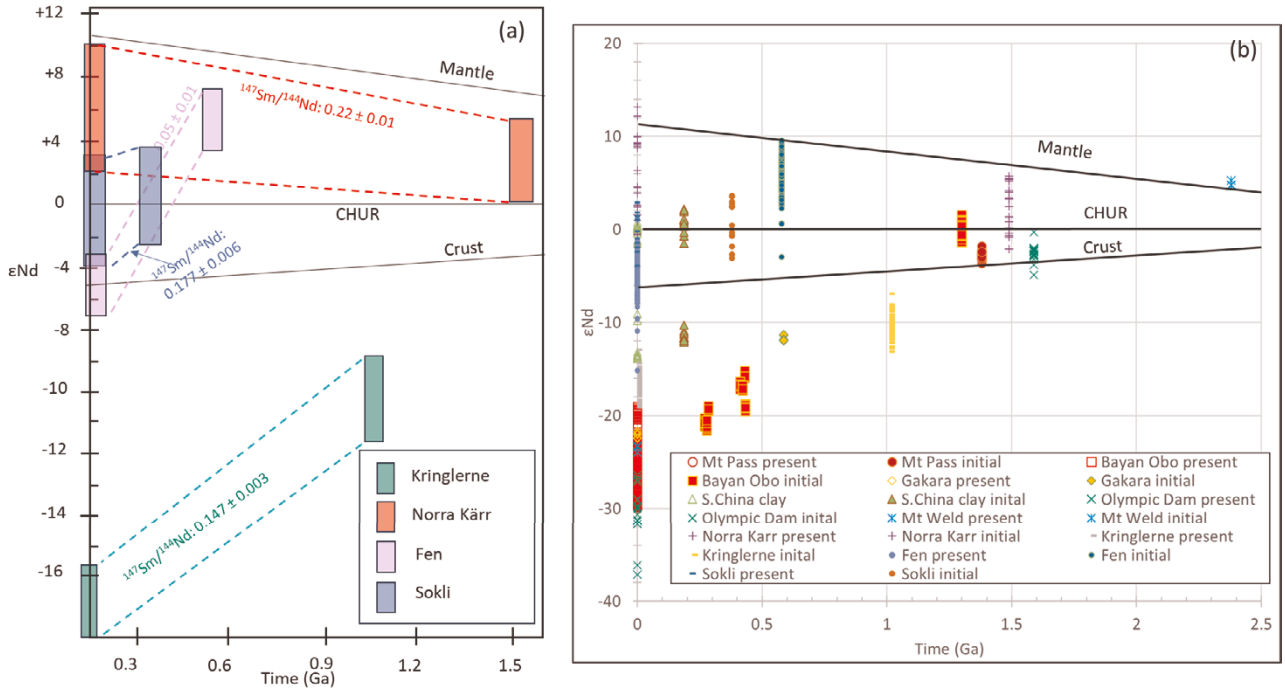


Figure 35. Sm–Nd diagrams showing the evolution of terrestrial Nd isotopes, with REE targets of this project and major REE deposits around the world. The data for major REE deposits are from the following references: Mountain Pass (Poletti et al. 2016); Bayan Obo (Li et al. 2021); Gakara (Lehmann et al. 1994); Olympic Dam (Johnson & McCulloch 1995); Mountain Weld (Graham et al. 2004).

2.3 Geo-forensic pilot study: Nd magnets

A neodymium (Nd) magnet is a type of permanent magnet made from an alloy of Nd, iron (Fe) and boron (B), forming a $Nd_2Fe_{14}B$ tetragonal microcrystalline structure. It is widely used in many applications such as electric motors, electric generators for wind turbines, loudspeakers and headphones. It has superior magnetic properties, such as high residual magnetism (a measure of the capability for storing magnetic energy), high coercivity (a measure of resistance to external magnetic resetting), in addition to other physical and mechanical properties, such as high tensile strength. Nd magnets represent the most important use of rare earth metals, accounting for 80% of the use of Nd in the EU according to the Horizon 2020 SCRREEN project[10].

NdFeB-based permanent magnets can be produced with various processing techniques, which dictate the microstructures of the magnets, such as grain size, alignment and the distribution of phases. Melt spinning, mechanical alloying and the HDDR (hydrogenation, disproportionation, desorption and recombination) process are commonly used for obtaining nanometre grain sizes, whereas the sintering process is commonly used in producing micron-sized grains (Fidler and Schrefl 1996). Typically, in sintered magnets for instance, a Nd magnet is made from pure boron, pure iron and rare earth metal, and the rare earth metal may include pure Nd, pure Pr–Nd and pure Nd oxides. Several other rare earth elements may be added as substituents and dopants, such as Dy, Tb, Cu, Co, Al, Ga and Nb, to improve the performance of the magnets (Fidler and Schrefl 1996).

The objective of this pilot study was to determine whether it is possible to distinguish Nd magnets based on the microstructure, chemical composition and Nd isotopes, and also to evaluate the possibility of tracing them to a specific rare earth deposit.

2.3.1 Analytical workflow

A total of 61 Nd magnet blocks were collected from different sources, including used magnets from personal collections, new magnets purchased from local dealerships, and magnet scraps purchased from online shops. Due to the lack of traceability, none of the collected magnets have information on the raw material origin, and due to commercial secrecy, the sellers of the new magnets were only willing to share the production year, grade and other information regarding the physical properties. Two types of Nd magnets were gathered and studied in this project (Fig. 36). The first type comprised novel magnets with a known production year (1999 to 2023) and grade (different Nd contents), and the other consisted of scrap magnets without information.

All the magnets were first demagnetized by heating to over 500 °C in an oven for about 20 minutes. The coating (Zn or Ni) of the demagnetized blocks was then removed by grinding. Two magnet blocks were drilled with a 1–2-mm diamond drill bit to produce NdFeB powders for solution analysis, while the other magnet blocks were made into epoxy mounts for *in-situ* laser ablation.

[10] https://scrreen.eu/wp-content/uploads/2023/08/SCRREEN2_factsheets_REE-EUROSTAT.pdf

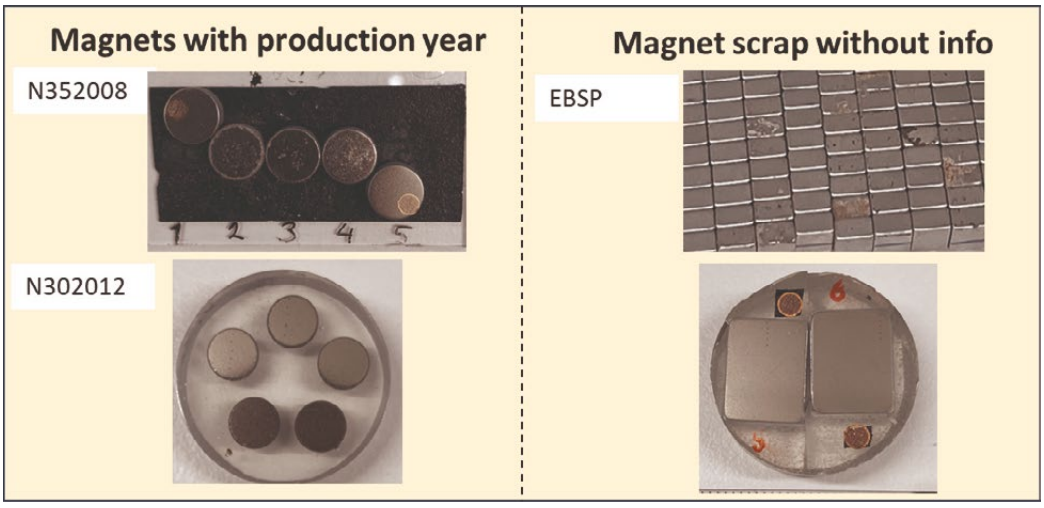


Figure 36. Images of selected samples of magnets with a known production year and without production information

2.3.2 Phase characterization

Nd-bearing minerals from the studied deposits and the NdFeB magnets were investigated with scanning electron microscopy (SEM). Samples were mounted in epoxy and coated with carbon (10 nm) to make them conductive. A range of SEM techniques was applied to the samples.

Composition

The magnets typically consist of a ground mass of hexagonal grains 1–5 µm in size that are rich in iron (over 60 wt%), but also include Nd and often a selection of other metals, including Pr, Ce and Al. The exact composition varies between magnets and between batches of magnets (Fig. 37). Within the groundmass, there are inclusions of other metals that appear to fill out the pore space within the ground mass and are therefore irregularly shaped or equant. These interstitial phases are richer in Nd (typically 40–60%), poor in Fe (0–3%) and typically contain a larger range of REEs (Pr, Ce, Ho, Dy and La), but also other metals, especially Cu, Nb, Co and Al. In more than half of the studied magnets, this interstitial phase is solidified as an exsolution in two different phases (see Fig. 37 for examples).



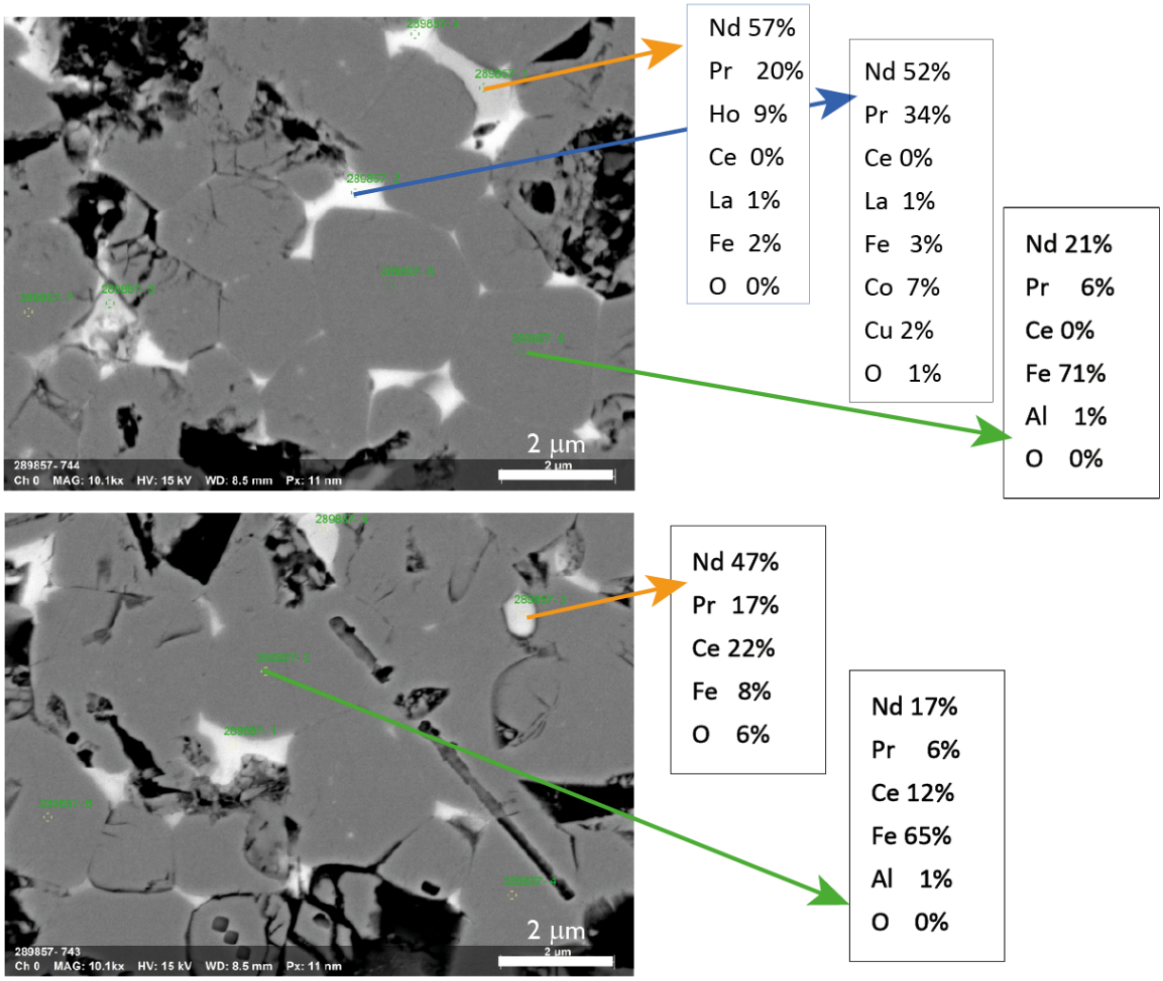


Figure 37. BSE images and EDS point analyses of two magnets (2018Magnet 2 on top and E-Bay Scrap Magnet 1 at the bottom) to visualize differences between the magnets. 2018Magnet2 shows more hexagonal grains in a small range of particle sizes. There are two interstitial phases with different compositions. E-Bay Scrap Magnet 1 has a more irregular grain size and grain shape, and only one interstitial phase, which is rich in Ce.

Internal variation within a magnet and within a batch

The internal variation within the magnets was tested by scanning the samples in two directions with AQM from side to side and performing element mapping for the Nd and Fe concentrations within the magnets. Most magnets are internally homogeneous down to a few wt% in variation, and only one sample displayed a larger deviation than this for some of the magnets. For magnets within the same batch, larger variations were recorded in a few sets, e.g., in magnets of the series NdN45_2022 and NdN35_2023 (Fig. 38).

Variation between batches of magnets

The variation between batches of magnets was found to be larger than the internal variation within batches, and especially larger than the variation within samples. The samples vary in grain size for the ground mass from 1 µm to 5 µm, and they vary in the composition of the ground mass (where the variation is in the Fe:Nd ratio), and especially for the interstitially formed grains rich in REEs (composition and concentration of interstitial material; e.g., one or two phases, presence of Ce, La or Nb, presence of Dy or Ho, amount of Pr, presence and amount of the lighter metals Fe, Cu and Al). There is a concentration

in the grain shape of the ground mass (more or less hexagonal, homogenous or varying grain size) and in the distribution and size of the interstitial phases. Most samples have hole in the sample surface, indicating that material might have been lost during the processing of the samples. An example of the variation is provided in Figure 39 for more details on all samples.

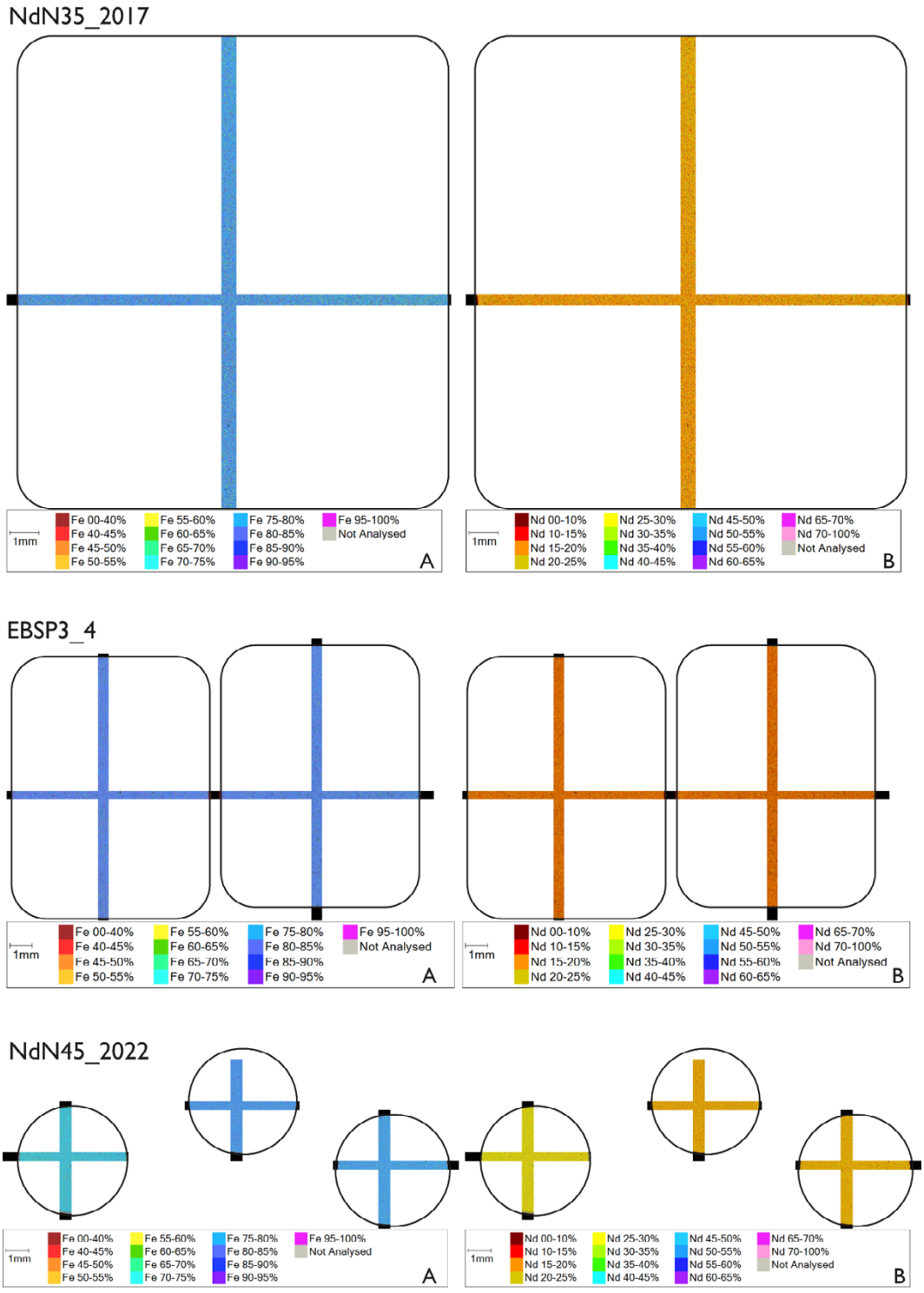


Figure 38. AQM element maps for Fe and Nd in magnets from three selected batches. The approximate shape of the entire magnet is indicated with a black square or circle. Analyses were only performed with one horizontal and one vertical line. Individual magnets are near-homogeneous in composition, but significant differences exist between magnets from the same batch and between batches.

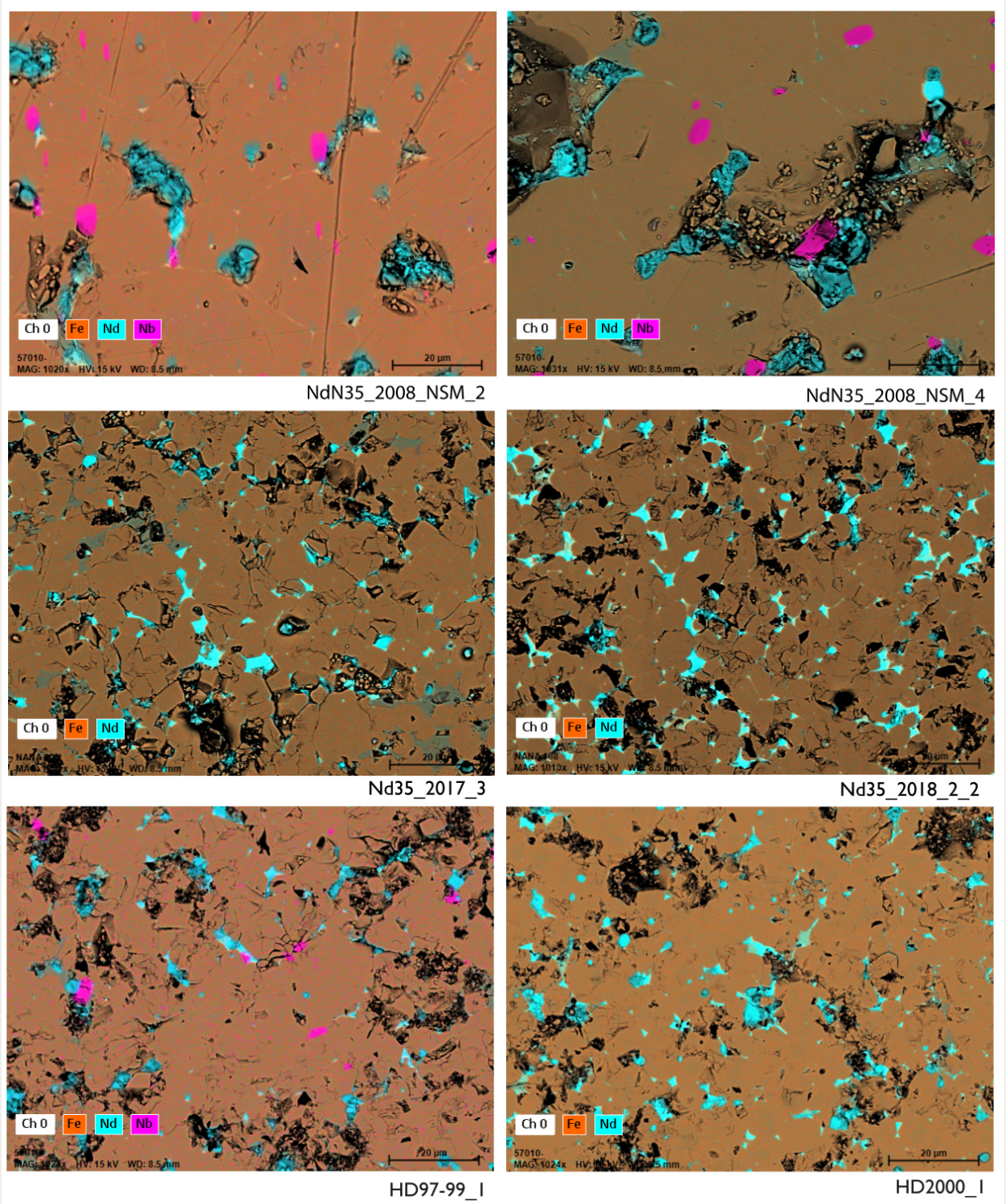


Figure 39. SEM_EDS element maps, showing the maximum signal per pixel (i.e., if Fe is the dominant mineral in a specific picture, only the relative Fe concentration is shown). Therefore orange colours indicate different Fe concentrations, blueish colours indicate different Nd concentrations and pinkish colours show where Nb is high. Note the difference in the distribution of interstitial Nd phases, different grain sizes of the matrix Fe-rich phase and differences in Fe concentrations (intensity of orange colour) between magnets of the same type produced at different times.

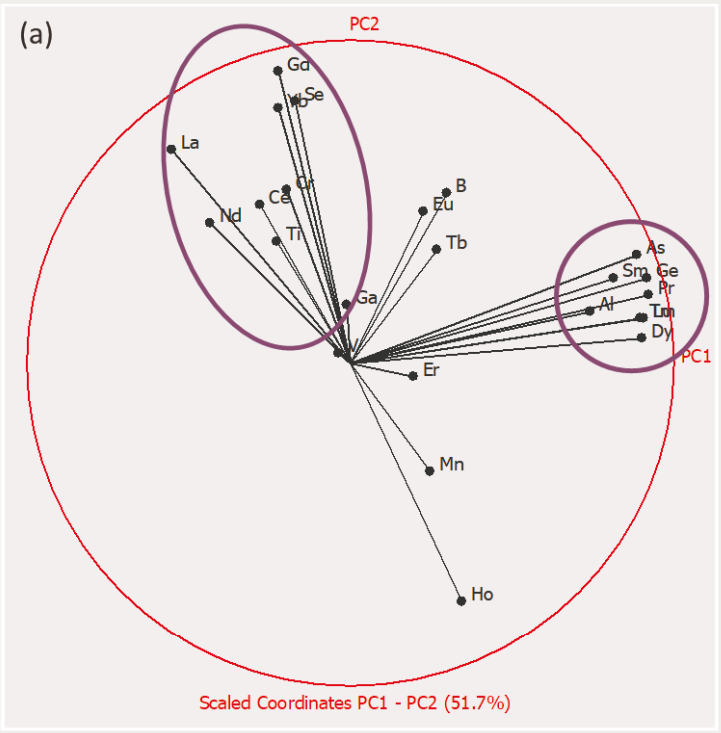
2.3.3 Trace elements

The 255 laser ablation analyses of 9 magnet samples produced in 1997–1999, 2000, 2008, 2012, 2017, 2018, 2021, 2022 and 2023 revealed many elements that have appreciable concentrations in the analysed magnets (Fig. 40). Apart from Nd, Fe and B, other major components (>1000 ppm) include Al, Mn, Cu, Co, Ga, Ge, As, Pr, Gd and Dy. Minor components (>10 ppm) include Ti, V, Cr, Se, Y, Ba, Sm, Tb, Ho and Er. They additionally contain some trace amounts (<10 ppm) of elements such as V, Eu, Tm, Yb, Lu and Pb.

Principle analysis identified two groups of elements that behaved distinctively in the magnets, as encircled in Figure 41a. Using elements from the two groups, discriminating diagrams can be used to differentiate the magnets. In the Al–Gd–Dy ternary plot in Figure 41b, magnets produced before 2012 appear to be enriched in Dy and Al and depleted in Gd, whereas those produced later are enriched in Gd but relatively depleted in Dy and Al. More importantly, the magnets separated very nicely in this compositional plot. This compositional variation indicates that manufacturers at different times used different recipes for producing magnet alloys. Nevertheless, due to the use of substituent and dopant elements in the making of magnets, it is nearly impossible to distinguish elements that were originally derived from Pr–Nd metal materials, and it is thus unlikely that these trace elements could be used to identify the origin of rare earth minerals unless the substituent and dopant elements share the same origin. From a geological perspective, the substituent Gd, Dy, Sm, Tb, Ho and Er may come from the same deposit as Pr–Nd, as they commonly occur together, whereas the other elements are normally not produced in REE mines. It should be noted, however, that the substituent rare earth elements are either monoisotopic or only consist of stable isotopes, meaning that their isotopic compositions in nature remain largely constant and cannot therefore be used for tracing.

It appears that the only information left from the original rare earth minerals is the materials themselves, namely Pr and Nd. Consequently, the ratio of Pr and Nd, as well as the Nd isotope composition, might be the only signatures that can be used as tracers.

Figure 40. A boxplot of element concentrations in the analysed Nd magnets. Note that the colour and shape of the symbols represent the production year and grade.



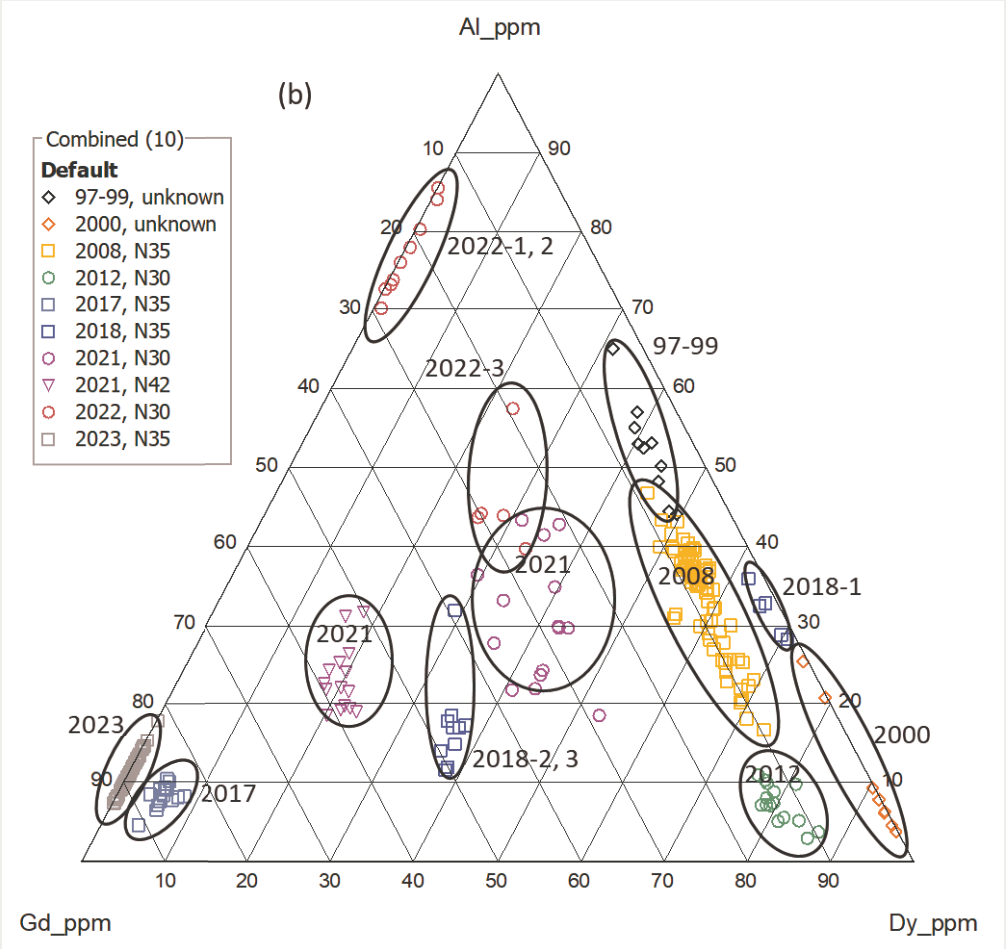


Figure 41. A PCA plot (a) and Al–Gd–Dy ternary plot (b) of trace elements in the Nd magnets examined in this project.

2.3.4 Nd isotopes

The Nd isotope composition of the magnets was determined with laser ablation and solution analysis by MC-ICP-MS. The solution analyses were conducted to determine whether the mineral processing and magnet production processes modify the isotope ratios of $^{146}Nd/^{145}Nd$, which is normally used for correcting instrumental mass bias in MC-ICP-MS. Solution analysis suggested that the magnets had $^{146}Nd/^{144}Nd$ ratios similar to natural Nd (Fig. 42).

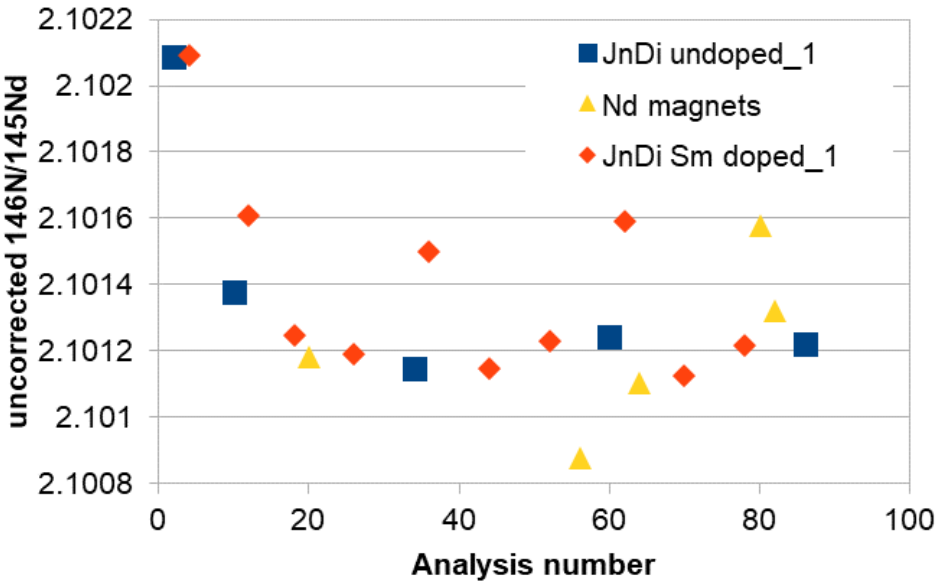


Figure 42. A diagram comparing $^{146}Ndd/^{145}Nd$ ratios between Nd magnets and JnDi

Laser ablation analysis suggested that the analysed magnets, including those with a known production year and scrap magnets, had a wide range of present-day εNd values from -7.5 to -30 (Fig. 43). Before 2012, the magnets had quite distinctive εNd values, with the ones manufactured between 1997 and 1999 having lowest and the ones made in 2008 the highest values. This feature might indicate that these magnets were made from rare earth materials with different origins. Comparing them with major REE-producing deposits around the world, the 1997–1999 magnets were most likely derived from Olympic Dam and Mountain Pass. The 2008 ones are most likely derived from REE clays of South China. The 2000 ones may come from Bayan Obo, or a mixture of Bayan Obo with Mt. Weld and/or Gakara. The 2012 magnets, as well as the ones produced in 2021 and two magnets without production years (EBSP1 and EBSP2), may have come from the same origin as the 1997-1999 magnets. Similarly, the ones made in 2017 and 2023, as well as multiple unknown magnets, might have come from the same origin as the 2008 magnets. The ones made in 2021 and one unknown magnet might have originated from the same source as the 2000 magnets. Examining the Al–Gd–Dy plot, we might infer that the doping recipe may have changed dramatically over the period of 20 years, even though the source of Nd remained the same. The only exception is the magnets manufactured in 2017 and 2023, which had very close doping compositions. This makes sense considering they were also close in production

years. Taking together both the trace element and Nd isotope data, it might suggest that these magnets were made by the same manufacturer, who had purchased Nd metals from three different sources and had changed their recipes multiple times during the past 20 years, and also reused some of the old recipes in a rather random way. Alternatively, it might indicate that these magnets were produced by multiple manufacturers who had different doping recipes.

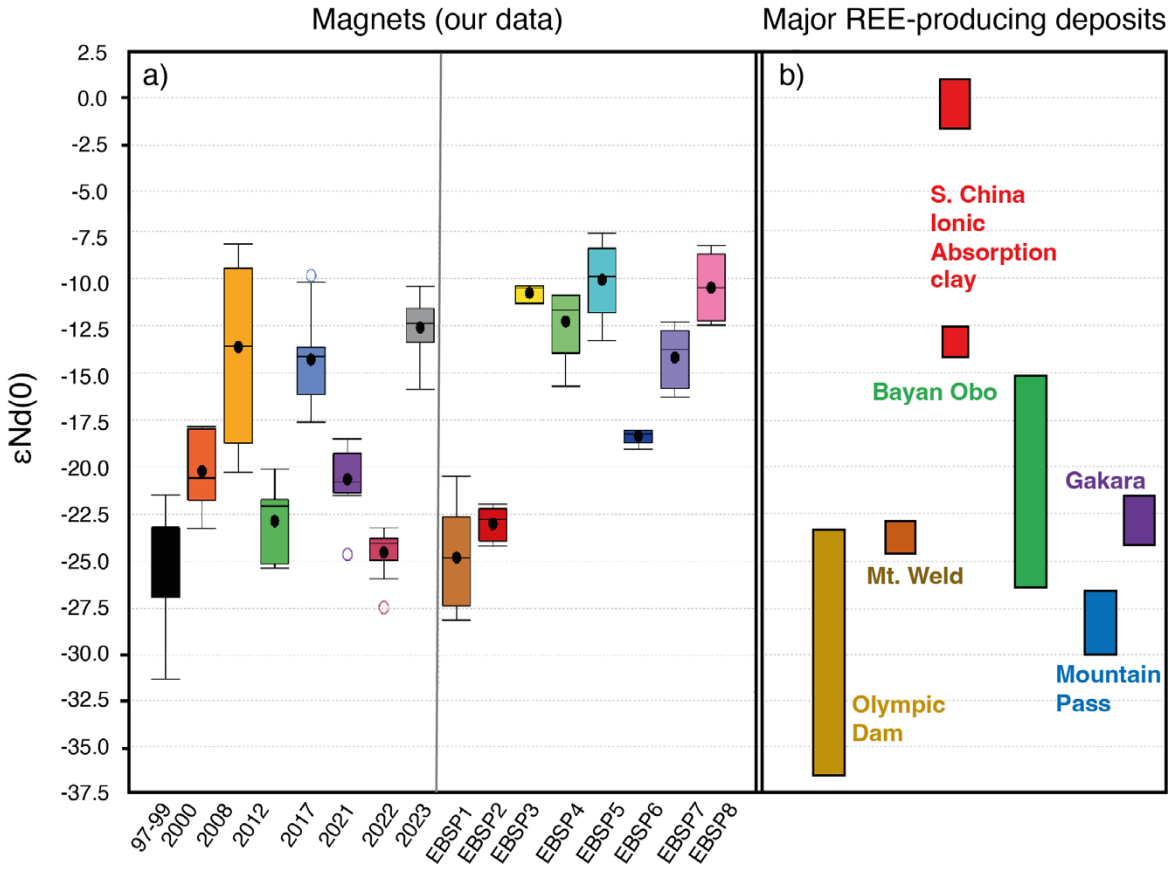


Figure 43. A diagram showing the Nd isotope ratios of Nd magnets compared to major REE-producing deposits. Sources of data are the same as Fig. 29.

3. Discussion

3.1 Feasibility analysis

To a wider extent, certifying an ore deposit or a mine requires full documentation of the mine information, including how it operates, as well as the signature of its ore minerals. As to the former, a few initiatives have aimed to generate certification standards (e.g., CERA 4in1) and novel ways of preserving and transmitting the information (e.g., blockchain). These techniques are well under development. The end results of these initiatives will be solutions for recording, standardizing, validating and verifying the required information for identifying a mine and its metal products. These solutions can help generate a document-based identity comparable to a person's passport. In the meantime, to increase verifiability and reliability, certain geo-signatures should be embedded in the databank of the document-based identity. As demonstrated in the previous sections, the geo-signature(s) should be homogeneous and thus representative, conservative and traceable, as well as unique and thus distinctive.

Homogeneity tests in the NSM project clearly demonstrated that REE deposits are variably heterogeneous in terms of most relevant geo-signatures, such as the mineral association, modal mineralogy, trace elements and isotopes. In general, alkaline intrusion-related REE systems are simpler and more homogeneous compared to carbonatite systems. The fundamental cause of this variability is differences in the mechanism of deposit formation as well as potential post-ore modification processes. Alkaline intrusion systems are commonly simple systems that form via magmatic differentiation at a relatively constant and higher pressure and temperature, whereas carbonatite systems are more dynamic systems that may involve extra magmatic segregation and hydrothermal overprinting at a range of pressures and temperatures. To obtain homogeneity, one needs to consider the so-called geochemical pairs, such as Zr/Hf, Nb/Ta and REE ratios (e.g., Pr/Nd, Sm/Nd), which show similar geochemical behaviours, and thus their ratios are relatively insensitive to variations in external conditions. Alternatively, one may need to narrow down the scope to a specific area and/or a specific ore-forming stage of the deposit, where and when the external conditions are relatively constant. It needs to be pointed out, however, that while some geo-signatures might show variation, the range itself might be unique when compared to other deposits worldwide, and therefore may be considered as a potential traceability indicator.

As to the conservativity of geo-signatures, the test study on eudialyte from Kringlerne clearly yet unsurprisingly revealed that all rock-scale information (e.g., texture, structure) and most of the mineral-scale signatures (textures, shape and size, modal mineralogy) would be eliminated due to crushing and grinding of ores. The mineral association, however, might be preserved at the sub-mineral scale. In the Kringlerne eudialyte concentrates, gangue minerals such as nepheline, arfvedsonite, sodalite and aenigmatite are still seen as individual fragments, aggregates or intergrowth. In terms of trace element signatures, REE oxalates produced from Kringlerne eudialytes principally contain rare earth elements, apart from carbon and oxygen, that are from the

leaching solutions. Other homogeneous elements that previously existed in the eudialytes, such as Zr/Hf, are not detectable with EDS analyses. Even though ICP-MS analyses, having lower detection limits, might detect these traces, most elemental information would generally have been lost in hydrometallurgical refining and separation. Encouragingly, however, the REE ratios (e.g., La/Nd, Pr/Nd) remain largely unaltered due to their very similar geochemical properties. In theory, isotopes are atoms of the same elements with the same number of protons but a different number of neutrons, and isotopes of the same element should therefore exhibit identical chemical behaviour, and their ratios will be very difficult to change. A change or, in scientific terms, fractionation of isotopes may occur in mass-dependent processes such as phase separation at high temperatures. More commonly, isotope ratios change due to radioactive decay of a parent nuclide that generates one of the isotopes. In the case of Nd isotopes, ^{143}Nd is generated by the decay of ^{147}Sm, and the present-day ^{143}Nd/^{144}Nd ratio would therefore be dependent on the time elapsed following the decay and the amount of Sm, or more precisely the Sm/Nd ratio. Analyses of Nd isotopes in REE oxalates revealed nearly comparable ^{143}Nd/^{144}Nd ratios compared to the original eudialyte concentrates. This observation was further verified by our magnet pilot study, in which Nd isotope analyses revealed that the man-made magnets had natural Nd isotopic ratios, for instance ^{146}Nd/^{145}Nd, meaning that the metal refining, alloying and magnet-producing process did not change the isotope compositions.

Our pilot study on Nd magnets, which aimed to evaluate whether it is possible to forensically identify the origin of REE materials used in the making of magnets, revealed dozens of elements with appreciable concentrations. These elements are most likely added to the major components Nd, Nd-Pr, Fe, and B as substituents and dopants during the making of Nd–Fe–B alloys. These added trace elements fall into two broad categories on a PCA diagram, probably attributed to the substitution of the Nd site and Fe site in the magnet formula. In an Al–Gd–Dy ternary plot, magnets produced in different years were clearly distinguished, signalling that the recipe for the substituents and dopants can potentially be used to trace and identify the manufacturer of a certain magnet. There is no direct relationship between the doping recipe and Nd isotope analysis results, but the latter appear to support the view that the Nd metals might have been derived from three different REE deposits.

To briefly summarise, homogeneous geo-signatures might exist at different scales, particularly geochemical pairs and isotope ratios. These geo-signatures would gradually diminish due to physical, chemical and electrolytical treatment during mineral processing and metal refining. The mineral association and some trace element ratios can persist until mineral beneficiation, whereas geochemical pairs (Zr/Hf, Nb/Ta, Pr/Nd, Sm/Nd) can be conservative until hydrometallurgical separation. The only geo-signature that remains unchanged is the Nd isotope ratios, in which ^{143}Nd/^{144}Nd is the most important tracer, whereas the other stable isotope ratios are not important, as they are not indicative of different sources. The use of chemicals in hydrometallurgical purification (e.g., solvent extraction) and the addition of other elements as substituents and dopants in the manufacture of Nd magnets may provide unique opportunities to complement Nd isotopes as traceability indicators.

3.2 Major challenges

In the NSM project, we have undertaken pioneering studies and obtained significant and first-hand knowledge on metal (particularly REE) traceability. Nevertheless, this study should not be considered comprehensive and conclusive. We have faced many challenges that remain to be addressed in future studies, which have many facets but can be categorized into four types.

Sampling

Proper and representative sampling lies at the heart of metal traceability studies, especially concerning homogeneity testing of ore deposits and magnet forensics. As demonstrated in section 2.1, a homogeneity study requires samples that can represent the entire deposit in terms of both space and time. It is by no means an easy task to collect all the necessary samples due to not-unlimited access to the mine site and drill cores, let alone due to some deposits still being in the early phase of exploration and mine development, where only limited samples are available. In the case of Kringlerne, only one sample of eudialyte concentrate was tested, which was Ce-poor, Ca-rich and homogeneous in composition. As such, it is different from eudialyte previously sampled from Kringlerne, in which eudialyte from a range of samples was found to be internally zoned and Ce-bearing (e.g., Borst et al. 2018). Furthermore, the analytical age obtained by LA-ICP-MS was different from that previously reported. This situation also holds for the other three targets, which are nevertheless slightly better. For forensic studies on magnets, obtaining the samples is not usually a problem, but obtaining key product information, such as the supplier or manufacturer, is impossible due to the very fact that these pieces of information are often considered business secrets by magnet traders. The lack of magnet information prohibits the checking and validation of interpretations.

An equally challenging issue exists when obtaining samples from various stages of the value chain, particularly hydrometallurgy and electrolysis. Only a few labs are capable of conducting the experiments, which may take a long time and be expensive, particularly if the studies aim at obtaining samples from the beginning of the value chain until the very end. This literally means a pilot-scale (tons of feeding materials) mineral beneficiation, which typically costs one to two million euros alone. Therefore, a comprehensive and conclusive traceability study would not be possible without comprehensive sampling, which requires long-term, large-scale financial supports.

Analytics

Due to the centuries-long development of analytical geochemistry, most rock and mineral samples can be analysed with fairly good precision and accuracy. Nevertheless, it can be anticipated that discrimination of ore deposits that are formed in proximity in terms of age and the process, for instance those within the same metallogenic belt or district, may require better precision and accuracy than that required by geological applications. This is particularly true for trace element and isotope determination by ICP-MS.

Analytical challenges have been encountered when analysing trace elements and isotopes in Nd magnets by laser ablation ICP-MS. For example, there is a lack of matrix-matched reference materials, resulting in a compromised

accuracy. Furthermore, the grain size of the magnets' ground mass is smaller than the spot of the LA-ICP-MS, and the distribution and composition of the interstitial phases rich in Nd is inhomogeneous, making it difficult to measure these phases. To circumvent this issue, NdFeB reference materials should be produced and characterized.

Social and environmental

The main principle of traceability is that it identifies the source of a commodity along the value chain. Traceability also strongly relies on responsible sourcing. However, REE mine projects at both Norra Kärr in Sweden and Sokli in Finland are contentious and opposed by the local community, ENGOs and reindeer herders because of their potential environmental and social impacts. Both companies operate in sensitive contexts prone to disputes, and the existence of such a dispute may not be good for their reputation. It may also constrain the benefit of their traceability, because appeals due to unsustainable production can be made regarding the projects. Even though production in Nordic countries, known for their high ESG standards, can add value to minerals, their traceability to dispute cases involving impacts on traditional livelihoods, such as reindeer herding in the case of Sokli, can challenge, denigrate and discredit their sustainability. Apparently, the role of local opposition and ENGOs in such cases is an issue that has not previously been discussed in this context.

3.3 Outlook

A metal traceability system is intended to be a sophisticated, scalable and affordable technique, as with any other supply chain traceability system. The development of such a system requires long-term and in-depth investigations. This project represents no more than a proof of concept designed to evaluate the possibility and feasibility of devising a geo-based tracing system, which concluded with a positive and encouraging results. In order to further validate the conclusion of this and preceding research and develop a working metal traceability system, a number of issues need to be considered, besides properly addressing the challenges described above.

Database construction

Due to limited resources, unequal efforts have been made to construct an in-focus, global REE traceability database. This does not disqualify uniqueness as the cornerstone of a traceability technique. Quite the opposite, the importance of having an accurate and thorough database cannot be overstressed. In any future studies on metal traceability, efforts should be made to build a database that covers a wider geography and includes as many REE deposits and prospects as possible. Relevant geo-signatures, particularly the mineral association, geochemical pairs and Nd isotopes, should be compiled as accurately as possible. Where data are lacking, analyses should be carried out to fill the gaps.

Probability modelling and unmixing modelling

Admittedly, this study could have benefited considerably from probability modelling. Such modelling requires the use of statistical and mathematical tools for generating a quantitative assessment of likelihood when comparing a geo-signature with possible sources. This helps to make data interpretation objective and reliable. Future studies should be directed towards this area of research.

It is a common practice for refineries to mix raw materials from different sources in order to improve facility efficiency. Modelling tools and methods should be made available to be able to distinguish different sources. Several software programs exist that have been applied to other fields of research, such as the diet of animals, but few studies have been undertaken to adapt the tools to metal traceability.

Digitalization

To the authors' best understanding, for traceability, geo-signatures need to be digitalized so that they can be recorded, stored and passed along the supply chain, as well as being readable or retrievable in whatever way. This could involve a series of codes that contains key information regarding the deposit and the derivative metals, such as coordinates, trace element ratios and isotope ratios. This coding system needs to be standardized to improve clarity and avoid potential ambiguity. Alternatively, it could simply be a bar code or QR code that is linked to a database that contains all the necessary information. Future studies need to be undertaken to evaluate the different options.

Development of magnet recipes for the dual purposes of doping and tracing

As postulated by this study, the doping elements in Nd magnets, as well as in other rare earth magnets and applications, may offer a unique opportunity for identifying and tracing a REE product, especially considering that the elements are added at a stage when Nd isotopes are the only surviving geo-signature. Since dozens of elements can be added, future studies could investigate how to make these elements useful for traceability purposes and how the modification of the recipe may or may not affect the magnet properties.

4. Conclusion

This proof-of-concept study aimed to explore the potential and feasibility of using geo-signatures as a tracing tool for identifying REE minerals and metals in the entire value chain. It combined a homogeneity test of four REE targets, a conservativity test of geo-signatures during mineral processing and refining, and uniqueness tests at the Nordic level to validate the geo-based traceability concept. The mineral association, some trace element ratios and Nd isotopes can be used for tracing mineral concentrates. Moving down the value chain, geochemical pairs (Zr/Hf, Nb/Ta, Pr/Nd, Sm/Nd) and Nd isotopes can be used for tracing REE compounds, while only $^{143}Nd/^{144}Nd$ can be used for tracing pure Nd and Nd–Pr metals if there are no overlaps with other sources. The use of chemicals in hydrometallurgical purification and the addition of other elements as substituents and dopants in the making of Nd magnets may provide unique opportunities to complement Nd isotopes as traceability indicators.

Acknowledgement

We thank Paavo Nikkola and Sari Lukkari for help with SEM-EDS analysis, Pasi Heikkilä for help with XRD analysis, Ester Jolis for help with µ-XRF, Hugh O'Brien, Minna Myllyperkiö, Matti Kurhila and Meiru Zhou for help with ICP-MS analysis, Seppo Töllikkö, Atte Halmesaari and Katariina Issukka for help with sample preparation, Arvi Arohonka (3R-Cycle oy) for providing services for REE separation, and Nima Hajir Azad for assistance in preparing the figures from the AQM data and EDS element mapping. Hans Kristian Schønwandt is acknowledged for fruitful discussions about the Kringlerne deposit and for the contact with Tanbreez.

Permission to use the REE mineral concentrate from the Kringlerne deposit was kindly granted by Tanbreez. The REE mineral concentrate for the Fen case study was kindly provided by the Norwegian University of Science and Technology, Trondheim, Norway (RareGreen project #21130, co-funded by EIT Raw Materials) and Rare Earth Norway AS. The Sokli samples were kindly provided by Krisztian Szentpeteri. The Norwegian Museum of Natural History in Oslo provided eudialyte samples from the Larvik Plutonic Complex. Sami Pietilä provided Nd magnets produced in the 1990s. Leading Edge Materials Corp. are thanked for supplying concentrates and drill core samples.

Nikolaos Arvanitidis carried out a detailed and critical review of the report, which significantly improved its quality. Päivi Kuikka-Niemi helped to check the reference list and citations. Special thanks to Marita Mutka and Johannes Klein for a great job in managing and organizing the project in the beginning, which laid a solid foundation for the smooth execution of the project until its end. This study has benefited from many people, whose contributions are not directly reflected in this report. We are indebted to our project manager, Lauri Solismaa, communications manager Kati Kiviniemi, and the advisory group consisting of Tommi Kauppila, Soili Solismaa and Asko Käpyaho. In addition, this study has received tremendous support from the WP2 team led by Leonardo Feltrin. This study formed WP1 of the Nordic Sustainable Minerals project (2022–2024), which was kindly funded by Nordic Innovation.

References

Adamas Intelligence 2022. Rare Earth Magnet Market Outlook to 2035. Adamas Intelligence.

Al Ani, T. & Sarapää, O. 2009. Rare earth elements and their mineral phases in Jammi carbonatite veins and fenites on the south side of Sokli carbonatite complex, NE Finland. Geological Survey of Finland, archive report M19/4723/2009/34. 24 p., 2 app. pages. Available at: https://tupa.gtk.fi/raportti/arkisto/m19_4723_2009_34.pdf

Al Ani, T. & Sarapää, O. 2013. Geochemistry and mineral phases of REE in Jammi carbonatite veins and fenites, southern end of the Sokli complex, NE Finland. Geochemistry: Exploration, Environment, Analysis 13(3), 217–224.

Al Ani, T., Heikura, P. & Sarapää, O. 2011. REE-mineralogy and geochemistry of selected drillcores from southern side of Sokli Carbonatite Complex, NE-Finland. Geological Survey of Finland, archive report 24/2011. 25 p. Available at: https://tupa.gtk.fi/raportti/arkisto/24_2011.pdf

Alves Dias, P., Bobba, S., Carrara, S. & Plazzotta, B. 2020. The role of rare earth elements in wind energy and electric mobility. EUR 30488 EN. Luxembourg: Publication Office of the European Union. doi:10.2760/303258, JRC122671

Andersen, T. 1984. Secondary processes in carbonatites: petrology of "rødberg" (hematite-calcite-dolomite carbonatite) in the Fen central complex, Telemark (South Norway). Lithos 17, 227–245.

Andersen, T. 1988. Evolution of Peralkaline Calcite Carbonatite Magma in the Fen Complex, Southeast Norway. Lithos 22, 99–112.

Andersen, T. 1989. Carbonatite-Related Contact Metasomatism in the Fen Complex, Norway – Effects and Petrogenetic Implications. Mineralogical Magazine 53, 395–414.

Banik, T.J., Miller, C.F., Fisher, C.M., Coble, M.A., Vervoort, J.D. 2018. Magmatic tectonic control on the generation of silicic magmas in Iceland: Constraints from Hafnarfjall-Skarðsheiði volcano. Lithos 318-319, 326–339. https://doi.org/10.1016/j.lithos.2018.08.022.

Bergstøl, S. & Svinndal, S. 1960. The carbonatite and per-alkaline rocks of the Fen area. Norges Geologiske Undersøkelse 208, 99–110.

Bohse, H. & Andersen, S. 1981. Review of the stratigraphic divisions of Kakortokite and lujavrite in southern Ilímaussaq. Rapport Grønlands Geologiske Undersøgels 103, 53–62.

Bohse, H., Brooks, C. K. & Kunzendorf, H. 1971. Field observations on the kakortakites of the Ilimaussaq intrusion, South Greenland. Rapport Grønlands Geologiske Undersøgelse 38. 43 p.

Borst, A. M., Friis, H., Andersen, T., Waight, T. E., Nielsen, T. F. D. & Smit, M. 2016. Zirconosilicates in the kakortokites of the Il´ımaussaq complex, South Greenland: implications for fluid evolution and HFSE-REE mineralization in agpaitic sys-tems. Mineralogical Magazine 80, 1–26.

Borst, A. M., Friis, H., Nielsen, T. F. D. & Waight, T. E. 2018. Bulk and Mush Melt Evolution in Agpaitic Intrusions: Insights from Compositional Zoning in Eudialyte, Ilímaussaq Complex, South Greenland. Journal of Petrology 2018, 1–23.

Borst, A. M., Waight, T. E. Finch, A. A., Storey, M. & Le Roux, P. J. 2019. Dating agpaitic rocks: A multi-system (U/Pb, Sm/Nd, Rb/Sr and 40Ar/39Ar) isotopic study of layered nepheline syenites from the Ilímaussaq complex, Greenland. Lithos 324–325 (2019), 74–88.

Bowell, R. J., Chapman, C., McDougall, C., Martindale, R. & Pittuck, M. 2021. Preliminary economic assessment of Norra Kärr rare earth deposit and potential by-products. SRK Consulting (UK) Limited. 328 p.

Brøgger, W. C. 1921. Die eruptivgesteine des Kristianiagebietes, IV. Das Fengebiet in Telemark, Norwegen. Det Norske Videnskaps Akademi i Oslo, Matematisk-naturvitennskapelig klasse 1920 9.

Climate Watch 2023. – with major processing by Our World in Data. Climate Watch, "Greenhouse gas emissions by sector".

Dahlgren, S., Heaman, L. & Krogh, T. 1990. Geological evolution and U-Pb geochronology of the Proterozoic central Telemark area, Norway. Geonytt 17, 38.

Deb, M. & Sarkar, S. C. 2017. How Do Mineral Deposits Form and Transform? A Systematic Approach. Minerals and Allied Natural Resources and their Sustainable Development: Principles, Perspectives with Emphasis on the Indian Scenario, 29–139.

Department of Industry, Science, Energy and Resources 2022. 2022 Critical minerals strategy. Available at: https://www.industry.gov.au/publications/critical-minerals-strategy-2022 [Accessed 29 September 2022]

Desaulty, A. M., Monfort Climent, D., Lefebvre, G., Cristiano-Tassi, A., Peralta, D., Perret, S., Urban, A. & Guerrot, C. 2022. Tracing the origin of lithium in Li-ion batteries using lithium isotopes. Nature communications 13(1), p. 4172.

Eerola, T. 2022. Corporate conduct, commodity, and place. Ongoing mining and mineral exploration disputes in Finland and their implications for the social license to operate. Resources Policy 76, 102568. Available at: https://doi.org/10.1016/j.resourpol.2022.102568

Elliott, H. A. L., Wall, F., Chakhmouradian, A. R., Siegfried, P. R., Dahlgren, S., Weatherley, F., Finch, A. A., Marks, M. A. W., Dowman, E. & Deady, E. 2018. Fenites associated with carbonatite complexes: A review. Ore Geology Reviews 93, 38–59.

European Commission 2020. Critical Raw Materials for Strategic Technologies and Sectors in the EU. A Foresight Study. Brussels: European Commission.

Fidler, J. & Schrefl, T. 1996. Overview of Nd–Fe–B magnets and coercivity. Journal of Applied Physics, 79(8), 5029–5034.

Fisher, C. M., Bauer, A. M., Luo, Y., Sarkar, C., Hanchar, J. M., Vervoort, J. D., Tapster, S. R., Horstwood, M. & Pearson, D. G. 2020. Laser ablation split-stream analysis of the Sm-Nd and U-Pb isotope compositions of monazite, titanite, and apatite–Improvements, potential reference materials, and application to the Archean Saglek Block gneisses. Chemical Geology 539, 119493.

Fitton, J.G., Saunders, A.D., Norry, M.J., Hardarson, B.S., Taylor, R.N. 1997. Thermal and chemical structure of the Iceland plume. Earth Planet. Sci. Lett. 153, 197–208. https://doi.org/10.1016/S0012-821X(97)00170-2.

Fjellborg, D., Beland Lindahl, K. & Zachrisson, A. 2022. What to do when the mining company comes to town? Mapping actions of anti-extraction movements in Sweden. Resources Policy 75, 102514. Available at: https://doi.org/10.1016/j.resourpol.2021.102514

Franzson, H., 1978. Structure and Petrochemistry of the Hafnarfjall-Skarðsheiði Central Volcano and the Surrounding Basalt Succession, W-Iceland. University of Edinburgh.

Garcia-Torres, S., Albareda, L., Rey-Garcia, M. & Seuring, S. 2019. Traceability for sustainability – literature review and conceptual framework. Supply Chain Management, Vol. 24, Issue 1. 85-106. doi:10.1108/SCM-04-2018-0152

Giardina, E. 2013. DNA fingerprinting. In: Maloy, S. & Hughes, K. (eds) Brenner's encyclopedia of genetics. Academic Press.

Gielen, D. & Lyons, M. 2022. Critical materials for the energy transition: Rare earth elements. Abu Dhabi: International Renewable Energy Agency.

Gonçalves, G. O., Lana, C., Scholz, R., Buick, I. S., Gerdes, A., Kamo, S. L., Corfu, F., Marinho, M. M., Chaves, A. O., Valeriano, C. & Nalini, H. A. 2016. An assessment of monazite from the Itambé pegmatite district for use as U–Pb isotope reference material for microanalysis and implications for the origin of the "Moacyr" monazite. Chemical Geology 424, 30–50.

Goodenough, K. M., Schilling, J., Jonsson, E., Kalvig, P., Charles, N., Tuduri, J., Deady, E. A., Sadeghi, M., Schiellerup, H., Müller, A., Bertrand, G., Arvanitidis, N., Eliopolous, D. G., Shaw, R. A., Thrane, K. & Keulen, N. 2016. Europe´s rare earth element resource potential: an overview of metallogenetic provinces and their geodynamic setting. Ore Geology Reviews, 72, 838–856.

Graham, S., Lambert, D. & Shee, S. 2004. The petrogenesis of carbonatite, melnoite and kimberlite from the Eastern Goldfields Province, Yilgarn Craton. Lithos, 76(1–4), 519–533.

Grohol, M. & Veeh, C. 2023. Study on the Critical Raw Materials for the EU 2023 Final Report. Directorate-General for Internal Market, Industry, Entrepreneurship and SMEs.

Harðardóttir S., Matthews, S., Halldórsson, S.A., Jackson, M.G. 2022. Spatial distribution and geochemical characterization of Icelandic mantle end-members: Implications for plume geometry and melting processes. Chemical Geology 604 https://doi.org/10.1016/j.chemgeo.2022.120930.

Harðarson, B.S., Fitton, J.G., Ellam, R.M., Pringle, M.S. 1997. Rift relocation – a geochemical and geochronological investigation of a palaeo-rift in Northwest Iceland. Earth Planet. Sci. Lett. 153, 181–196. https://doi.org/10.1016/S0012-821X(97)00145-3.

Högdahl, K., Andersson, U. B. & Eklund, O. (eds) 2004. The Transscandinavian Igneous Belt (TIB) in Sweden: a review of its character and evolution. Geological Survey of Finland, Special Paper 37. 125 p. Available at: https://tupa.gtk.fi/julkaisu/specialpaper/sp_037.pdf

IEA 2021. The Role of Critical Minerals in Clean Energy Transitions. Licence: CC BY 4.0. Paris: IEA. Available at: https://www.iea.org/reports/the-role-of-critical-minerals-in-clean-energy-transitions

IPCC 2021. Climate Change 2021: The Physical Science Basis. Contribution of Working Group I to the Sixth Assessment Report of the Intergovernmental Panel on Climate Change [Masson-Delmotte, V., P. Zhai, A. Pirani, S. L. Connors, C. Péan, S. Berger, N. Caud, Y. Chen, L. Goldfarb, M. I. Gomis, M. Huang, K. Leitzell, E. Lonnoy, J. B. R. Matthews, T. K. Maycock, T. Waterfield, O. Yelekçi, R. Yu & Zhou, B. (eds)]. Cambridge, United Kingdom and New York, NY, USA: Cambridge University Press. 2391 p. doi:10.1017/9781009157896

IPCC 2022. Climate Change 2022: Impacts, Adaptation and Vulnerability. Contribution of Working Group II to the Sixth Assessment Report of the Intergovernmental Panel on Climate Change [Johnsen, O., Ferrarris, G., Gault, R. A., Grice, J. D., Kampf, A. R. & Pekov, I. V. 2003. The nomenclature of eudialyte-group minerals]. Canadian Mineralogist 41, 785–794.

Jóhannesson B., Th. I. Sigfússon, H. Fransson, Ö. Erlendsson, B.S. Harðarson, E. R, Þórhallsson, Á. B. Árnason, K. Azrague, M. R. K. Wiik, S. Vares, A. Kronlöf, P. Koskinen, Vehmas, T. 2016. GREENBAS: Sustainable Fibres from Basalt Mining. Nordic Council of Ministers 2016. TemaNord 2016:564, ISSN 0908-6692.

Johnsen, O., Ferraris, G., Gault, R. A., Grice, J. D., Kampf, A. R. & Pekov, I. V. 2003. The nomenclature of the eudialyte-group minerals. Canadian Mineralogist 41, 785–794.

Johnsen, O., Grice, J. D. & Gault, R. A. 2001. The eudialyte group: a review. In: Sørensen, H. (ed.) The Ilímaussaq complex, South Greenland: status of mineralogical research with new results. Geology of Greenland Survey Bulletin 190, 65–72.

Johnson, J. P. & McCulloch, M. T. 1995. Sources of mineralising fluids for the Olympic Dam deposit (South Australia): Sm-Nd isotopic constraints. Chemical Geology 121(1–4), 177–199.

Jonsson, E., Harlov, D., Majka, J., Högdahl, K. & Persson-Nilsson, K. 2016. Fluorapatite-monazite-allanite relations in the Grängesberg apatite-iron oxide ore district, Bergslagen, Sweden. American Mineralogist 101, 1769–1782.

Jonsson, E., Nysten, P., Bergman, T., Sadeghi, M., Söderhielm, J. & Claeson, D. 2019. REE mineralisations in Sweden. In: Sadeghi, M. (ed.) Rare earth elements distribution, mineralisation and exploration potential in Sweden. Geological Survey of Sweden, Rapporter & Meddelanden 146, 20–111.

Jonsson, E., Törmänen, T., Keiding, J. K., Bjerkgård, T., Eilu, P., Pokki, J., Gautneb, H., Reginiussen, H., Rosa, D., Sadeghi, M., Sandstad, J. S. & Stendal, H. 2023. Critical metals and minerals in the Nordic countries of Europe: diversity of mineralisation and green energy potential. Geological Society of London, Special Publication 526, 95–152.

Kalvig, P. 2022. Rare Earth Elements (REE) Geology, technologies, and forecast. MiMa rapport 1/2022, 253 p.

Kramm, U., Kogarko, L. N., Kononova, V. A. & Vartiainen, H. 1993. The Kola Alkaline Province of the CIS and Finland: Precise Rb-Sr ages define 380-360 Ma age range for all magmatism. Lithos, 30(1), 33–44.

Krumrei, T. V., Villa, L. A., Marks, M. A. W. & Markl, G. 2006. A 40Ar/39Ar and U/Pb isotopic study of the Ilímaussaq Complex, South Greenland: implications for the 40K decay constant and the duration of magmatic activity in a peralkaline complex. Chemical Geology 227, 258–273.

Lèbre, É., Stringer, M., Svobodova, K., Owen, J. R., Kemp, D., Côte, C., Arratia-Solar, A. & Valenta, R. K. 2020. The social and environmental complexities of extracting energy transition metals. Nature communications 11(1), 1–8.

Lee, M. J., Garcia, D., Moutte, J., Williams, C. T. & Wall, F. M. 2004. Carbonatites and phoscorites from the Sokli Complex, Finland.

Lehmann, B., Nakai, S. I., Höhndorf, A., Brinckmann, J., Dulski, P., Hein, U. F. & Masuda, A. 1994. REE mineralization at Gakara, Burundi: Evidence for anomalous upper mantle in the western Rift Valley. Geochimica et Cosmochimica Acta, 58(2), 985–992.

Li, X. C., Yang, K. F., Spandler, C., Fan, H. R., Zhou, M. F., Hao, J. L. & Yang, Y. H. 2021. The effect of fluid-aided modification on the Sm-Nd and Th-Pb geochronology of monazite and bastnäsite: Implication for resolving complex isotopic age data in REE ore systems. Geochimica et Cosmochimica Acta, 300, 1–24.

Liu, S. L., Fan, H. R., Liu, X., Meng, J., Butcher, A. R., Yann, L., Yang, K. F. & Li, X. C. 2023. Global rare earth elements projects: New developments and supply chains. Ore Geology Reviews, p.105428.

Liu, Z.-C., Wu, F.-Y., Yang, Y.-H., Yang, J.-H. & Wilde, S. A. 2012. Neodymium isotopic compositions of the standard monazites used in U-Th-Pb geochronology. Chemical Geology 334, 221–239.

Ma, Y., Stopic, S. & Friedrich, B. 2019. Hydrometallurgy Treatment of an Eudialyte Concentrate for Preparation of Rare Earth Carbonate. Johnson Matthey Technol. Rev. 63(1), 2–13.

McDonough, W. F. & Sun, S.-S. 1995. The composition of the Earth. Chemical Geology 120, 223–253.

Natural Resources Canada 2021. Canada's critical minerals list 2021. Available at: https://www.nrcan.gc.ca/sites/nrcan/files/mineralsmetals/pdf/Critical_Minerals_List_2021-EN.pdf [Accessed 29 September 2022]

O'Brien, H. & Hyvönen, E. 2015. The Sokli carbonatite complex. Mineral deposits of Finland, 305–325. Elsevier.

Paton, C., Hellstrom, J., Paul, B., Woodhead, J. & Hergt, J. 2011. Iolite: Freeware for the visualisation and processing of mass spectrometric data. Journal of Analytical Atomic Spectrometry 26, 2508–2518.

Pfaff, K., Krumrei, T., Marks, M., Wenzel, T., Rudolf, T. & Markl, G. 2008. Chemical and physical evolution of the 'lower layered sequence' from the nepheline syenitic Ilímaussaq intrusion, South Greenland: Implications for the origin of magmatic layering in peralkaline felsic liquids. Lithos 106, 280–296.

Poletti, J. E., Cottle, J. M., Hagen-Peter, G. A. & Lackey, J. S. 2016. Petrochronological constraints on the origin of the Mountain Pass ultrapotassic and carbonatite intrusive suite, California. Journal of Petrology 57(8), 1555–1598.

RCS Global and ICMM 2017. Blockchain for Traceability in Minerals and Metals Supply Chains. London: Opportunities and Challenges.

Rosa, D., Kalvig, P., Stendal, H. & Keiding, J. K. 2023. Review of Critical Raw Material Resource Potential in Greenland. MiMa rapport 2023/1. 124 p.

Sadeghi, M., Arvanitidis, N. & Ladenberger, A. 2020. Geochemistry of rare earth elements in bedrock and till, applied in the context of mineral potential in Sweden. Minerals 10(4), p. 365.

Sæther, E. 1957. The alkaline rock province of the Fen Area in southern Norway. Trondheim: Det Kgl. Nor. Vidensk. Selsk. Skr. 1957, p. 148.

Saunders, A.D., Fitton, J.G., Kerr, A.C., Norry, M.J., Kent R.W. 1997. The North Atlantic Igneous Province. In: Mahoney, J. J. and M. F. Coffin eds. Large Igneous Provinces: Continental, Oceanic, and Planetary Flood Volcanism, Geophys. Monogr. 100, Am. Geophys. Union, Washington DC, 45–93.

Saxon, M., Leijd, M., Forrester, K. & Berg, J. 2015. Geology, mineralogy, and metallurgical processing. Symposium on critical and strategic materials. British Columbia Geological Survey Paper 2015-3 of the Norra Kärr heavy REE deposit, Sweden.

Schønwandt, H. K., Barnes, G. B. & Ulrich, T. 2016. A description of the world-class rare earth element deposit, Tanbreez, South Greenland. Elsevier: Rare Earth Industry, Chapter 5, 73–85.

Schønwandt, H. K., Barnes, G. B. & Ulrich, T. 2023a. Assimilation and extensive metasomatism of agpaitic rocks from the transitional layered kakortokite, Ilímaussaq Intrusion. South Greenland. Resource Geology 73(1), e12320. Available at: https://doi.org/10. 1111/rge.12320

Schønwandt, H. K., Barnes, G. B. & Ulrich, T. 2023b. Perthite in nepheline syenite from the kakortokite unit in the Ilímaussaq Complex, South Greenlan. Journal of Geosciences 68(2023), 203–211. doi:10.3190/jgeosci.375

Short, M., Apelt, T., Moseley, G., Mounde, M. & La Touche, G. D. 2015. Amended and restated prefeasibility study – NI 43-101 – Technical report for the Norra Kärr rare earth element deposit. GBM Consultants Ltd.

Sjöqvist, A. S. L. 2021. Ample rare elements. A geochemical anomaly in the Earth´s crust at Norra Kärr. PhD thesis, Department of Earth Sciences, University of Gothenburg.

Sjöqvist, A. S. L., Cornell, D. H., Andersen, T., Erambert, M., Ek, M. & Leijd, M. 2013a. Three compositional varieties of rare-earth element ore: eudialyte-group minerals from the Norra Kärr alkaline complex, southern Sweden. Minerals 3, 94–120.

Sjöqvist, A. S., Zack, T., Honn, D. K. & Baxter, E. F. 2020. Modification of a rare-earth element deposit by low-temperature partial melting during metamorphic overprinting: Norra Kärr alkaline complex, southern Sweden. Chemical Geology 545, p. 119640.

Sjöqvist, A., Leijd, M., Jonsson, E. & Andersson, U. B. 2013b. The Norra Kärr REE-Zr project. In: Jonsson, E. et al. (eds) Mineral Deposit Research for a high-tech world. 12th Biennial SGA Meeting. Excursion Guide Book SWE3, SWE6 & SWE7, 36–48.

Sovacool, B. K., Ali, S. H., Bazilian, M., Radley, B., Nemery, B., Okatz, J. & Mulvaney, D. 2020. Sustainable minerals and metals for a low-carbon future. Science 367(6473), 30–33.

Sungha, K. 2012. A Short Review on Basalt Fiber. International Journal of Textile Science 2012, 1(4): 19-28. DOI: 10.5923/j.textile.20120104.02.

Temper, L., del Bene, D. & Martinez-Alier, J. 2015. Mapping the frontiers and front lines of global environmental justice: the EJAtlas. Journal of Political Ecology 22, 255–278. Available at: https://doi.org/10.2458/v22i1.21108

Thirlwall, M.F., Gee, M.A.M., Taylor, R.N., Murton, B.J., 2004. Mantle components in Iceland and adjacent ridges investigated using double-spike Pb isotope ratios. Geochim. Cosmochim. Acta 68 (2), 361–386. https://doi.org/10.1016/S0016-7037(03)00424-1.

Törnebohm, A. E. 1906. Katapleiit-syenit, en nyupptäckt varietet af nefelinsyenit i Sverige. Sveriges geologiska undersökning C 199, 1–54.

UN Global Compact Report 2014. A Guide to Traceability: A Practical Approach to Advance Sustainability in Global Supply Chains. Available at: https://www.unglobalcompact.org/library/791

Upton, B. G. J. 2013. Tectono-magmatic evolution of the younger Gardar southern rift, South Greenland. Geological Survey of Denmark and Greenland, Bulletin 29. 124 p.

Van Den Brink, S., Kleijn, R., Tukker, A. & Huisman, J. 2019. Approaches to responsible sourcing in mineral supply chains. Resources, Conservation and Recycling 145, 389–398.

Vartiainen, H. & Paarma, H. 1979. Geological characteristics of the Sokli carbonatite complex, Finland. Economic Geology 74(5), 1296–1306.

Vartiainen, H. & Wooley, A. R. 1976. The petrography, mineralogy and chemistry of the fenites of the Sokli carbonatite intrusion, Finland.

Vartiainen, H. 1980. The petrography, mineralogy and petrochemistry of the Sokli carbonatite massif, northern Finland. Geological Survey of Finland, Bulletin 313. 126 p. Available at: https://tupa.gtk.fi/julkaisu/bulletin/bt_313.pdf

Watne, T. 2023. The Fen Carbonatite complex in Telemark, Norway. A potential European source of rare earth elements. Oral presentation given at the Fennoscandian Exploration and Mining in Levi, Finland, 1st November 2023.

White, W. M. 2020. Geochemistry. John Wiley & Sons.

Yang, Y. H., Wu, F. Y., Li, Q. L., Rojas-Agramonte, Y., Yang, J., H., Li, Y., Ma, Q., Xie, L. W., Huang, C. & Fan, H. R. 2019. In situ U-Th-Pb dating and Sr-Nd isotope analysis of bastnäsite by LA-(MC)-ICP-MS. Geostandards and Geoanalytical Research 43, 543–565.

Table of figures

Figure 1.	Generic diagram showing the primary value chain of REEs from mine to finished product. The upstream activities (in blue) are generally performed in or near the mining facility. The mid- and downstream activities (in red) involve advanced processing stages, each handled by companies specializing in that particular phase. These steps are primarily dominated by Chinese companies. Figure from Kalvig (2022).	8
Figure 2.	Location of very large to medium-sized deposits of REE resources in the Nordic countries. Case study deposits in this project are mentioned on the map.	10
Figure 3.	A schematic diagram showing that external stakeholders, including the general public, governments, international organizations and non-government organizations, are exerting pressure on supply chain participants for transparency, which can only be achieved using traceability techniques.	11
Figure 4.	Geo-chemical analysis techniques ranked according to their cost and value information (a) and their spatial resolution and detection limit (b). Figures from von der Heyden et al. (2020), originally adapted, respectively, from Becker et al. (2016) and from Reich et al. (2017) and Stromberg et al. (2019).	16
Figure 5.	Schematic diagrams showing the general concept of metal traceability (a), a theoretical framework for performing the proof of concept (b), and an analytical framework for rare earth elements in the Nordic Sustainable Minerals project (c).	17
Figure 6.	A diagram of the geo-certification methodology for the Nordic Sustainable Minerals project, illustrating the workflow for producing a lab-scale REE value chain, the sampling strategy and the analytical measurements in relation to the three traceability requirements. See the text for details.	19
Figure 7.	A schematic diagram showing the primary value chain (in blue) from mineral exploration to magnet use design, the secondary chain for tailings and side streams (in dark blue), the re-use/repurposing chain (in brown), the recycling chains (in green) and the waste chain (in red). In this project, the NSM traceability methodology (highlighted with red fingerprints) was applied at the mining stage (REE ore) and to finished magnets and scrap magnets.	20
Figure 8.	A geological map of the Ilímaussaq Complex showing the location of the Kringlerne deposit to the south. From Upton (2013).	21
Figure 9.	Composition of the eudialyte concentrate – EURARE project (Ma et al. 2019).	22
Figure 10.	Backscattered electron (BSE) images of eudialyte studied by Borst et al. (2018) displaying various types of typical zonation in the ore mineral from the Kringlerne deposit. a) A sector-zoned eudialyte crystal with overgrowth at the rim of the crystal, sample from the black kakortokite sublayer; b) Subhedral eudialyte with a sector-zoned core, sample from the white kakortokite sublayer; c) Complex sector and oscillatory zonation, sample from the red kakortokite sublayer. Abbreviations: Arf = arfvedsonite, EGM = eudialyte group mineral. Figure modified from Borst et al. (2018).	23
Figure 11.	SEM-AQM mineral map of the Kringlerne eudialyte concentrate. 93% of the sample consists of Ca eudialyte.	24
Figure 12.	Backscattered electron (BSE) image of the studied eudialyte concentrate from Kringlerne (sample ID 202202193).	25
Figure 13.	SEM-AQM element map of the Kringlerne eudialyte concentrate. Eudialyte grains are internally homogeneous for their major cations, a) Na, b) Ca, c) Si and d) Zr.	26

Figure 14.	Boxplot showing a comparison between the mineral concentrate analysed and literature results from Kringlerne (Borst et al. 2018). Normalising values are the chondritic values of McDonough and Sun (1995), whereas the anomalies are calculated using the neighbouring elements, namely and , where the subscript N indicates normalisation to chondritic values.	27
Figure 15.	Rare element fractionation trends as suggested by Borst et al. (2018). Sample ID 202202193 also displays a positive and negative trend, possibly related to the position of the analysis during the laser ablation experiment. Density plots illustrate subtle variation in the and ratios. Normalising values are the chondritic values of McDonough and Sun (1995).	28
Figure 16.	Variation in the ratios Ta_N/La_N, La_N/Sm_N and Gd_N/Lu_N through the kakortokite–lujavrite sequence compared to the data of Pfaff et al. (2008).	28
Figure 17.	A) Initial εNd values compared to literature data for the layered kakortokites. Khibina and Lovozero have also been plotted for comparison. B) Reproducibility of analysis by laser ablation MC-ICP-MS. Mean data from Borst et al. (2019) are also presented to allow comparison between TIMS and laser data.	29
Figure 18.	Geological map of Norra Kärr. (Source: Saxon et al. 2015)	31
Figure 19.	A box & whisker plot of all elements analysed by LA-ICP-MS. The x-axis and y-axis present the element and concentration in ppm, respectively. The colour of the box corresponds to the colour of the symbol in the legend.	36
Figure 20.	Selected homogeneous trace element bi-variate plots for eudialyte of the Norra Kärr deposit	37
Figure 21.	Simplified geological map of the Fen complex, showing the location of the samples used in this study and examples of the REE-bearing minerals analysed.	38
Figure 22.	Compositional variation in REE-F-carbonates. a) TREO+Y_2O_3 versus Eu anomaly. b) Strontium versus Eu anomaly.	40
Figure 23.	Monazite compositional variations. a) Strontium versus uranium concentrations. b) Strontium versus yttrium.	41
Figure 24.	a) Average epsilon neodymium value for REE-F-carbonates in the Fen Fe-dolomite carbonatite. n = number of analyses. b) Neodymium isotopic composition of REE-F-carbonate and monazite from various REE deposits around the world.	42
Figure 25.	A geological map of the Sokli P–REE–Nb deposit (modified from the data of the Finnish Minerals Group)	44
Figure 26.	The Sokli mine project and surrounding protected areas in Savukoski, Eastern Lapland.	45
Figure 27.	A box plot of trace elements in apatite of the Sokli deposit	47
Figure 28.	Trace elements and ratios of the Sokli apatite analysed by LA-ICP-MS	49
Figure 29.	Map showing the names of key topographical features in the area of the Hafnarfjall-Skarðsheiði central volcano. Inset: simplified geological map of Iceland. The red box indicates the setting of the volcano.	51
Figure 30.	Simplified geological map of the Hafnarfjall-Skarðsheiði central volcano showing the extent of main eruptive phases. Note the Brekkufjall phase. The black box indicates the approximate location of the stratigraphical unit of interest.	52
Figure 31.	(a) Sample BTR-5. Photomicrograph showing a fine-grained andesite with flow-aligned groundmass and microcrystic plagioclase laths in plane polarized light. The black dots show the interspersed opaque minerals and the brownish grains are pyroxene. A vesicle filling in lower left corner with quartz and clay (probably mixed layer clay). (b) TAS classification plot showing the compositional variation within the Brekkufjall Phase of the Hafnarfjall-Skarðsheiði central volcano. The blue square denotes the basaltic andesite of BTR-5.	53

Figure 32.	A 3D relative elevation map of the southern half of the stratigraphical unit of interest (A). Also shown is the location of the electrical substation.	54
Figure 33.	Whole-rock eNd_t versus $^{87}Sr/^{86}Sr$ for basalt and related rocks from the North Atlantic Igneous Province (NAIP) and Iceland. The Iceland array is defined by the compositional domains labelled PB (picrites), OT (olivine tholeiites), QT (quarts tholeiites) and AB (alkali basalt). B. The same as A, but showing the complete range for the NAIP. From Saunders et al. (1997). C. Whole-rock eNd versus eHf in the volcanics from the Hafnarfjall -Skarðsheiði central volcano plotted against the Iceland array (see key for details). Also indicated is the terrestrial array (Banik et al. 2018).	57
Figure 34.	Whole-rock Zr/Y versus Nb/Y from basalts within the neovolcanic zones of Iceland defining the Iceland array. Also shown for comparison are the compositional fields for Zr/Y versus Nb/Y in other parts of the NAIP and MORB.	58
Figure 35.	Sm–Nd diagrams showing the evolution of terrestrial Nd isotopes, with REE targets of this project and major REE deposits around the world. The data for major REE deposits are from the following references: Mountain Pass (Poletti et al. 2016); Bayan Obo (Li et al. 2021); Gakara (Lehmann et al. 1994); Olympic Dam (Johnson & McCulloch 1995); Mountain Weld (Graham et al. 2004).	60
Figure 36.	Images of selected samples of magnets with a known production year and without production information	62
Figure 37.	BSE images and EDS point analyses of two magnets (2018Magnet 2 on top and E-Bay Scrap Magnet 1 at the bottom) to visualize differences between the magnets. 2018Magnet2 shows more hexagonal grains in a small range of particle sizes. There are two interstitial phases with different compositions. E-Bay Scrap Magnet 1 has a more irregular grain size and grain shape, and only one interstitial phase, which is rich in Ce.	63
Figure 38.	AQM element maps for Fe and Nd in magnets from three selected batches. The approximate shape of the entire magnet is indicated with a black square or circle. Analyses were only performed with one horizontal and one vertical line. Individual magnets are near-homogeneous in composition, but significant differences exist between magnets from the same batch and between batches.	64
Figure 39.	SEM_EDS element maps, showing the maximum signal per pixel (i.e., if Fe is the dominant mineral in a specific picture, only the relative Fe concentration is shown). Therefore orange colours indicate different Fe concentrations, blueish colours indicate different Nd concentrations and pinkish colours show where Nb is high. Note the difference in the distribution of interstitial Nd phases, different grain sizes of the matrix Fe-rich phase and differences in Fe concentrations (intensity of orange colour) between magnets of the same type produced at different times.	65
Figure 40.	A boxplot of element concentrations in the analysed Nd magnets. Note that the colour and shape of the symbols represent the production year and grade.	67
Figure 41.	A PCA plot (a) and Al–Gd–Dy ternary plot (b) of trace elements in the Nd magnets examined in this project	68
Figure 42.	A diagram comparing $^{146}Ndd/^{145}Nd$ ratios between Nd magnets and JnDi	69
Figure 43.	A diagram showing the Nd isotope ratios of Nd magnets compared to major REE-producing deposits. Sources of data are the same as Fig. 29.	70

Appendices

Appendix 1. Sample preparation and analytical method

A1.1 Mineral beneficiation of the Kringlerne sample 202202193

The sample, originally provided by the company Tanbreez, was processed to produce a Kringlerne eudialyte concentrate as part of the EURARE project. The rock ore sample was crushed to -1.5 mm and classified by sieving into the size fractions of +0.5 mm, -0.5+0.355 mm, -0.355+0.25 mm and -0.25+0.125 mm. The fractions of the sample were separately processed by dry high intensity magnetic separation (DHIMS) to separate the rare earth minerals (mainly eudialyte) from other gangue minerals. The process included two stages. First, the sample of each fraction was processed at a lower field intensity (~0.6 Tesla) and the iron-containing minerals, such as aenigmatite and arfvedsonite, which are more magnetic than eudialyte, were separated as the tailings. The concentrate from the first stage was further processed at a higher field intensity (>0.7 Tesla). The non-magnetic minerals with diamagnetism, such as albite and nepheline, were removed and the eudialyte concentrates were obtained.

A1.2 Micro-XRF and mineral identification

The first geochemical survey for Sc mineral locations was performed using the micro-X-ray fluorescence (μ-XRF) spectrometer system M4 Tornado plus instrument from Bruker at the Geological Survey of Finland (GTK). The instrument is equipped with an Rh X-ray 30-Watt Rh anode target, two simultaneously operating 30 mm^2 XFlash® silicon drift detectors (SDD) with an energy resolution of <145 eV at 275 kcps (measured on MnKα) via beryllium windows and poly-capillary optics. Scanning and sample navigation is carried out via a motorized stage that moves the sample beneath the static X-ray beam. No sample preparation was needed. All data acquisition was performed with an accelerating voltage of 50 kV and a beam current of 600 μA, using a fixed spot size of 20 μm under 2 mbar vacuum. The samples were mapped in separate runs using a step size of 20 μm and a pixel dwell time of 20 ms/pixel.

We used the Advanced Mineral Identification and Characterization System (AMICS) to conduct the μ-XRF mineral identification. The M4 Tornado Plus is equipped with AMICS software, which allows mineral identification using μ-XRF datasets. The collected X-ray spectral data are evaluated and compared with a reference list of known mineral spectra, using χ2 fingerprinting for a best-match mineral classification. Mineral classification can be further refined using various clustering techniques and/or manual manipulation and evaluation of XRF spectral attributes, and the data repeatedly reclassified to resolve unclassified X-ray points (unknowns). The final product is a mineral-class map with one mineral-class label (single or specific mineral mixture) per pixel, which allows us to quantify mineral properties such as abundance and size, as well as association.

A1.3 Backscattered electron and electron micro-probe analysis

At GTK, backscattered electron (BSE) images were obtained at the SEM Laboratory in Espoo using a Hitachi SU3900 scanning electron microscope equipped with an Oxford Instruments EDS-spectrometer X-Max 20 mm^2 (SDD).

Spot analysis and WDS imaging were performed with a JEOL JXA-iHP200F field-emission electron microprobe analyser (FEG-EMPA) at the Geological Survey of Finland (GTK) using wavelength-dispersive spectrometry (WDS). The accelerating voltage and beam current were set to 15 kV and 20 nA for the spot measurements. A defocused beam diameter set to 5 µm was used and for apatite set to 10 µm. Test measurements were performed to ensure that the set conditions did not cause element migration during apatite measurements. The analytical results have been corrected using the XPP on-line correction program (Pouchou & Pichoir 1991). Natural and synthetic minerals and metals were used as standards, and a detailed description of standards and measurement settings can be found in the supplementary information. The relative accuracy has been determined by measuring selected standards as unknowns and is better than 3% for major elements and better than 5% for minor elements.

Element mapping was performed on the same instrument using a 20 kV accelerating voltage, 100 nA beam current and a focused beam. The dwell time per pixel was set to 50 ms. The elements were assigned on the spectrometers to have only two sweeps per image with the beam sensitive elements F, Ca, K and Na set to the first sweep. The images were quantified using the XPP online correction program (Pouchou & Pichoir 1991) and the background was determined using the mean atomic number (MAN) correction method (Donovan & Tingle 1996). More information can be found in the supplementary information.

At GEUS, samples were imaged by applying a backscattered electron (BSE) detector. Analyses are typically performed on polished surfaces and result in a greyscale image. The signal emitted by the individual phases is mainly dependent on the average atomic number and density of the phases that are imaged. A dense, heavy material has a higher electron density and therefore yields bright values on a greyscale image, while phases with mainly light elements appear dark in this image. The BSE images were used to guide the laser-ablation analyses for trace elements and also Nd isotopes.

Chemical analyses can be performed with one or more energy dispersive spectroscopy (EDS) detectors. Interaction of the primary electron beam from the SEM with the sample causes the emission of secondary electrons from the sample. If an inner shell electron is removed from the atom, one of the other shell electrons will translocate to the inner shell, and the energy of this shell transition is emitted as an X-ray. The energy of this X-ray photon is dependent on the distance between the two shells, and this distance is characteristic of the atom. By measuring the specific energy of this X-ray photon, it can be assigned to a specific element and thus be used to quantify the chemistry of the sample. EDS analyses are typically performed manually, by setting points on features of interest in the sample, but a scan for all elements present in a predefined area on the surface of the sample can also be performed, referred to as element mapping.

BSE imaging and EDS analyses can be combined and automated as automated quantitative mineralogy (AQM). For SEM-AQM analyses, a mosaic of BSE frames of a representative part of the sample is taken. Each frame in the mosaic is thereafter analysed with EDS detectors in a grid with a user defined step size of 20 µm between EDS analytical spots. Each analysis is completely deconvoluted and the resulting chemistry for the pixel is returned to the software, which is then interpreted as a mineral species and assigned a colour: this is then one pixel in the false-coloured mineral map/phase map. The classification of phases is operator-based. As a second step, classification schemes for element mapping were performed for Na, Ca, Zr and Si. Further details of the software and applied method can be found in Keulen et al. (2020). Analyses were performed with acceleration voltages of 15 kV, a 120 μm^2 aperture and an EDS throughput rate of 275 kcps/detector.

A1.4 LA-ICP-MS analysis

Trace element analyses were performed using a double-focusing single collector inductively coupled plasma mass spectrometer (ICP-MS) (AttoM, Nu Instruments Ltd., Wrexham, UK) coupled with an Analyte 193 nm ArF excimer laser-ablation system (Photon Machines, San Diego, USA) housed at the Espoo Research Lab of the Geological Survey of Finland (GTK). Samples were ablated in a helium (He) atmosphere (0.4 to 0.1 L/min) within a HelEx two-volume ablation cell, and the ablated aerosol was carried with a He flow mixed with Ar (gas flow = 0.85–0.95 L/min) prior to entering an ICP. The gas mixture was optimized daily for maximum sensitivity. The laser was set to output 5 mJ energy with 2–5% variation. The laser energy delivered to the samples was set between 30% and 80% for different minerals to achieve optimum ablation. By focusing on a 30 µm to 60 µm circular spot, the laser generated 2–8 J/cm^2 fluence. In general, ferromagnesian silicates, oxides, carbonates, phosphates, sulphides and sulphates were ablated with lower fluence, whereas feldspars and fluorite were ablated with high fluence. The laser was run at a pulse frequency of 5 Hz for 200 shots. Each measurement was initiated with a 20-second baseline measurement followed by switching on the laser for 40 seconds for signal acquisition. Analyses were conducted using time resolved analysis (TRA) with continuous acquisition of data for each point (generally following the scheme of primary standard, quality control standards, 10–20 unknowns). For all mineral phases except sulphides, USGS basaltic glass GSE-2g was used as the primary standard. BHVO-2g, BCR-2g and NIST610 were used as quality controls for all except rutile and monazite, in which matrix-match standards were used, i.e., R10 and TS-MNZ, respectively. For sulphides, FeS1 was used as the primary standard and FeS5 and FeS6 as the quality controls.

Data reduction was performed with GLITTER4.4.4 software, and reference values for the aforementioned standards were taken from GeoReM. Internal standards were a major element that had been measured by electron microprobe or EDS or using the stoichiometric value if the former two analyses were not available.

At NGU, trace elements in bastnasite, parasite, synchisite and monazite were collected by LA-ICP-MS at the Norwegian Laboratory for Mineral and Materials Characterisation (MiMaC) of the Norwegian Geological Survey (NGU). We used a Photon Machines Analyte Excite 193 nm excimer laser coupled to an Agilent 8900 Triple Quadrupole ICP-MS. We used an energy of 4 J/cm^2,

a repetition rate of 5 Hz and a spot size of 10 um. Ablations were carried out for 40 s, followed by 5 s of washout and 30 s of baseline measurements. Ablations were carried out in a He atmosphere and the sample aerosol was transported to the ICP-MS by a He carrier gas, with additional Ar added to the He sample in a mixing bulb before the plasma torch. The conditions were optimized on a daily basis and the total He was approximately 0.75 L/min. All isotopes were measured with integration times between 0.005 and 0.0065 s.

We used common reference glasses as primary and secondary reference materials. These glasses were NIST610, NIST 612, GSE and GSD. Data reduction was performed in iolite 4 (Paton et al. 2011) with the 3D trace element data reduction scheme. First, the on-peak baselines are subtracted from each channel using the automatic spline fit. We mostly used NIST610 as a primary reference material, but for some elements we used a calibration curve based on some or all of the glass reference materials. We used ^{140}Ce for internal standardisation using stochiometric amounts for each mineral and the GeoReM preferred values for the glasses.

A1.5 Solution MC-ICP-MS

Solution analysis of Sm–Nd isotopes in Kringlerne eudialyte, Norra Kärr eudialyte wet ores, REE oxalate and Nd magnets were carried out with a Neoma MS/MS MC-ICP-MS, coupled to a Teledyne (Photo Machine) Analyte Excite 193 nm excimer laser at GTK's Espoo Research Lab. The Neoma instrument was only installed in mid-June, so the data quality might suffer from poor tuning.

Kringlerne eudialyte samples consisted of pure mineral separate hand-picked from eudialyte concentrates produced through magnetic separation (Appendix 1). Norra Kärr wet ores were fine-grain powdered materials contained in water. REE oxalate consisted of fine powders produced from Kringlerne eudialyte concentrates through chemical leaching. Magnet powders were milled from Nd magnet blocks with drilling. Between 120–200 mg of powdered silicate and magnet sample and about 5 mg of REE oxalate samples were spiked with a ^{149}Sm–^{150}Nd tracer. The sample–spike mixture was dissolved in HF-HNO_3 in sealed Teflon bombs in an oven at 180 °C (felsic rocks) or in Savillex screw-cap beakers on a hot plate (mafic rocks) for 48 hours. Prior to dissolving the residue in 6.2 N HCl, the fluorides were gently evaporated using HNO_3. Conventional cation exchange chromatography was used for separation of the light rare earth elements, and Sm and Nd were separated by a modified Teflon-HDEHP (hydrogen di-ethylhexyl phosphate) method. The total procedural blank was <0.6 ng for Nd and <1.2 ng for Sm. The sample was diluted down to 100 ppb Nd and Sm in a disposable 2-mL beaker in 1.5 mL 2% HNO_3. Sm and Nd were separated through ion exchange using AG50W-X12 resin.

Nd isotopes were measured with a static mode on the Neoma. Before measurement, the sensitivity was maximized and accuracy was monitored with JnDi-1. Nine masses, ^{142Nd}, ^{143}Nd, ^{144}(Nd+Sm), ^{145}Nd, ^{146}Nd, ^{148}Nd, ^{150}Nd, ^{147}Sm and ^{149}Sm, were monitored with Faraday cups and 10^{11} ohm resistors. Data reduction was performed with a built-in evaluation program in Qtegra, which handles Sm interference with ^{147}Sm assuming a natural abundance. Mass bias correction was performed with internal normalization to a ^{146}Nd/^{144}Nd ratio of 0.7219, assuming an exponential law.

A1.6 LA-MC-ICP-MS

At GTK, Nd isotopes of Kringlerne eudialyte and Nd magnets were collected using a Nu Plasma multi-collector inductively coupled plasma mass spectrometer (MC-ICP-MS) coupled with a Photon Machines Analyte G2 193 nm excimer laser. For eudialyte and magnets, the laser was run with a raster scan mode at an energy of 5 J, 50–30% output, a repetition rate of 10 and 5 Hz, and a spot size of 110 µm and 50 µm. Analysis started with 5–10 seconds of preablation, followed by 20 s of washout and 20 s of baseline measurements. Ablations were carried out in a He atmosphere and the sample aerosol was transported to the ICP-MS by a He carrier gas, with additional Ar as the makeup gas to improve sensitivity before entering plasma torch. The conditions were optimized on a daily basis and the total He varied between 0.3 and 0.5 L/min. The multicollector was run in a static mode with a low mass resolution (Δm/m = 400). Masses of ^{143}Nd, ^{144}(Nd+Sm), ^{145}Nd, ^{146}Nd, ^{147}Sm and ^{149}Sm were monitored with six Faraday cups. Before analysis, the instrument was tuned to maximum sensitivity and good accuracy with an in-house eudialyte standard (KHI-EUD, which is a eudialyte megacrystal from the Khibiny complex, ^{143}Nd/^{144}Nd: 0.512906). The same KHI-EUD was analysed twice before and after a block of five unknowns.

Data reduction was performed with an in-house spreadsheet, which conducts baseline subtraction, isobaric interference removal and mass bias correction. To remove isobaric interference of ^{144}Sm on ^{144}Nd, the Sm mass fractionation is calculated with an exponential law based on the ^{147}Sm/^{149}Sm ratio of 1.0868. For magnets, ^{142}(Nd+Ce), ^{143}Nd, ^{144}(Nd+Sm), ^{145}Nd, ^{146}Nd, and ^{147}Sm were monitored with six Faraday cups. The multicollector was run in a static mode with a low mass resolution (Δm/m = 400). Before analysis, the instrument was tuned to maximum sensitivity and good accuracy with Bananeira and Coqueiro monazites (Gonçalves et al. 2016).

Sm–Nd isotopes in apatite from Sokli and eudialyte from Norra Kärr were analysed with a Neoma MS/MS MC-ICP-MS coupled to a Teledyne (Photo Machine) Analyte Excite 193 nm excimer laser. The laser was run in a raster scan mode at an energy of 5 J, 40% output, a repetition rate of 10 and 5 Hz, and a spot size of 110 µm. Analysis started with 5–10 seconds of preablation, followed by 20 s of washout and 20 s of baseline measurements. The Neoma was run in a static mode and monitored nine masses, ^{142Nd}, ^{143}Nd, ^{144}(Nd+Sm), ^{145}Nd, ^{146}Nd, ^{148}Nd, ^{150}Nd, ^{147}Sm and ^{149}Sm, with Faraday cups and 10^{11} ohm resistors. Data reduction was performed with a built-in evaluation program in Qtegra, which handles interference removal and mass bias correction using the same principle as outlined above.

At the Norwegian Geological Survey (NGU), Nd isotopes of monazite and bastnasite were collected using a laser ablation multi-collector inductively coupled plasma mass spectrometer (LA-MC-ICP-MS) in the Norwegian Laboratory for Mineral and Materials (MiMaC). We used a Photon Machines Analyte excite 193 nm excimer laser coupled to a Nu Plasma 3 MC-ICP-MS. For bastnasite and most monazite, the laser used an energy of 4 J/cm^2, a repetition rate of 5 Hz and a spot size of 10 um. For monazite analysed in session 13697, we used 3 J/cm^2, 10 Hz and a 15 µm spot size. Ablations were carried out for 30 s, followed by 5 s of washout and 20 s of baseline measurements. Ablations were carried out in a He atmosphere and the sample aerosol was

transported to the ICP-MS by a He carrier gas, with additional Ar added to the He-sample in a mixing bulb before the plasma torch. The conditions were optimized on a daily basis and the total He varied between 0.3 and 0.5 L/min. Oxides generated in the plasma had a considerable effect on the accuracy of the data, and oxide formation was thus monitored and minimized at the beginning of each analytical session by moving the plasma torch. In addition, the magnet setting was offset from the centre of the peak by 0.05 amu. We analysed masses 143–150 in multi-collection mode on Faraday cups coupled with 10^{11} ohm resistors. As a primary standard, we used ZME for bastnasite (Yang et al. 2019) and Manangoutry for monazite (Liu et al. 2012). As control samples, we analysed Bananeira and Coquiero monazites (Gonçalves et al. 2016) and LZ1384 bastnasite (Liu et al. 2012). The primary reference materials were analysed at the beginning and end of each session and after every fifth unknown sample.

Data reduction was performed in iolite 4 (Paton et al. 2011) with a DRS from Fisher et al. (2020). First, the on-peak baselines are subtracted from each channel. Then, an isobaric interference correction of Sm on masses 144, 148 and 150 is applied. For this correction, the Sm mass fractionation is calculated with an exponential law based on the $^{147}Sm/^{149}Sm$ ratio of 1.0868. After Sm interference correction, the Nd fractionation is calculated using $^{146}Nd/^{144}Nd$ with an exponential law using the canonical ratio of 0.7219. In the LA data, elemental fractionation between Sm and Nd is observed and is corrected for with a downhole fractionation correction and normalization to the $^{147}Sm/^{144}Nd$ ratio of the primary reference material (Fisher et al. 2020).

References for Appendix 1

Pouchou, J. L. & Pichoir, F. 1991. Quantitative analysis of homogeneous or stratified microvolumes applying the model PAP. In: Heinrich, K. F. J. & Newbury, D. E. Electron Probe Quantitation. Plenum Press, 31–75.

Donovan, J. J. & Tingle, T. N. 1996. An improved mean atomic number background correction for quantitative microanalysis. Microscopy and Microanalysis 2(1), p. 1–7.

Appendix 2. REE oxalate production with hydrometallurgy

(Appended as a separate report)







GEOLOGICAL
SURVEY OF
NORWAY
- NGU -





Geological Survey of
Denmark and Greenland





Direktoratet for mineralforvaltning
med Bergmesteren for Svalbard





NAALAKKERSUISUT
GOVERNMENT OF GREENLAND